Durham E-Theses

Electron paramagnetic resonance of rutile pigments

Eggleston, H. S.

How to cite:

Use policy

Electron Paramagnetic Resonance

of

Rutile Pigments

by

H.S. Eggleston, B.Sc., M.Sc

(Grey)

A Thesis submitted to the University of Durham

in Candidature for the degree of Doctor of

Philosophy

January, 1982

CONTENTS

ABSTRACT

An Electron Paramagnetic Resonance study of rutile (TiO_2) pigments doped with either iron or chromium has been performed. The spectra of the Cr^{3+} ion has been observed and confirmed by computation. In iron doped pigments a signal with $g = 4.28$ was observed and has been attributed to the Fe^{3+} ion in a site of rhombic symmetry. The effect of irradiation by light on the Fe^{3*} ion in a substitutional site has been examined and seen to be different from that for single crystal samples ; only wavelengths longer than 700 nm affect it. A light-generated line was observed with 'g' values $g_{11} = 2.010$, $g_1 = 2.005$. The response of this line is related to the concentration of iron. The data has been analysed and correlates reasonably well with accepted models for the positions of the defect centres within the band gap.

ACKNOWLEDGEMENTS

CHAPTER 1

RUTILE

Rutile is widely used as a white pigment in paint, paper and plastics. The high refractive index gives it excellent light scattering properties which, apart from making it ideal for "brilliant white"paints, has led to the production of gemstones with a fire and brilliance superior to diamonds (De Vare (1951) Moore (1948)). The properties of rutile have been summarized in three reviews by Cronemeyer (1952), Grant (1959) and Frederickse (1961).

Rutile is just one of the three polymorphic forms of titanium dioxide. The other two are anatase and brookite which are metastable and can be transformed into rutile by heating to 1000° C and 850° C respectively (Shannon and Prewitt (1969)). The three forms are listed in Table 1.1.

Type	Crystallographic System	Unit Cell Dimensions (nm)	Band Gap (eV)
Rutile	Tetragonal D_{4H}^{14}	a = 0.4594 c = 0.2958	3.03
Anatase	Tetragonal D_{4H}^{19}	a = 0.3783 c = 0.951	3.23
Brookite	Orthorhombic V_{H}^{15}	a = 0.5435 b = 0.9166 c = 0.5135	3.26

Table 1.1 : Structural forms of TiO_2

Amorphous TiO_2 can be precipitated from sulphate or chloride solutions, but hydrolysis by direct boiling of chloride solutions will produce rutile directly. The production of pigments is discussed in section 1.5. Large
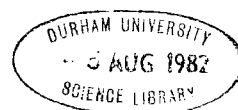
crystals are grown by the Verneuil flame fusion method ; these crystals are black due to a large number of oxygen vacancies but after heating in oxygen become transparent with a slight yellow colour. Fully stoichiometric rutile is a colourless transparent insulator with a band gap of 3.03 eV (Croneymeyer (1952), Grant (1959)), while crystals with an oxygen deficiency, of the form $Ti_{1+x}O_{2-x}$, are black, have a band gap dependent on x and are n-type semi-conductors.

1.1 THE UNIT CELL

The tetragonal (001) axis is called the 'c' axis and the (010) and (100) axes are called the 'a' axes. The unit cell is shown in Fig 1.1 (Von Hippel (1962)).

Each titanium atom is at the centre of a slightly distorted oxygen octahedron with principle axis in the $\left[110\right]$, $\left[001\right]$ and $\left[1\bar{1}0\right]$ directions. These provide a more useful axis system for discussing E.S.R. results and are labelled x,y,z respectively. They are shown in Fig 1.2, where it can be seen that there are two different titanium sites differing only by a rotation of 90° about the c-axis (Anderson and Kolberg (1973)).

The convention adopted to determine a direction in the crystal requires two angles θ and ϕ. Here θ is the angle between the field and the z axis and ϕ is the angle in the x-y plane between the x-axis and the projection of the field in the x-y plane.

In rutile each titanium ion is surrounded by an octahedron of oxygen atoms. The structure can be thought of as being formed of stacks of these octahedra, parallel to the 'c' axis, adjacent stacks being rotated by 90°. This structure leads to channels parallel to the 'c' axis which can be considered as oxygen octahedra with the central titanium ion missing. Alternatively rutile can be considered as being composed of layers of -O-O-Ti-O-O-Ti- chains perpendicular to the 'c' axis and orientated at right angles to the layers above and below.
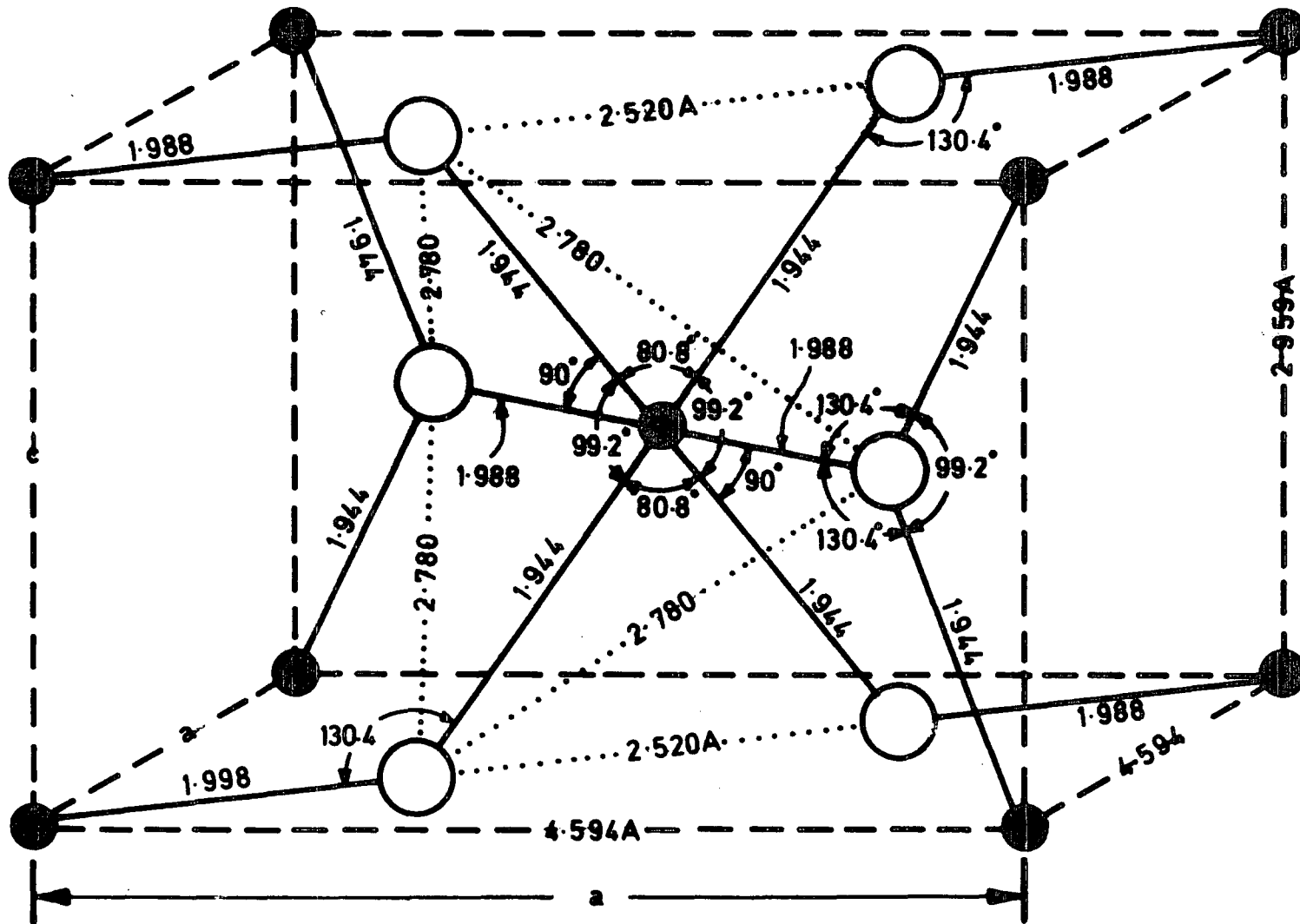
FIG. 1·1 UNIT CELL OF RUTILE,
(AFTER VON HIPPEL)

- ● Ti^{4+} ions
- ○ O^{2-} ions
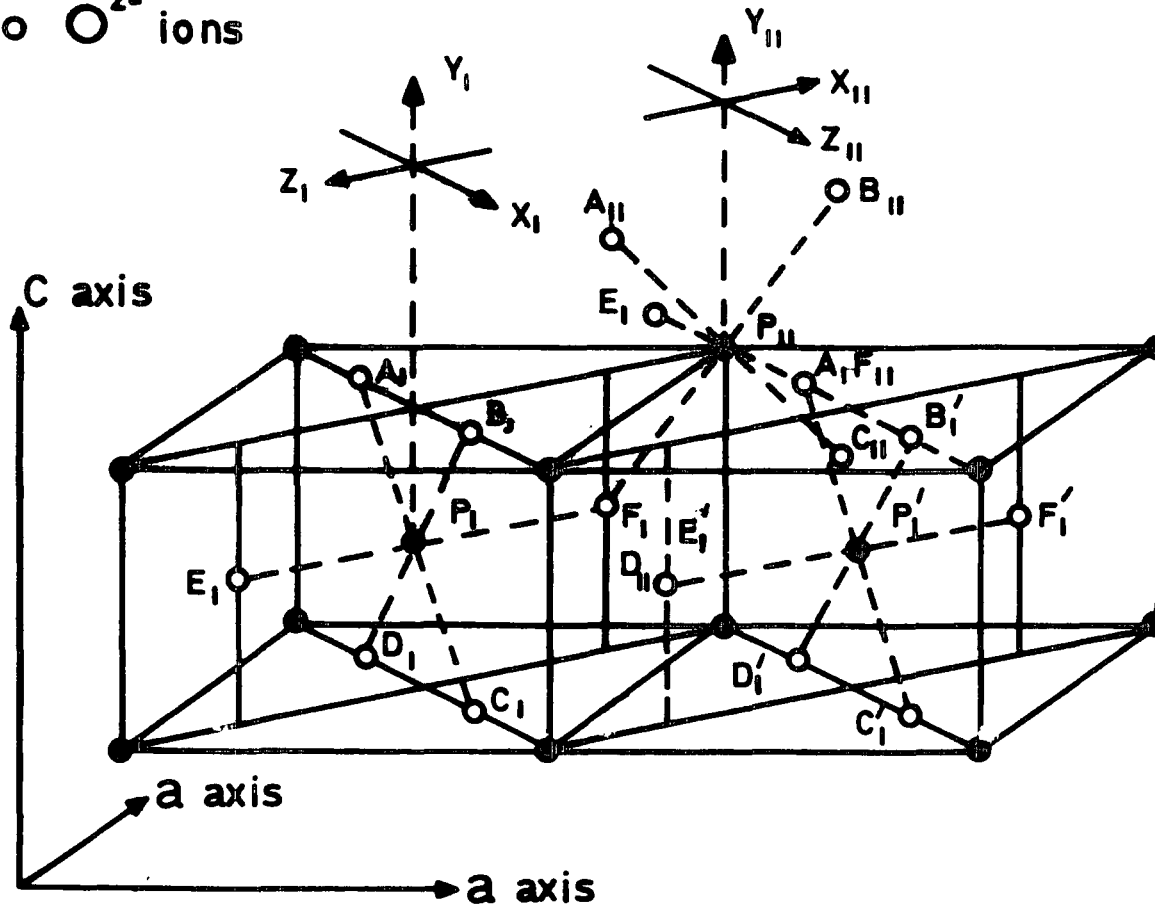
FIG. 1·2 CRYSTAL STRUCTURE AND AXIS OF SUBSTITUTIONAL SITES IN RUTILE. (AFTER ANDERSSON AND KOLBERG).

1.2   IMPURITY SITES

Impurity ions may take up either substitutional or interstitial sites. Paramagnetic ions substituting for Ti^{4+} will have magnetic axes parallel to the x,y and z axes. As the lattice has two different titanium sites differing only by a rotation of 90° around the y axis, we would expect to see two E.P.R. spectra rotated by 90° about this axis (Fig 1.2).

The existence of open channels parallel to the y axis results in easy diffusion of impurities in this direction. Ions may take up a position in the centre of these channels (Fig 1.3). There are four of these interstitial sites (in Fig 1.3) which differ only by a rotation of $\pm \alpha$ and $90 \pm \alpha$ where $\alpha = 12.6^{\circ}$, around the y axis (Kersen and Volger (1973)). Thus for a paramagnetic ion distributed over these sites we would expect to see a fourfold E.P.R. spectrum with the principle axes along the y axes and in the x-y plane, the latter axes making angles of $\pm \alpha$ and $90 \pm \alpha$ with the $\begin{bmatrix}110\end{bmatrix}$ directions. Small interstitial ions would not appreciably distort the lattice. Low and Offenbacher (1965), first considered the space available to accommodate an ion at an interstitial site ; subsequently, having reviewed a recent set of ionic radii given by Shannon and Prewitt (1969), Kersen and Volger (1973) concluded that ions with radii in the region of 0.63-0.82 $\overset{\circ}{A}$ might prefer these interstitial positions.

Huntington and Sullivan (1967) suggested the existence of a second-class of interstitial sites on $\left(\frac{1}{2},0,^{n}/4\right)$ type positions with n odd (i.e. points marked Δ in Fig 1.3). These sites are surrounded by four O^{2-} ions, two at a distance of 1.77 $\overset{\circ}{A}$ and two at 1.74 $\overset{\circ}{A}$. Energy calculations for the two types of sites showed that the difference in energy between the occupancy of one type of site or the other is small and might depend on the charge and radius of the interstitial ion. A fourfold E.P.R. spectrum could be expected also from ions in this type of site with an angle $\alpha \simeq 12.6$. For all impurity positions the spectra can be uniquely characterized by the g values along the principle axes and the angle α, i.e. g_x, g_y, g_z and α. For substitutional ions $\alpha = 0$.
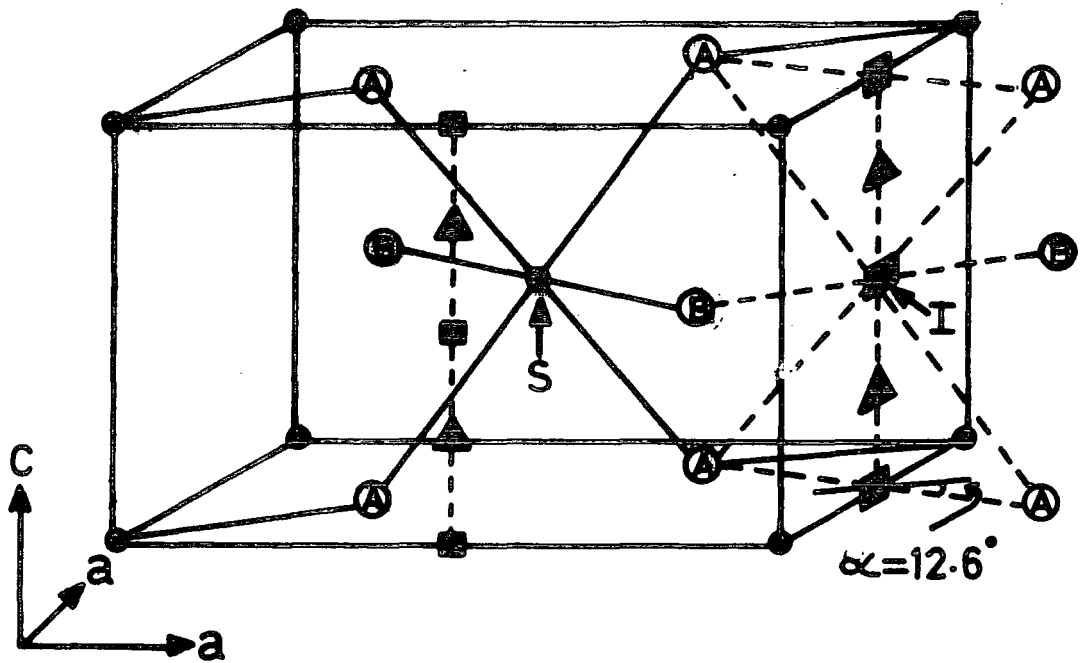
● Ti^{4+} $C = 2.959 Å$

○ O^{2-} $a = 4.594 Å$

■ $\frac{1}{2} O \frac{1}{2}$

▲ $\frac{1}{2} O \frac{1}{4}$

FIG. 1·3 CRYSTAL STRUCTURE OF RUTILE (TiO_2) SHOWING A UNIT CELL AND SOME $\frac{1}{2}O\frac{1}{2}$ (■) AND $\frac{1}{2}O\frac{1}{4}$ (▲) TYPE INTERSTITIAL SITES. THE POSITION AROUND THE OCTAHEDRALLY CO-ORDINATED SUBSTITUTIONAL ION S AND AROUND THE INTERSTITIAL SITE I ARE INDICATED. (AFTER KERSSEN AND VOLGER).

Rutile shows large variations from stoichiometry. When heated in a reducing atmosphere (vacuum, hydrogen, CO or titanium powder) rutile loses oxygen and becomes a n-type semiconductor. (The as-grown crystals need to be heated in O_2 as mentioned above). Two reducing reactions have been thought possible:-

$$TiO_2 \longrightarrow TiO_{2(1-x)} + x\ O_2\uparrow + 2\ x\ V_O^{2+} + 4\ x\ e^- \qquad (1.1)$$

$$TiO_2 \longrightarrow (1-x)TiO_2 + x\ O_2\uparrow + x\ Ti_I^{4+} + 4\ x\ e^- \qquad (1.2)$$
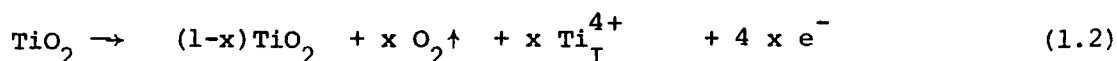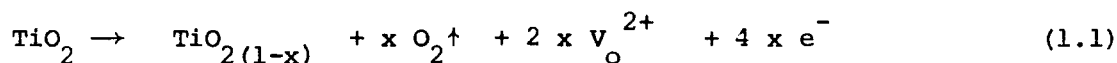
where V_O is an oxygen vacancy,

Ti_I is an interstitial titanium ion.

(the V_O or Ti_I can capture one or more electrons).

Initially, it was thought that the first reaction dominated but later E.P.R. results showed the presence of interstitial Ti^{3+} ions. To explain the results of many different experiments, both processes have to be used. Which predominates depends on the temperature, atmosphere and partial pressure of oxygen when the sample is reduced. However, it appears that $V_O-Ti_I^{3+}$ and $Ti_I^{3+} - Ti_I^{3+}$ complexes form and more exotic formations have been suggested to explain all the results (Kersen and Volger (1973)).

Recent work by Gibb and Anderson (1972) and Blanchin et al (1980) has shown that crystallographic shear planes can form in slightly reduced rutile. These are formed by the removal of whole planes of oxygen atoms parallel to either the $\begin{bmatrix} 132 \end{bmatrix}$ or $\begin{bmatrix} 121 \end{bmatrix}$ planes. The main impurity ions frequently found in rutile are listed in Table 1.2. The ions discussed in this thesis, Fe^{3+} and Cr^{3+}, enter the lattice substitutionally, replacing Ti^{4+}; how the change compensation takes place is not known.

TABLE 1.2 :   Properties of ions which are usually present in rutile (after Kersen and Volger).

Ionic Species	Ionic Radius ($\overset{\circ}{A}$)	Isotope	Natural Abundance (%)	Nuclear Spin	Nuclear Moments (μ_n)
O^{2-}	1.36	^{16}O	99.5	0	
		^{18}O	0.5	0	
Mg^{2+}	0.72	^{24}Mg	78.7	0	
		^{25}Mg	10.1	$\frac{5}{2}$	− 0.885
		^{26}Mg	11.2	0	
Al^{3+}	0.530	^{27}Al	100.0	$\frac{5}{2}$	+ 3.64
Si^{4+}	0.400	^{28}Si	92.2	0	
		^{29}Si	4.7	$\frac{1}{2}$	− 0.55
		^{30}Si	3.1	0	
Ti^{3+}	0.67	^{46}Ti	8.0	0	
Ti^{4+}	0.605	^{47}Ti	7.3	$\frac{5}{2}$	− 0.79
		^{48}Ti	74.0	0	
		^{49}Ti	5.5	$\frac{7}{2}$	− 1.10
		^{50}Ti	5.2	0	
Cr^{3+}	0.615	^{52}Cr	90.5	0	
		^{53}Cr	9.5	$\frac{3}{2}$	− 0.47
Fe^{3+}	0.645	^{54}Fe	5.8	0	
		^{56}Fe	91.6	0	
		^{57}Fe	2.2	$\frac{1}{2}$	< 0.05
		^{58}Fe	0.3	0	
Cu^{2+}	0.72	^{63}Cu	69.1	$\frac{3}{2}$	2.23
		^{65}Cu	30.9	$\frac{3}{2}$	2.38

1.3   E.P.R. OF IMPURITIES

Electron paramagnetic resonance provides a technique of examining

paramagnetic impurities and defects in a lattice which, like rutile, is

formed of diamagnetic ions. The resulting spectra can provide information

about the charge state of the defect, its local environment, and the inter-

actions between impurities. This work is concerned with pigments in which

much of this information is lost, or at least, very difficult to distinguish

from the effects of looking at a large collection of randomly orientated

crystallites. This problem is discussed in Chapter 3. The observed spectra

is described in terms of a "Spin Hamiltonian" in which a small set of para-

meters give the complete angular dependence of the spectra and amplitude of

the transition (see Abragam and Bleaney (1970), Assenheim (1966) or Al'tshuler

and Kozyres (1974) for details).

1.3.1 Spin Hamiltonian Formalism

A free ion with a total angular momentum, J, placed in a magnetic

field will have energy levels given by :-

$$W = g\beta H M_j \tag{1.3}$$

where   W   = Energy

β = Bohr magneton

H   = Magnetic field

M_j = Angular momentum quantum number

g is the Landé factor given by (Abragam and Bleaney (1970)) :-

$$g = 1 + \frac{J(J + 1) + S(S + 1) - L(L + 1)}{2J (J + 1)} \tag{1.4}$$

L   = Orbital angular momentum

S   = Spin angular momentum

If an alternating field of frequency ν is placed at right angles to

H, photons will be absorbed if :-

$$h\nu = g \beta H \tag{1.5}$$

and $M_j = \pm 1$ as these are the only allowed transitions. Experimentally it is found to be more convenient if ν is kept constant and H is varied to find the absorption. If there is only one electron (i.e. L = 0) then $g = 2.0023191$. The difference from 2 is due to small corrections which can be calculated using quantum electrodynamics.

When a paramagnetic ion is placed in a solid it will interact with neighbouring ions in one, or both, of two ways :

(a) Interactions between the magnetic dipoles

(b) Interactions between the paramagnetic ion and neighbouring dia- magnetic ions.

In doped rutile the distances between the paramagnetic ions will, in general, be considerably larger than the distance between paramagnetic ions and diamagnetic ions. Thus the predominant interaction is the second. The charge of the diamagnetic ion sets up strong internal fields which, to a good approximation, can be considered to be static. This internal field is called the crystal or ligand field.

The crystal field has a large effect on the ions. Firstly, it lifts the degeneracy of the ground state forming a number of new levels. This is called the zero-field splitting. The splitting, and number of components, depends on the symmetry and strength of the crystal field. In the 3d, or iron group, the crystal field is of moderate strength being larger than the spin-orbit coupling but smaller than the Coulomb interaction. The crystal field changes the resonance condition and absorption can take place at several values of field. This is called the fine structure. Other interactions which can affect the energy levels include the hyperfine structure which is due to interactions between the electrons and the nucleus with a non-zero nuclear spin.

A 'g' value can be defined by equation 1.5. In general this 'g' value will be different from the Landé splitting factor and to minimize confusion is

called the spectroscopic splitting factor. As the crystal field has a certain symmetry, the 'g' value need not be isotropic and in the most general case 'g' can be represented by g_{ij}, which is called, rather loosely, a tensor.

The behaviour of the energy levels is conventionally represented by a Spin Hamiltonian ; this includes terms which are spin dependent but neglects those which only add a constant to the energy of the levels, since we are only interested in the differences between the levels.

A Spin Hamiltonian can be derived by considering the different interactions and summing various contributions. These interactions are :- Coulombic forces between both electrons and electrons and the nucleus, also between electrons with the crystal field, spin-orbit and spin-spin interactions, the Zeeman term which is responsible for paramagnetism, electron nuclear forces, a nuclear contribution and a term due to diamagnetism (Abragam and Bleaney (1970), Taylor et al (1975)). The Coulombic forces are independent of field and can be neglected. The Zeeman term is very important as it is the field dependent term which gives rise to the observed transitions, while the crystal field which gives rise to the fine structure is the largest term in the Spin Hamiltonian for rutile. The other terms represent small corrections and can be ignored. The nuclear spin of iron is 0 (Table 1.1), and so there are no hyperfine contributions. A reasonably general Spin Hamiltonian, which represents the observed energy levels, is (Taylor et al (1975))

$$\mathcal{H} = \beta \underline{S}.\underline{g}.\underline{H} + \underline{S}.\underline{D}.\underline{S} \qquad (1.6)$$

where $\underline{S}$ = Electron spin operator

$\underline{H}$ = Applied magnetic field

$\underline{g}$ = Spectroscopic splitting

$\underline{D}$ = Fine Structure interaction tensor

In this approximation terms, due to higher order fine structure interactions, have been ignored.

The substitutional sites in rutile have orthorhombic symmetry and the Spin Hamiltonian must have the same symmetry. A general spin Hamiltonian for S state ions in orthorhombic symmetry without any hyperfine interactions is (Bleaney and Trenham (1951), Bleaney and Stevens (1953)).

$$\mathcal{H} = g_{ij} \underline{H} \cdot \underline{S} + D \left[S_z^2 - \frac{S}{3}(S+1) \right] + E(S_x + S_y) + \frac{a}{6} \left[\left(S_x^4 + S_y^4 + S_z^4 - \frac{S}{5}(S+1) \right)(3 S^2 + 3S - 1) \right]$$

$$+ \frac{F}{180} \left[35 S_z^4 - 30 S (S+1) S_z^2 + 25 S_z^2 - 6S(S+1) + 3S^2 (S+1)^2 \right] \quad (1.7)$$

where D and E are fine structure constants and a and F are due to quadrupole interactions.

Other higher order terms exist, but are of little importance. In fact, the E.P.R. spectra of many impurity S state ions in rutile are adequately described by including just the first three terms.

In equation (1.7) the first term can be simplified. The $\underline{g}$ factor is represented by a 3 x 3 matrix, g_{ij}, (which is not a true tensor quantity). The quantity g_{ij} can then be diagonalized by a suitable similarity transform which is equivalent to changing the principle axes of the matrix. In Section 2 the use of a set of axes x, y, z, was described. Using these as the principle axis, g_{ij} is diagonal, i.e.

$$g_{ij} = 0 \quad (i \neq j) \quad (1.8)$$

$$g_{11} = g_x, \quad g_{22} = g_y, \quad g_{33} = g_z$$

so that g_{ij} can be represented by a vector g_i. In fact in Fe/TiO_2

$g_x = g_y = g_z$ so that g_i can become a numerical constant (Carter and Okaya (1960)).

Exact diagonalization of (1.7) is difficult and a computer has to be used as described in Appendix 2.

1.3.2 Fe^{3+} ($^6S_{5/2}$, $3d^5$)

Iron, in a trivalent state, substitutes for Ti^{4+} as shown in Fig 1.3. As there are two sites differing only by a rotation of 90° about the y axis, the E.P.R. spectra exhibits, in general, two lines for each transition.

Fe^{3+} has spin $^5/2$ and so an isolated ion will have a six-fold degenerate ground state. In rutile, the degeneracy is lifted by the crystal field and three pairs of levels are formed. These levels are Kramers doublets and the remaining degeneracy is lifted by an applied magnetic field (Figs 1.4 and 1.5). The levels can be labelled $\pm \frac{1}{2}$, $\pm \frac{3}{2}$, $\pm \frac{5}{2}$ in order of ascending energy. These do not strictly represent the spins of the level because the states are admixtures of spin states of the form

$$a\left|\frac{1}{2}\right> + b\left|\frac{-3}{2}\right> + c\left|\frac{5}{2}\right> \quad \text{or} \quad d\left|\frac{-1}{2}\right> + e\left|\frac{3}{2}\right> + f\left|\frac{-5}{2}\right> = \left|A\right>$$

where A is a label for one of the observed levels. Another way of labelling the states is 1, 2...6 in order of ascending energy and this leads to less confusion.

This explains why transitions between $+\frac{3}{2} \rightarrow -\frac{3}{2}$ are observed. The states are not pure spin states so the forbidden $\Delta m = 2$ transition can occur through mixtures of appropriate spins.

The Spin Hamiltonian used to describe the observed spectra is (Carter and Okaya (1960)).

$$\mathcal{H} = g\,\underline{H}.\underline{S} + D\left[S_z^2 - \frac{35}{12}\right] + E\left(S_x^2 - S_y^2\right) + \frac{a}{6}\left(S_x^4 + S_y^4 + S_z^4 - \frac{707}{16}\right)$$

$$+ \frac{7}{36}\,F\left[S_z^4 - \frac{95}{14}S_z^2 + \frac{81}{16}\right] \tag{1.9}$$
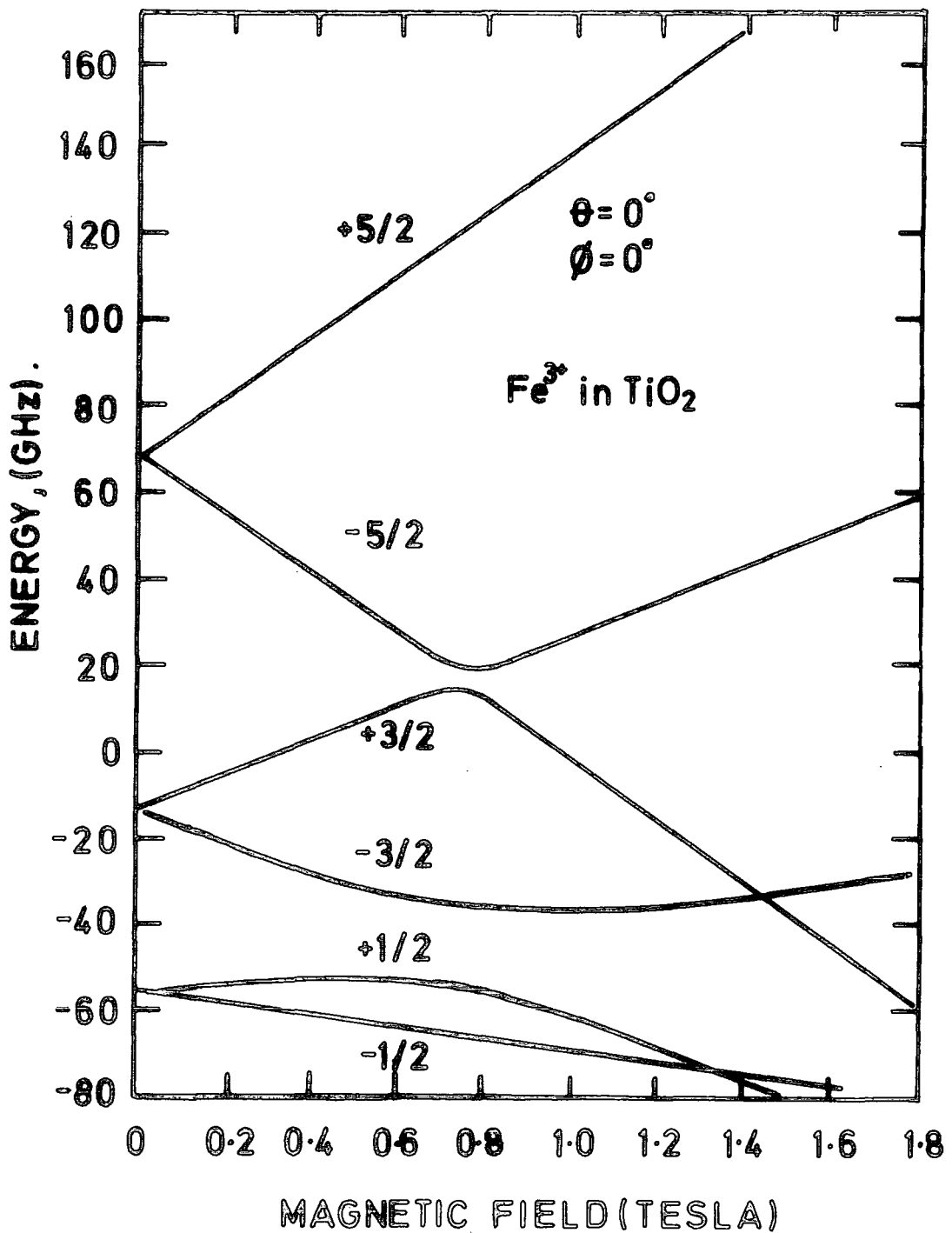
FIG. 1·4. CALCULATED ENERGY LEVELS AS A FUNCTION
OF FIELD STRENGTH FOR THE FIELD IN THE Z
DIRECTION ($\theta=0°, \phi=0°$). THE NUMBERS ON THE
LEVELS ARE FOR IDENTIFICATION. (AFTER
D. L. CARTER AND A. OKAYA).
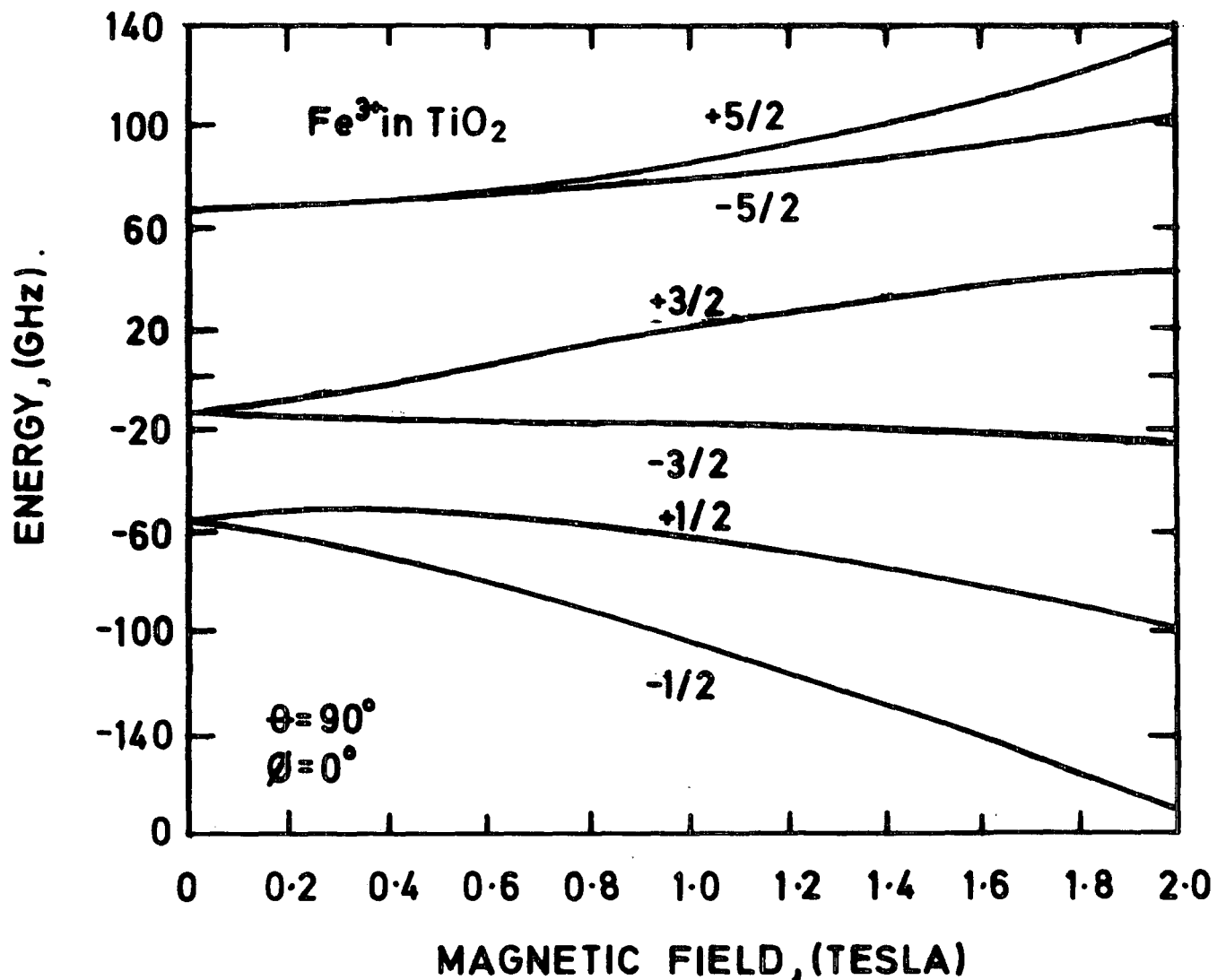
FIG. 1·5. CALCULATED ENERGY LEVELS AS A FUNCTION OF FIELD STRENGTH FOR THE FIELD IN THE X DIRECTION (θ=90, $\emptyset$=0). THE NUMBERS ON THE LEVELS ARE FOR IDENTIFICATION. (AFTER D.C.CARTER AND A.OKAYA).

The constants have been derived experimentally by various authors and a comparison is made in Table 1.3. Lichenberger and Addison (1964) included in their Spin Hamiltonian a term

$$C \left[\left(7 \, s_z^2 - \frac{3S}{4} \right) \left(s_x^2 - s_y^2 \right) + \left(s_x^2 - s_y^2 \right) \left(7 \, s_z^2 - \frac{3S}{4} \right) \right]$$

but as they conclude that the constant C equals zero there is no need to consider it further.

Carter and Okaya's values give better results at, or near, zero field and they claim that the signs of their constants agree with intensity measurements between 1.4 and 4.2 K. These are the values which shall be used.

Experimentally, frequencies of about 9 GHz were used. The photon energy is too small to stimulate transitions between different doublets (except at fields higher than were used) so only three transitions would be expected. In fact only two transitions can be seen. This is because the transition probability between the '5' and '6' states is small and the population of these states is less than for lower levels, so we would not expect to see it at all.

In analyzing the experimental results, it appears that the 3 or 4 transition could not be seen with the magnetic field along the y ('c') axis. In Fig.1.6 the explanation becomes clear. The separation between these two levels increases until it reaches a maximum of about 8 GHz and then decreases again with increasing magnetic field. Thus the microwave radiation is unable to stimulate transitions in the range being considered.

Additional spectra resulting from complexes of Fe^{3+} and an interstitial proton and Fe^{3+} and a nearby oxygen vacancy have also been reported (by Anderson and Kollberg (1973)).

TABLE 1.3 :   Spin Hamiltonian Parameters for Fe^{3+}/TiO_2.

Parameter	Carter & Okaya (1960)	Schollmeier (1966)	Lichenberger & Addison (1964)	Units
g	2.000 ± 0.005	2.000 ± 0.005	2.000 ± 0.0005	
D	20.35 ± 0.01	20.35 ± 0.01	20.38 ± 0.01	GHz
E	2.21 ± 0.07	2.21 ± 0.07	2.06 ± 0.01	GHz
F	-0.5 ± 0.3	-0.5 ± 0.3	0.68 ± 0.02	GHz
a	1.10 ± 0.1	+1.10 ± 0.1 (diag elements)	-0.84 ± 0.04	GHz
		-1.10 ± 0.1 (off diag elements)		GHz
C	–	–	0.00 ± 0.01	GHz
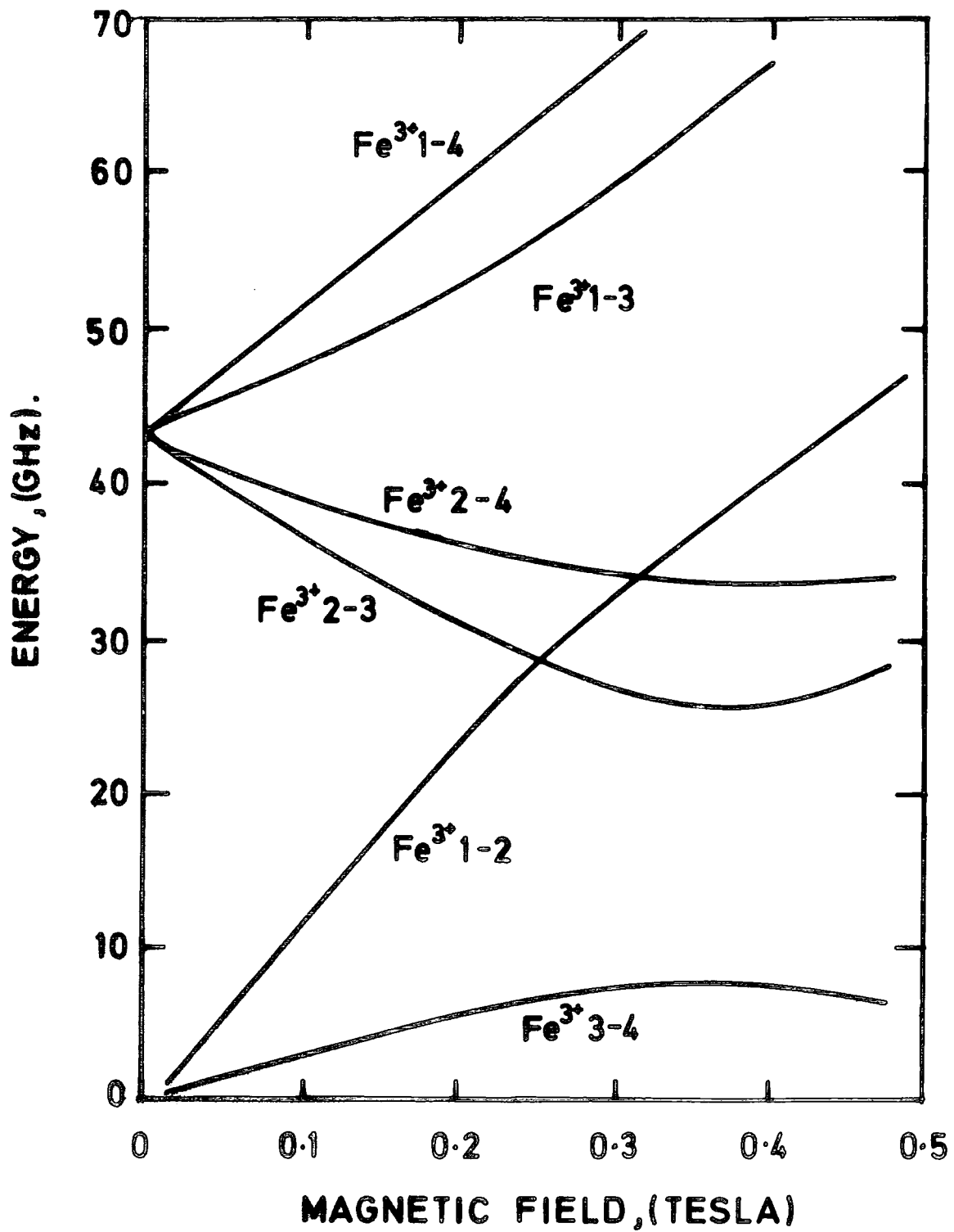
FIG. 16. ISOGON PLOT OF THE Fe^{3+} SPECTRUM FOR THE MAGNETIC FIELD ALONG THE c AXIS.

1.3.3 Other Impurities

The spectra of impurity ions in rutile is well known and lists of the Spin Hamiltonian parameters are available from various sources including Low and Offenbacker's review (1965) and Assenheim's book (1966) which include extensive bibliographics.

Only chromium and iron have been examined in this work. Chromium exhibits a spectra of a substitutional ion although there is also a weaker unexplained spectra. Cr^{3+} has a $3d^3$ configuration which is split by the crystal field into two Kramers doublets. The hyperfine splittings of the Cr^{53} isotope (9.5% abundance, $I = 3/2$) have been observed. A spectra attributed to Cr^{5+} formed by annealing in an electric field has been reported by Sochava (1972). Complexes of Cr^{3+} with a second or third nearest neighbour oxygen vacancies have also been observed. (Ikebe (1969), Sochava (1970)).

The Spin Hamiltonian parameters have been given by Gerritsen and Sabiskey (1963), Gerritsen and Harrison (1959) and (1960) and Sierro et al (1960) as $g_x = g_y = g_z = 1.97$

$$D = 0.55 \text{ cm}^{-1} \qquad E = 6.27 \text{ cm}^{-1}$$

The spectra of a trapped hole associated with aluminium substituting for Ti^{4+} have been reported by Zwingel (1976). These are excited by U.V. irradiation and seem to be associated with charge transfer from other (e.g. Fe^{3+} and Cr^{3+}) impurities causing the well-known photochromic behaviour of rutile (Faughnan and Kiss (1960), Clark et al (1970)).

1.3.4 E.P.R of Defects

It was mentioned above that in nonstoichiometric rutile it is not known exactly how charge compensation takes place but it is likely to be due to a combination of oxygen vacancies and interstitial Ti^{3+} ions. E.P.R. observations of three defects have been reported by various authors, some in 'pure' rutile and others in doped and reduced samples. In fact, as mentioned below, Al is needed to make good crystals so the observation of

centres in combination with Al^{3+} is not surprising. The observations are listed in Table 1.4.

1.3.5 E.P.R. of Adsorbed Ions

In the pigments supplied by Tioxide International Ltd., the individual grains were about 0.5 μm in diameter and had a surface area of about 7 metres² per gram. Thus there is considerable scope for ions to be adsorbed. E.P.R. of adsorbed species on rutile has been reported by several authors and their results are summarized in Table 1.5. Oxygen, nitrogen and nitrogen radicals have all been observed giving rise to spectra with 'g' values near the free electron value.

1.4 TRAPPING LEVELS IN RUTILE

Thermoluminescence (T.L) and Thermally Stimulated Conductance (T.S.C) have been used to look at shallow levels but these techniques cannot say much about deep levels apart from inferring that these levels exist.

These deep impurity levels of iron group impurities in rutile have been examined by Mizushima, Tanaka, Asai, Iida, and Goodenough (1973 and 1979) using two different magnetic resonance methods. The first method relies on moving the Fermi level and looking for changes of valence state while in the second crystals are irradiated with monochromatic radiation of energy less than the band gap, and the resulting valence changes are monitored.

In the interpretation of their data, Mizushima et al have used a model mainly based on a semi-empirical theoretical calculation first made by J.W.Allen (1964), and consequently the validity of the energy level diagram,they suggest,is limited by the exactness of the assumptions made in Allen's calculation. In the following section, an outline of Allen's method is given and it will be seen that it is probable that Mizushima's energy level scheme may be subject to errors amounting to at least 1 eV.

1.4.1 Theoretical Determination of Energy Levels

The method due to J.W.Allen (1964) can be summarised as follows.

TABLE 1.4 :   E.P.R. of Defects in Rutile.

g_{110}	$g_{1\bar{1}0}$	g_{001}	Notes	Interpretation	Refs
$g_x=1.974$	$g_y=1.977$	$g_z=1.941$	x,y are 19° from <110> in 001	Interstitial Ti^{3+} Interstitial M^+	1 2
1.965	1.965	1.935		F centre	3
1.975	1.978	1.953		Subst. Ti^{3+}	4
1.9777	1.9743	1.9436	Pt.doped crystal	" Ti^{3+}	5
$g_x=1.916$	$g_y=1.953$	1.814	reduced Al-doped	$Ti^{3+}-Al^{3+}.Al^{3+}$	6
$g_x=1.850$	$g_y=1.885$	1.932	"	$Ti^{3+}-Ti^{3+}-Al^{3+}-Al^{3+}$	6
$g_x=1.962$	$g_y=2.040$	1.704	"	"	6
1.965	1.965	1.965	"	F centre	6
$g_x=1.835$	$g_y=1.915$	1.825	"		6
1.980	1.978	1.956	Ti <450°C	F centre-trivalent impurity	7
1.923	1.896	1.793	Al doped	$Ti^{3+}-Al$	7
1.923	1.912	1.828	"		7
1.924	1.957	1.78	Reduced in H_2		7
1.985	1.989	1.932	"		7
1.964	1.971	1.971	"		7
1.964	1.994	1.928	Ti doped		7
1.954	1.979	1.950	"		7
1.92	1.89	1.80	irrad. γ-rays at 77 K		8
2.00	4.50	3.43	"		8
1.964	1.914	1.935	"		8
1.935	1.985	1.989	neutrons at room temp.		9
1.969	1.983	1.989	" at 140 K	F centre	10
1.991	1.9503	1.9503	" "	Ti^{3+}	10
1.998	1.973	1.971	"	Ti^{3+}	10
1.966	1.980	1.987	neutrons at 140 K - γ-ray annealed at 79 K	Ti^{3+} interstitial	10
$g_x=2.0192$	$g_y=2.0261$	2.0034	UV at 10 K	hole trapped - Al^{3+}	11
2.0197	2.0189	2.0030	" + anneal.	"	11

Refs : 1- Chester (1961 ; 2 - Shen et al (1974) ; 3 - Bogomolov et al (1968) ;
    4 - Gerritsen et al (1962) ; 5 - Chandrashekhev (1976) ;
    6 - Kersen and Volger (1973) ; 7 - Chester (1964) ; 8 - Young et al (1961) ;
    9 - Weeks (1961) ; 10 - Purcell (1971) ; 11 - Zwingel (1976).

TABLE 1.5 :

Species	g values	Refs
O_2^-	$g_1 = 2.030,\quad g_2 = 2.008$ $g_3 = 2.004$	Naccache et al, 1971
O_2^-	$g_1 = 2.020,\quad g_2 = 2.009$ $g_3 = 2.003$	"
?	$g = 2.003 \quad \Delta H = 3$ symmetric	Van Hooff, 1968
produced by U.V. irradiation of N_2O.	$g_{11} = 2.011,\quad g_1 = 2.002$	Shevets & Kazamskii (1971)

When an electron is taken from an impurity ion and put into the conduction band the configuration of that ion changes from d^n to d^{n-1}. Consequently, to find the depth of the impurity below the conduction band it is necessary to find the difference between these two levels. Using the approximations of crystal-field theory, the configuration energies can be written down. (These have been tabulated for transition metal ions by Griffith (1961)). To clarify the procedure it is useful to consider as an example the behaviour of divalent and trivalent cobalt (d^7 and d^6). These have energies given by

$$E(d^7) = -7U' + 21 A' - 43 B' + 14 C' - 3/5 \Delta' \qquad (1.10)$$

$$E(d^6) = -6U'' + 15 A'' - 35 B'' + 7 C'' - 2/5 \Delta''. \qquad (1.11)$$

In these equations the contributions represented by U' and U'' arise from the core and spherically symmetrical part of the crystal potential ; the terms involving the Racah parameters A' and A'' originate from electrostatic interactions within the d-shell and shift the energy of the shell as a whole ; the quantities B' and B'', C' and C'' are electrostatic terms which split the degeneracy of the d-electrons and finally Δ' and Δ'' are due to crystal-field splittings. We note here that although B, C and Δ can be measured experimentally, (from optical measurements on crystals) the parameters U and A are more difficult to determine. If it is assumed that $U' \simeq U''$, $A' \simeq A''$, $B' \simeq B''$, and $C' \simeq C''$ a series of equations can be written having the form

$$E(d^{n-1}) - E(d^n) = \phi + 3\eta + 6B + 3/5 \Delta(2+) + Q5(\Delta3+) \left[\text{for } n=3, Cr^{2+} \right]$$

and
$$\qquad (1.12)$$

$$E(d^{n-1}) - E(d^n) = \phi + 5\eta - 7C + 2/5 \Delta(2+) . \left[\text{for } n = 6, Fe^{2+} \right] \quad (1.13)$$

for each value of n lying within the limits $1 \leqslant n \leqslant 10$. Griffith has shown that for free ions U and A vary linearly with atomic number and if it is assumed that this is also true for ions in crystals their values can be estimated. It can thus be seen that for a substance like ZnS, (where B, C and Δ are known), the problem can be solved using two known energy levels to determine ϕ and η. A difficult problem arises, however, for rutile since no energy levels are known, neither are the values of B, C and Δ. The authors quoted above have resorted to making a series of approximations and estimates based on the few results known for other oxides ; (the only experimental result in doped TiO_2 is $\Delta = 17,500 \ cm^{-1}$ for the Cr^{3+} ion). This means that the errors in the calculations taken as a whole could be large. When discussing his results, Allen gives a range of error of about 2/3 eV for some levels, even in situations where the parameters are quite well known. As regards TiO_2, where there is a great lack of basic information, the results could be in error by a considerably larger amount. The results are given in Figure 1.7.

1.4.2 Experimental Determination of Energy Levels

(a) Lithium Doping

Lithium atoms in interstitial sites in rutile make shallow donors and these consequently can supply electrons which raise the Fermi level. The valence states of the impurity ions can be detected using E.P.R. and, as the Energy of the Fermi level is related to the Li concentration, the Fermi level can be swept up from E_F to the conduction band. It is important to note here that the exact relationship between the Fermi level energy and the lithium concentration is not known ; the information available using this method is therefore limited, but nevertheless it has been used by Mizushima et al (1973,1979) and the results they obtained are reproduced (Fig 1.8).
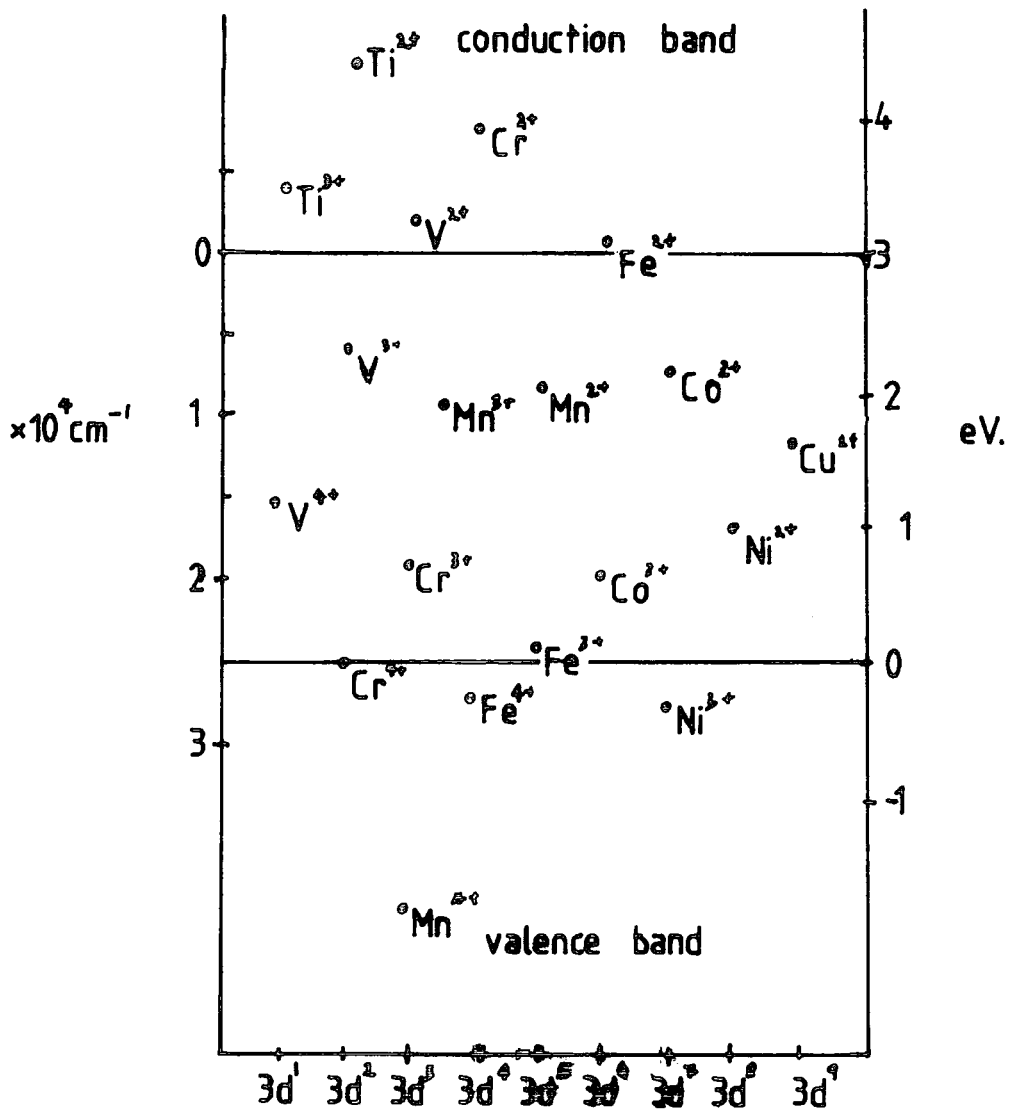
FIG.1·7   PREVIOUSLY PROPOSED ENERGIES OF IMPURITY-ION IN RUTILE
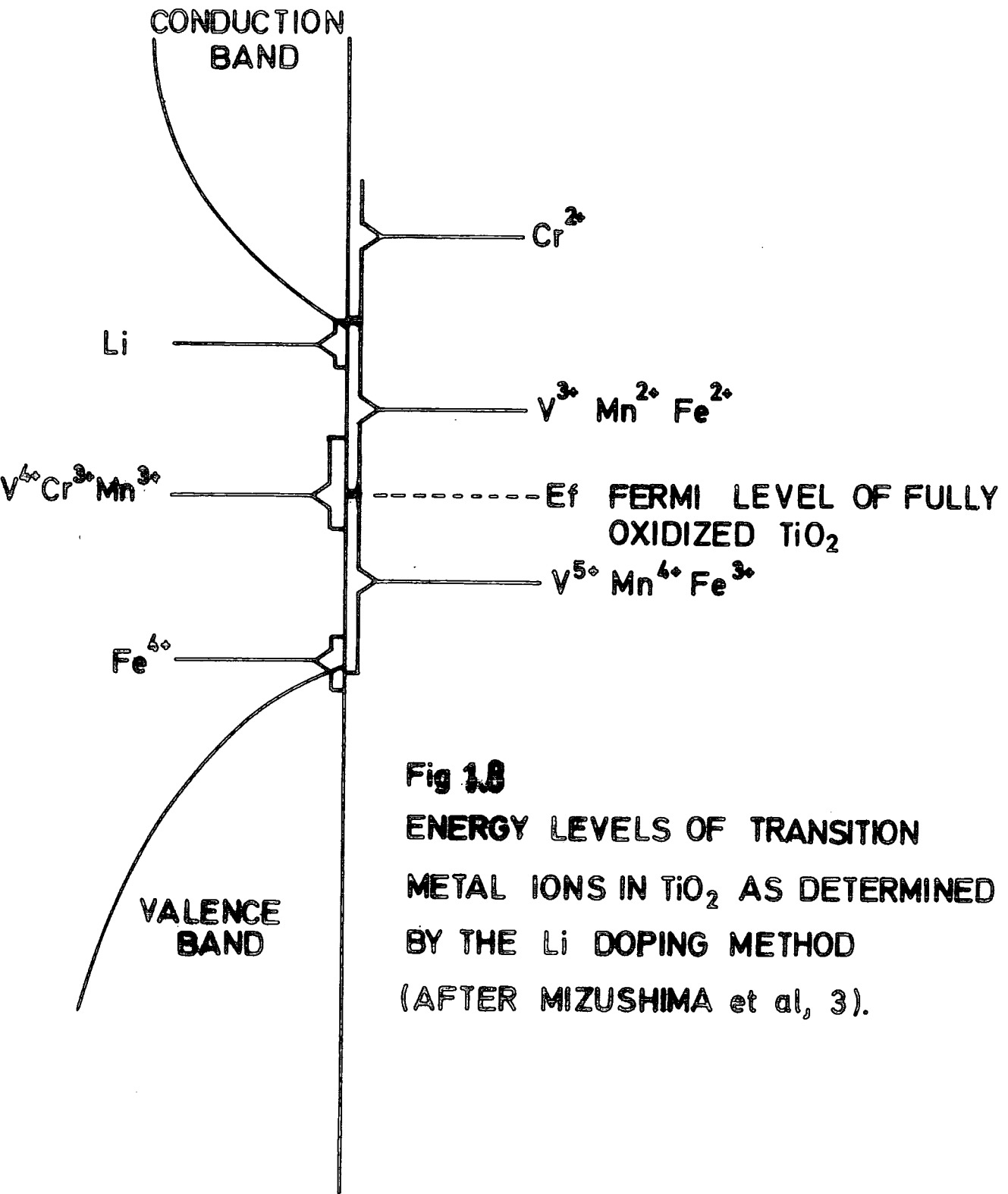
Fig 1.8
ENERGY LEVELS OF TRANSITION
METAL IONS IN TiO_2 AS DETERMINED
BY THE Li DOPING METHOD
(AFTER MIZUSHIMA et al, 3).

(b) <u>Photosensitive E.P.R.Measurements</u>

In the papers reviewed, measurements of the effect of optical irradiation on E.P.R. were used to determine the position of paramagnetic impurities in the band gap. The amplitude of the E.P.R. signal (which is proposed to the number of ions of a particular impurity with the same valency and environment) and the wavelength of the light used, (i.e. the photon energy), are reported for each of the ions V^{4+}, Cr^{3+}, Fe^{3+} and Mn^{4+} and the results are explained in terms of Fig.1.7.

Figures 1.9 and 1.10 indicate the type of variation of E.P.R. signal amplitude observed under various conditions. In Figure 1.10 the specimens have been exposed to an intense white light, before irradiation with monochromatic light, which sets up a metastable distribution between the 'bands' E_1 and E_2 and the impurities; the times t_1 and t_2 are defined below.

(c) <u>Experimental Procedure</u>

Three separate procedures were used. In each case the signal amplitude was measured as a function of time after the start of irradiation with monochromatic light. The time was labelled t_1, t_2 and t_3 to distinguish the conditions. The procedure was :-

1. A monochromatic irradiation following a virgin dark state (time denoted by t_1).

2. The dark state was followed by irradiation with intense white light and the electrons allowed to form a metastable distribution in the dark before the monochromatic radiation was applied (time denoted by t_2).

3. The intense white light was followed by irradiation at 415 m in order to establish a different metastable distribution (time denoted by t_3).

Fig 1.11 shows diagramatically the procedure.

To summarise briefly, the E.P.R. signals from V^{4+}, Cr^{3+}, Fe^{3+} and Mn^{4+} were monitored and the changes in amplitude as a function of the wavelength of the monochromatic irradiation were plotted.

Fig. 1·9 Spectra of the change ΔI in ESR signal intensity from $t_1 = 0$ to $t_1 = 2$ min for four impurity-cation states in oxidized TiO_2 at 77 K irradiated by monochromatic light

ΔI (arbitrary scale)

3.0   2.5   2.0   1.5 eV

(a)

V^{4°

600

400   500   600   700   800   mμ

0

400   500   600   700   800   mμ

(b)

Cr^{3°

ΔI

2.5   2.0   1.5 eV

3.0

600   500   600   700   800   mμ

(c)

Fe^{3°

ΔI

2.5   2.0   1.5 eV

3.0

0.5

(d)

700   500   mμ

600   500   600

Mn^{6°

" Mn^{3° "

ΔI

3.0   2.5   2.0   1.5 eV
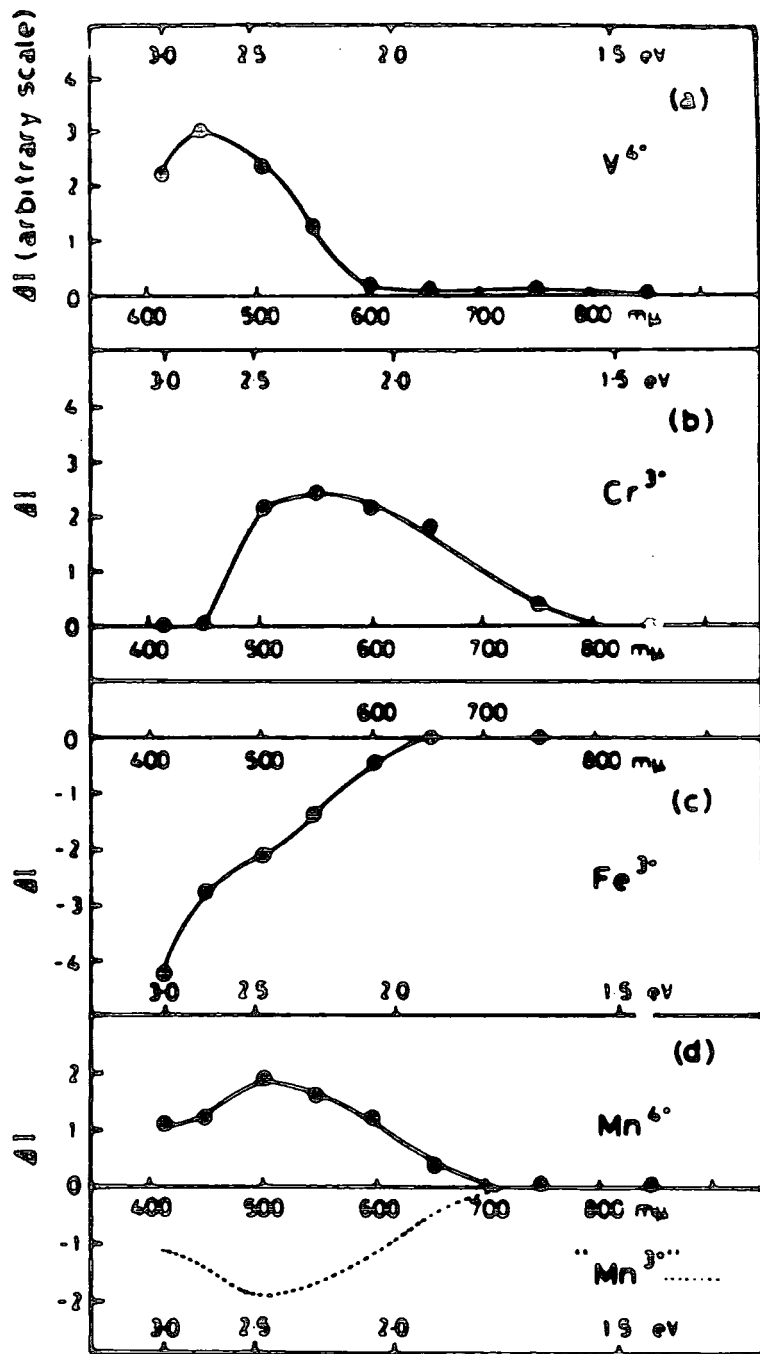
Wavelength monochromatic light (mμ)
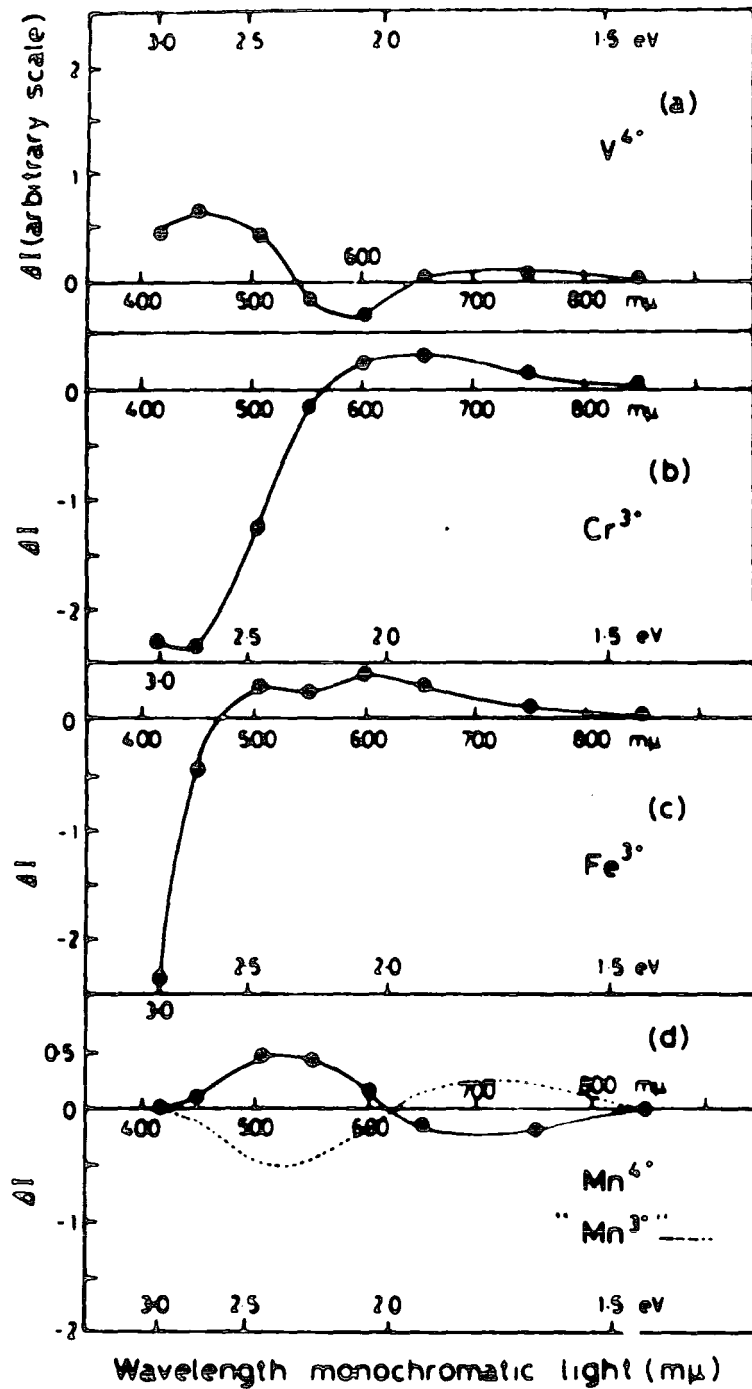
Fig.1-10 Spectra of the change ΔI in ESR signal intensity from $t_2 = 0$ to t_2 2 min for the same impurity-cation states in the same TiO$_2$ crystals as in Fig. 10 at 77 K and irradiated by monochromatic light.
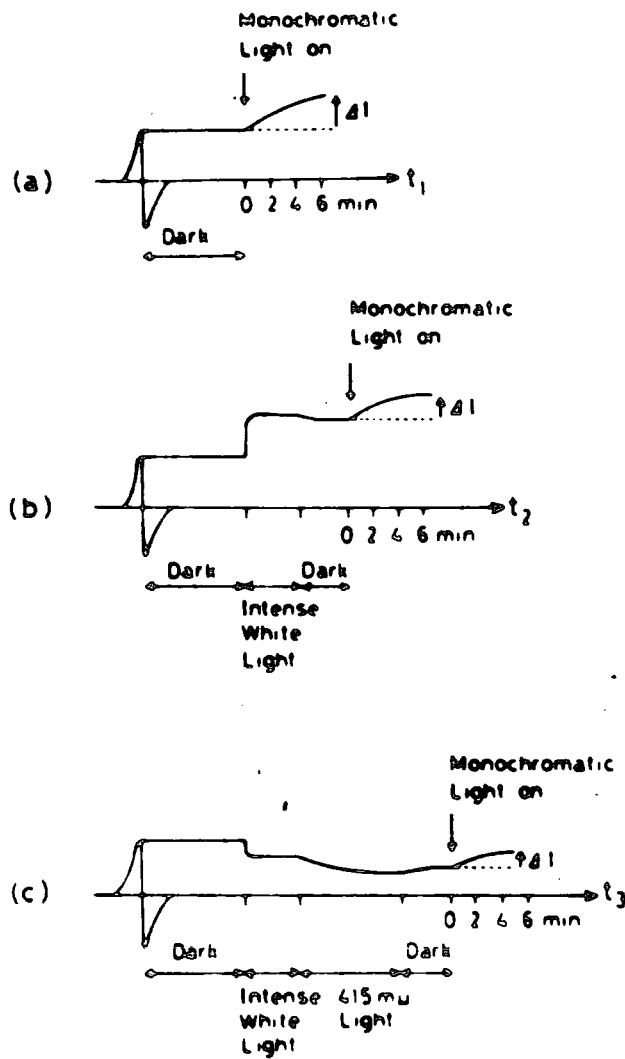
Fig.1·11 Schematic representation of the variation of ESR signal intensity (which is proportional to peak of the derivative in our case) with time for three different types of experiment. Definitions of the irradiation times before reading photocurrent or ESR signals: (a) t_1 follows a virgin dark state, (b) t_2 follows a dark interval following irradiation by an intense white light, (c) t_3 follows a dark state following a period of illumination with 415 mμ light after irradiation by an intense white light.

(d) Results

There were larger differences between ions and by finding the energies of the light at which the concentration of the ion increased or decreased, estimates of the depth of the 4 ions below the conduction band could be made. One of these (Mn^{3+}) was about 1 eV lower than the previous estimates. It may also be noted that photocurrent experiments and analysis of E.P.R. results revealed two bands of states. The first one was centred at 2 eV below E_c and appeared to be due to surface states (E_1). The second band lay 2 eV below E_c and was attributed to bulk defect states (E_2), probably introduced by the doping techniques used in these experiments (the bulk states are possibly cation vacancies).

The results are summarised in Figure 1.12. When this is compared with Fig 1.7, departures from the theoretical model can be seen to be significant.

1.5   RUTILE PIGMENTS

Rutile pigments are made using one of two processes, the sulphate and the chloride methods.   Darby and Leighton (1977) give a review of these processes and of the industrial aspects. The sulphate process uses ilmenite ($FeTiO_3$) which is ground and digested with concentrated sulphuric acid at an elevated temperature. The resultant sulphates of iron and titanium are leached from the bulk with water or dilute acid. The resultant fluid is filtered and then concentrated by evaporation. This fluid is now hydrolysed to precipitate acidic hydrated titanium, which is collected by filtration and after washing, heating and calcination yields titanium dioxide. This can result in either anatase or rutile depending on the exact conditions of the process.

However, all the pigments studied in this thesis were made using the chloride process. This consists of the formation of titanium tetrachloride, by heating with chlorine, purification of this and then oxidation of the

Conduction Band

————————————————————————————— —√Fe^{2+}(+0.1eV) 0

-1

—— Mn^{3+}(-1.9eV)
—— V^{4+}(-2.1eV)   -2

—— Cr^{3+}(-2.7eV)
//////////////////////////——Fe^{3+}(-3.0eV) -3eV
/////////////////↓ Mn^{4+}///////
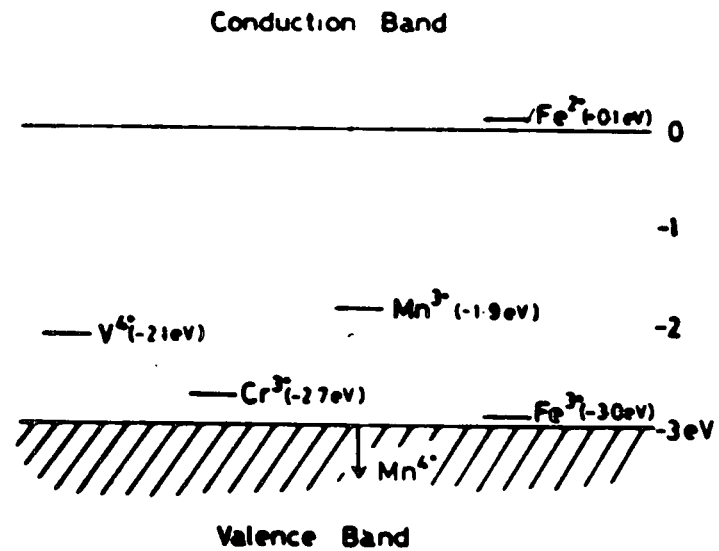
Valence Band

Fig.1-12 Location of M^{m+}:$3d^n$ levels in TiO$_2$ as determined by photosensitive ESR spectra. These are to be compared with Fig. 1.
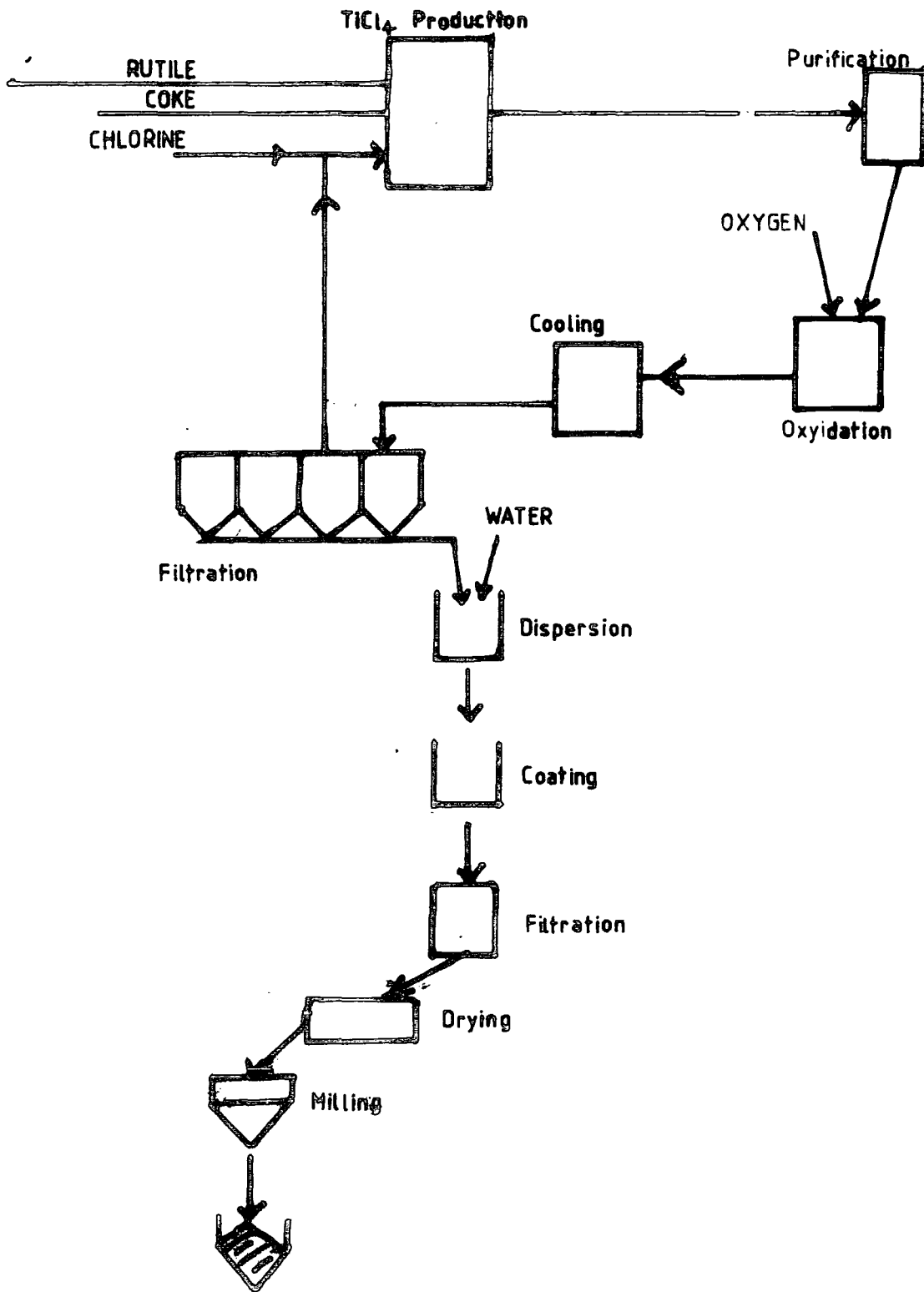
FIG. 1.13   PRODUCTION OF RUTILE PIGMENTS
             BY THE CHLORIDE PROCESS

titanium tetrachloride in oxygen to form rutile. The chlorine can be recovered and reused, (Fig 1.13). The oxidation process takes place at a temperature in the range 1200-1600°C and takes approximately one minute (see Tioxide International Ltd : BTP 182).

Alumina is added to the pigments to promote the formation of rutile (Goni and McPherson (1980)). It is known that single crystals that do not contain alumina are highly distorted and strained (Kersen and Volger (1973)) and it is thought that Al_2O_3 performs a similar function in these pigments.

The properties of the pigment are very important in determining the type and durability of the points produced. Some pigments are coated to enhance their properties (Turner 1967, Darby and Leighton (1977)). Pigments are used in a wide variety of products for example, plastics, paper, rubber, leather, soap and printing inks as well as paints and the properties required for each vary and so a variety of pigment grades is produced (Tioxide International : BTP 182). It was hoped in this work to be able to determine some of the ways in which the pigments interact with light, a process which is important in the degradation of the resulting products.

CHAPTER 2

EXPERIMENTAL METHODS

2.1   ELECTRON PARAMAGNETIC RESONANCE

All the E.P.R. measurements were performed using a Varian V4502-15 X-band spectrometer fitted with an Oxford Instrument E.S.R.9 liquid helium cryostat which allowed measurements to be made in the temperature range 3.8 K ⟶ 300 K.

2.1.1 The Varian V4502-15 Spectrometer

A block diagram of the machine is given in Fig 2.1. The magnet is a V.3605 12" electromagnet controlled by a VFR 5203 field regulated power supply which uses a Hall effect probe to monitor the field in the magnet gap. This system is claimed to be capable of setting the desired field to 0.1 mT with a 1 part in 10^5 repeatability and a resolution of 0.002 mT.   In practice a proton magnetometer was used to measure the field.

The V-4500-41A bridge uses a Klystron to generate the microwaves, which are connected to the bridge which use a conventional hybrid-tee system to connect to the sample cavity and the detector crystal.   The AFC uses a 10 kHz oscillator which modulates the Klystron power supply and a 100 kHz signal is used to modulate the magnetic field through coils in the sides of the cavity. This 100 kHz modulation means that the recordings are of the differentiate of the absorption line. Care must be taken to stop the line shapes being distorted and broadened.   Fig 2.2 shows how this system works. The rest of the machine is fairly conventional and needs no explanation.

2.1.2 E.S.R. 9 Cryostat

The E.S.R. 9 is a continuous flow cryostat designed to be operated from 3.8 K up to 300 K. Liquid helium is sucked out of its flask through a flexible syphon into a stainless steel feed capillary which takes coolant

Modulation Unit

Reference

Radio Frequency Control Unit (P.S.D)

Oscilloscope

Sweep for 'scope x axis

A.F. Phase-detected Signal

Selector Panel

Signal

Recorder

Phase Sensitive Detected Signal

A.F.C. Signal

100 kHz Field Modulation Unit

Bridge Output

Microwave Bridge

Klystron Power Supply

Waveguide

X-Band Cavity

Hall Effect Field Sensor

Electromagnet

Magnet Power Supply & Linear Field Sweep Unit
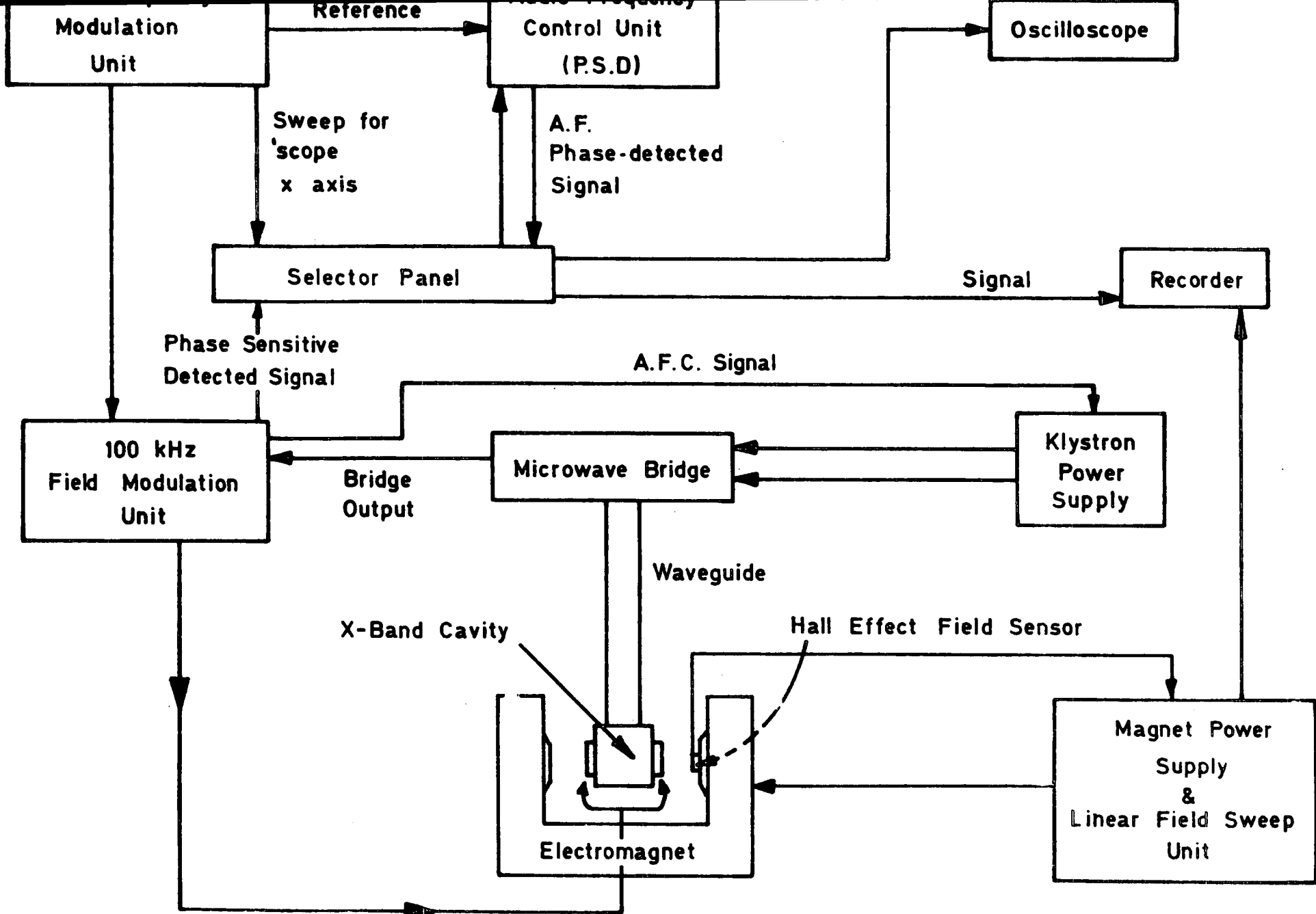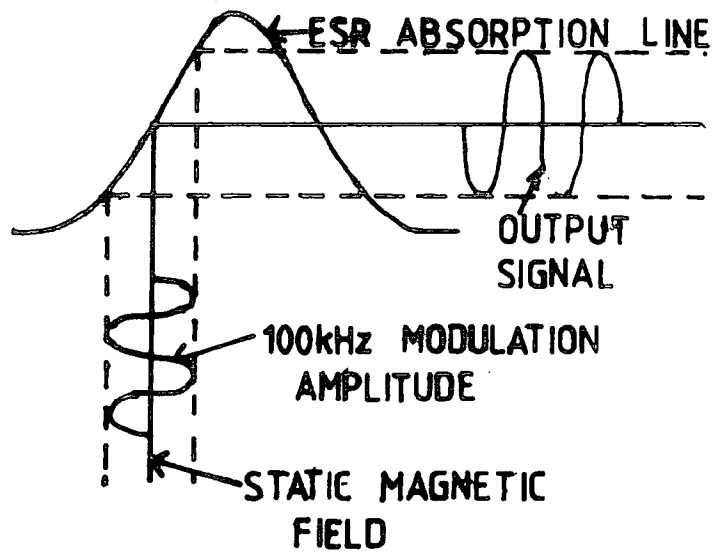
FIG. 2·1   BLOCK   DIAGRAM   OF   E.P.R.   SPECTROMETER

a) SIGNAL RESULTING FROM FIELD MODULATION
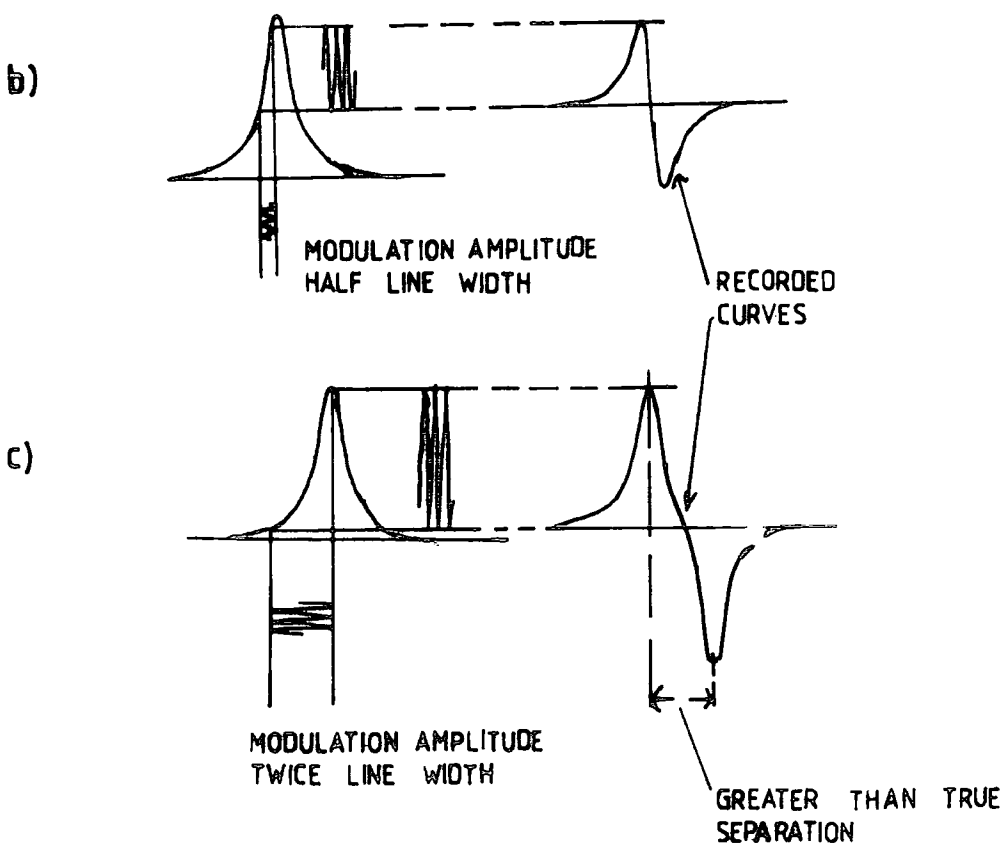
b)

c)

FIG 22   OPERATION OF FIELD MODULATION OF AN E.S.R.
          SPECTROMETER.

through the body of the cryostat to the bottom of the sample. It flows over a heater, thermocouple and then the sample (Fig 2.3). The gas is then sucked out of the cryostat and through an annular space around the feed. capillary to cool the syphon. The helium is pumped with a diaphragm pump to avoid contamination of the gas with pump oil. The temperature can be controlled by adjusting either the heater current or the flow rate. The temperature was controlled by an Oxford Instruments D.T.C2 temperature control which can maintain a constant temperature to within a tenth of a degree.

2.1.3 Irradiation Facilities

The end wall of the cavity was slotted so that it had a transmittance of 50% for optical radiation but did not degrade its microwave properties. The source of the light was a 250 watt Mg lamp focussed by a lens on the sample. Filters and a shutter could be placed in front of the cavity. A $CuSO_4$ filter was needed to block the IR radiation and a tungsten lamp could provide IR when needed.

2.1.4 Sample Holder

Single crystal samples could be held in place in a slotted 'spectrosil' quartz rod which was rotated about an axis at right angles to the magnetic field.

'Spectrosil' quartz was used because it has a very low amount of paramagnetic impurities and so does not contribute spurious signals.

Powders were held in 2 mm bore tubes, sealed at one end. About 0.05 grams were sufficient although up to twice as much could be used. The open end of the tube had to be connected to a vacuum system. This was because if there is any residual gas in the tube, it will condense and solidify and when the temperature rises again, the powder is smeared over the inside of the tube as the gas boils.

FIG. 2·3   CRYOSTAT AND IRRIADIATION FACILITIES

To vacuum pump.

Sample Tube

Waveguide to Bridge.

N_2 gas to remove H_2O.

Sample Space for filters & shutter.

250 Watt Mercury Lamp

Iris

Thermocouple

Heater

Cavity

Lens

To vacuum system.

Liquid Helium Inlet.

Gaseous Helium Outlet to Suction Pump.
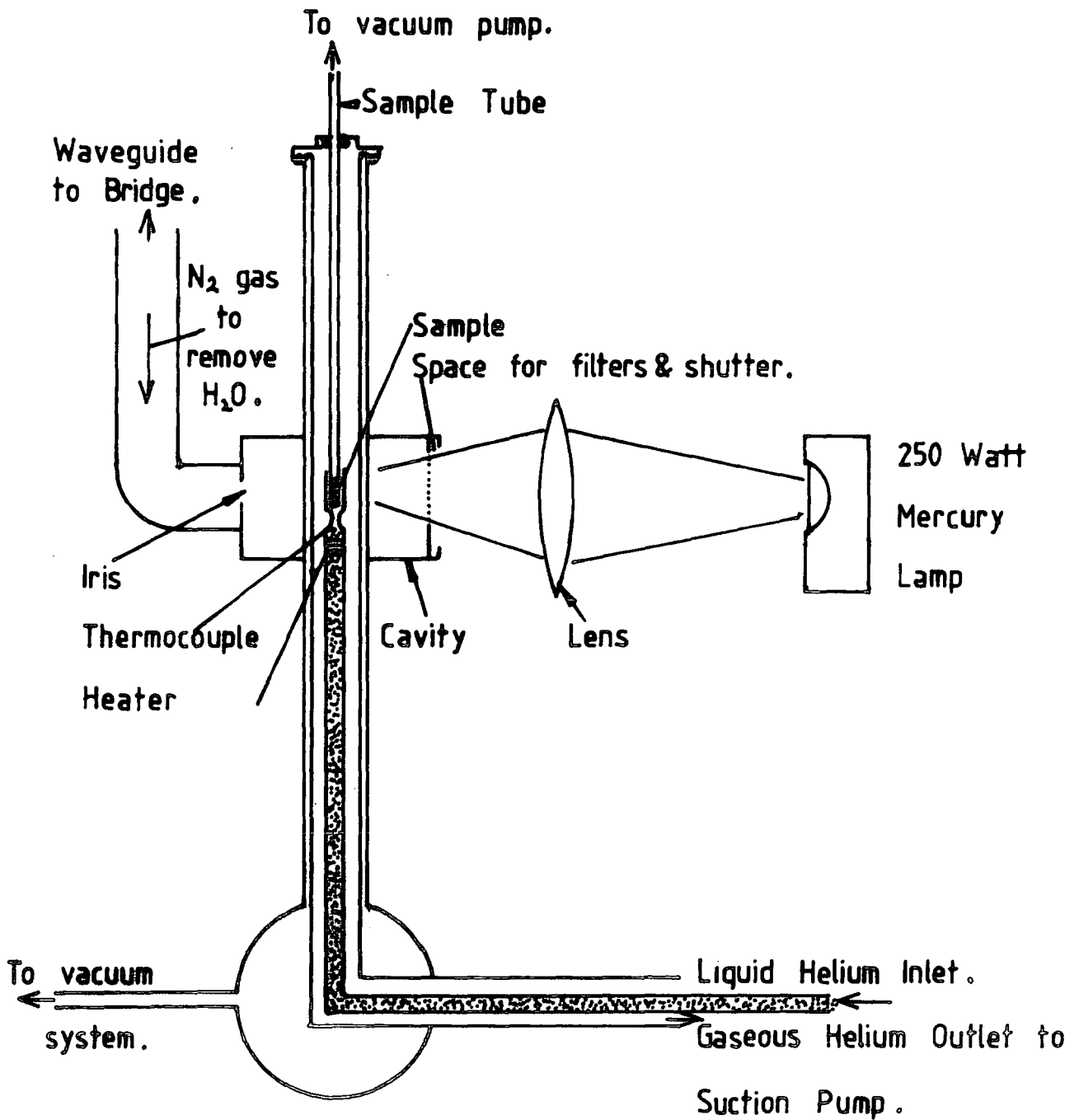
2.2 SAMPLE PREPARATION

The pigment samples used were produced by the chloride process by Tioxide International Ltd and supplied by their Central Laboratories in Stockton on Tees, Cleveland, England. Several samples were provided which had differing amounts of Al_2O_3 added during manufacture to promote the formation of rutile as opposed to anatase. The samples were at least 99.9% rutile.

They were then doped with iron or chromium. First a solution of Fe Cl_3 or Cr Cl_3 was mixed with the pigments. 100 ml of solution was added to 20 grams of TiO_2 powder, the density of the solution being chosen to arrive at the required Fe or Cr dopant concentration. The mixture was then dried and then heated to $600^{\circ}C$ for 12 hours. The doped pigments were analysed by X-ray fluorescence and mass spectroscopy. If the powders were immersed in HF to etch the outermost layers and then reanalyzed, a different dopant concentration was found. The amount of etch is expressed in terms of weight loss. Typically the results of this are shown in Table 2.1.

TABLE 2.1 :   XII Powder Analysis

Desired Dopant Concentration	Analysis Fe	
	As doped	5% Etch
10	30	10
50	60	30
100	100	50
150	110	60
250	170	100
500	290	150
1000	670	500

Full analysis of all the samples used are given in Appendix 1.

One sample (KENT) was prepared by taking a heavily doped single crystal ($\sim$ 1% Fe) and grinding it to a fine powder. The single crystal
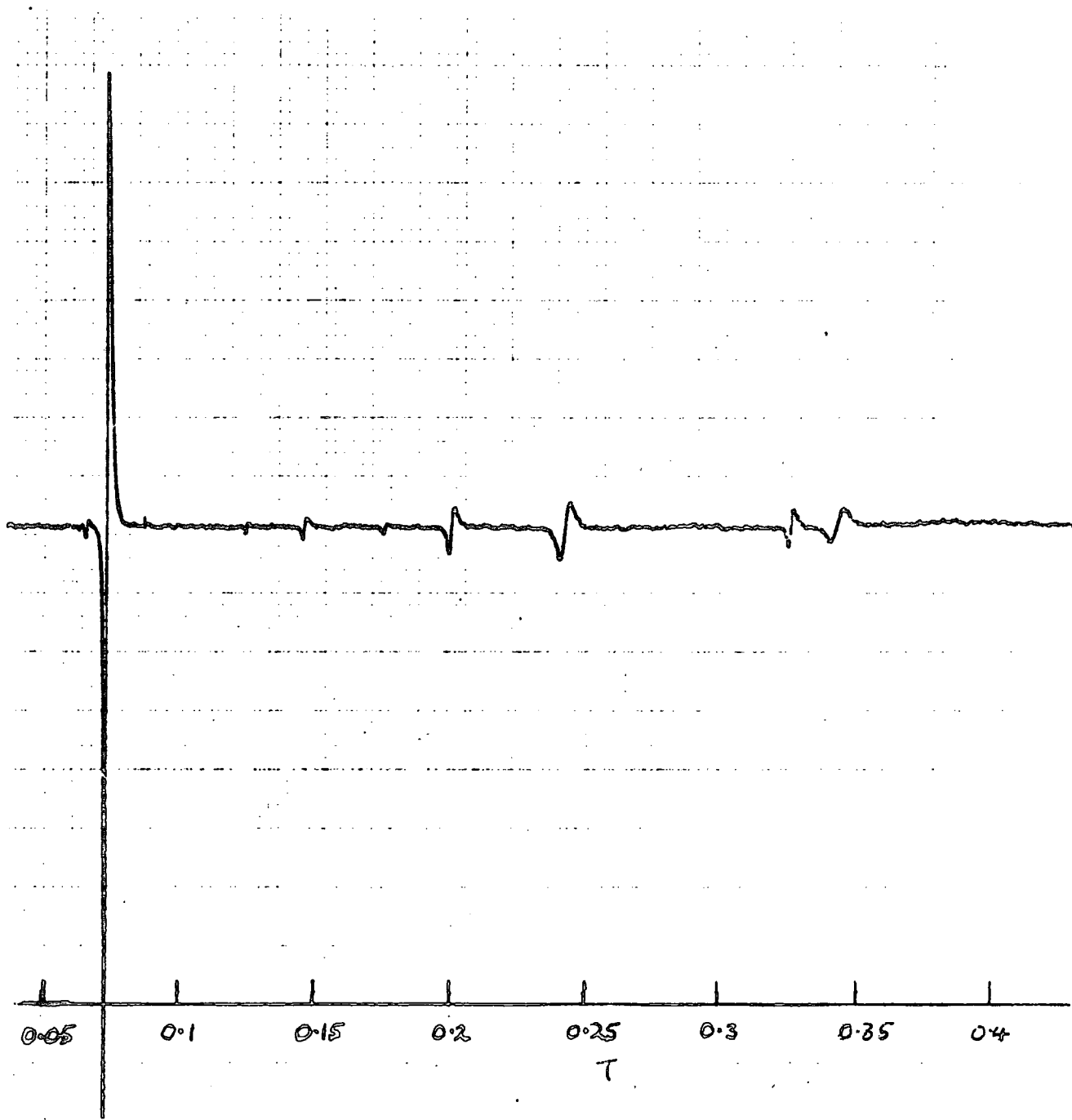
FIG. 2.4 : Spectrum of single crystal Fe/TiO$_2$;

H//c, 9.096 GHz.   1.5% Fe

FIG. 2.5: ISOFREQUENCY DIAGRAM OF IRON SPECTRA OBSERVED IN IRON DOPED RUTILE
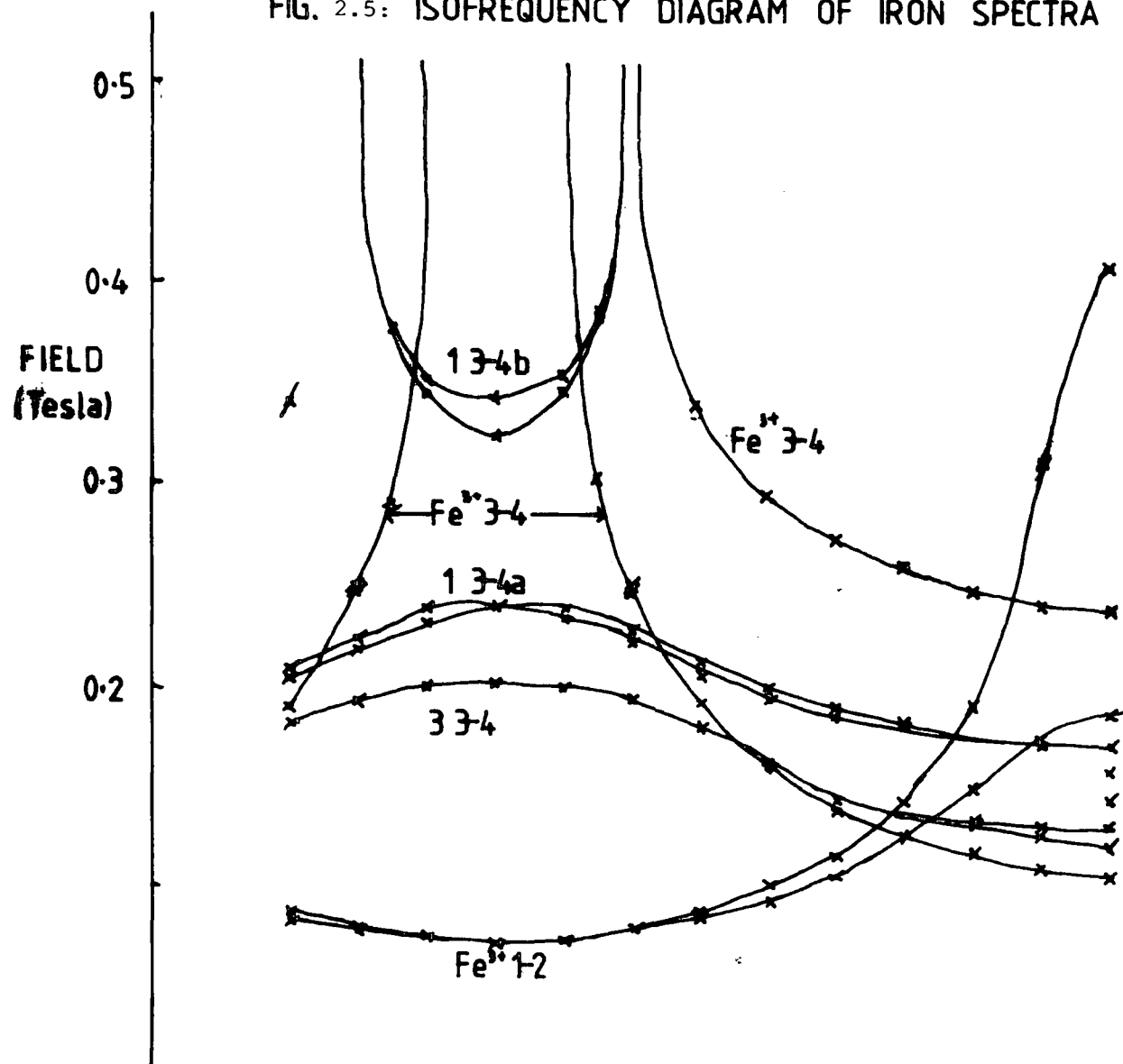
had a red colour which is characteristic of iron precipitates on lattice defects (Anderson et al (1974)).   An EPR study of the single crystal Fig 2.4, showed other spectra.

Plotting an isofrequency plot of these spectra, Fig 2.5, enabled them to be associated with some of the iron complexes identified by Anderson and Kolberg (1973).

X-Ray Powder photographs of the samples showed that all the powders were rutile and no lines of other stfuctures were observed.   Some samples were examined using X-ray diffractometer and infra-red absorbtion techniques.   The results are discussed later in Chapter 5.

CHAPTER 3

E.P.R. POWDER SPECTRA

3.1   INTRODUCTION

A method of deriving powder lineshapes, suitable for use in rutile, has been described in a M.Sc.Thesis (Eggleston (1980)) and in a subsequent paper, Eggleston and Thorp (1981); in Eggleston (1980),the technique was applied only to Fe^{3+} substitutional ions. Briefly, the method relies on the fact that in rutile the ground state of the Fe^{3+} ion, which has spin 5/2, is split into three Kramers doublets. These are, at X-band, spaced far enough apart for there to be no transitions between doublets. The resultant energy levels are given in Fig 3.1.   The transition in the highest doublet is very weak and is not observed. The two remaining transitions are treated separately as two S = 1/2 transitions with a very anisotropic g factor. This gives two separate transitions each with a Spin Hamiltonian of the form :-

$$\mathcal{H} \quad = \quad g_i \ \beta \ H \tag{3.1}$$

To derive a powder spectra, a resonance condition of the form,

$$h\nu \quad = \quad f(H) \tag{3.2}$$

is required.

A powder will contain crystallites orientated at random, so to simulate a powder we must examine the absorbtion for each orientation with respect to the magnetic field and sum all these contributions to the final absorbtion spectra. If S(H) is a shape function which represents the normalized
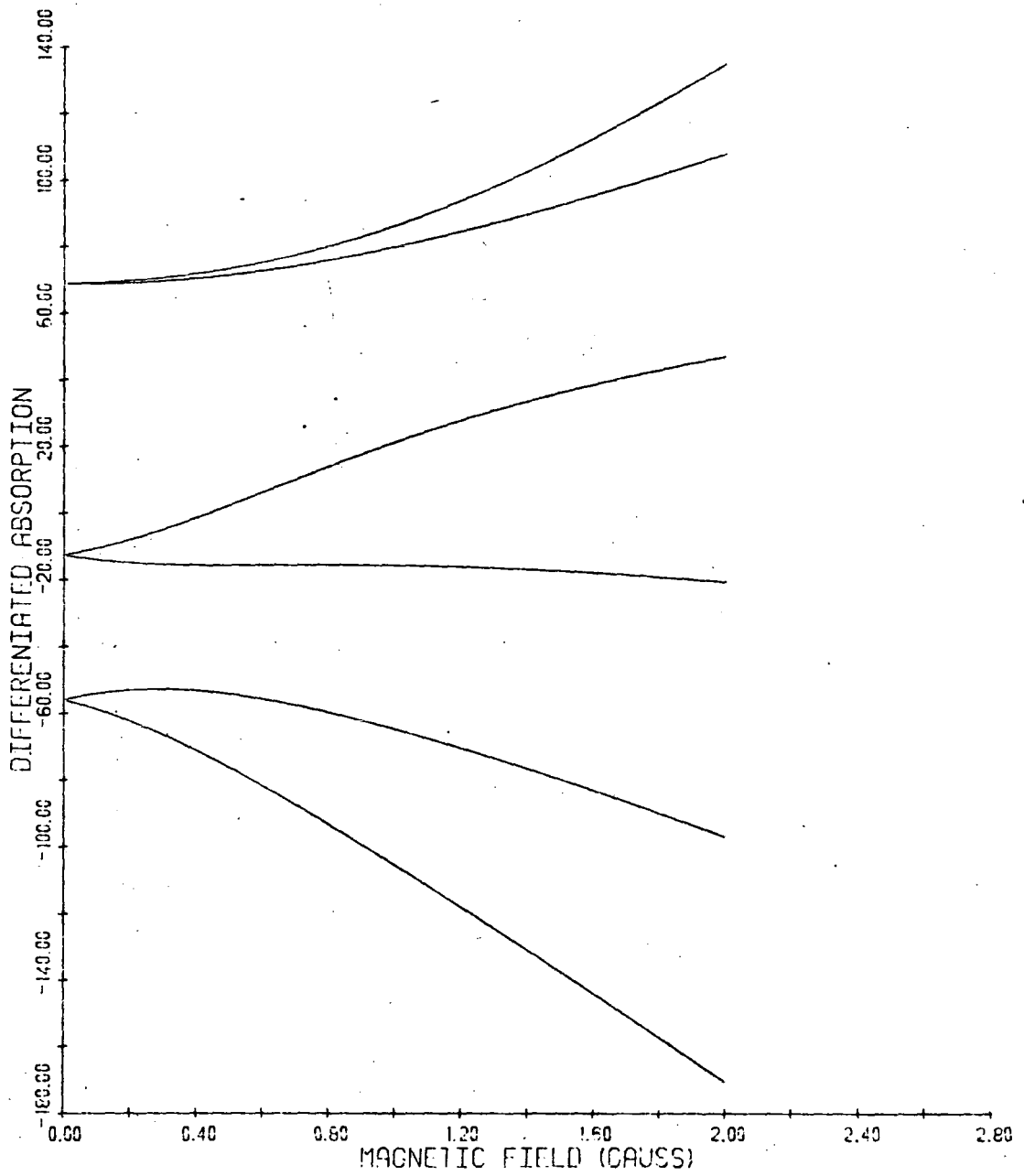
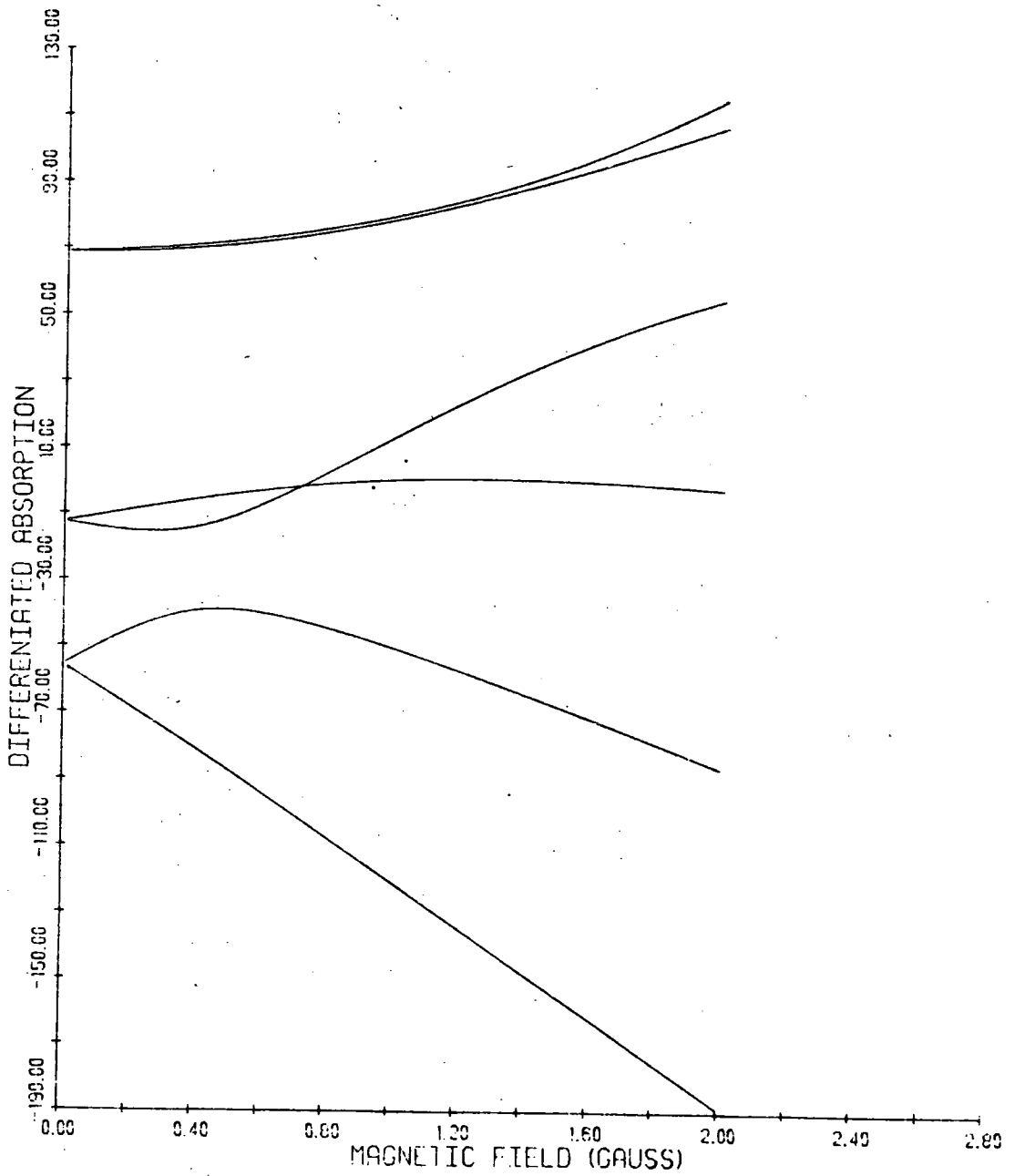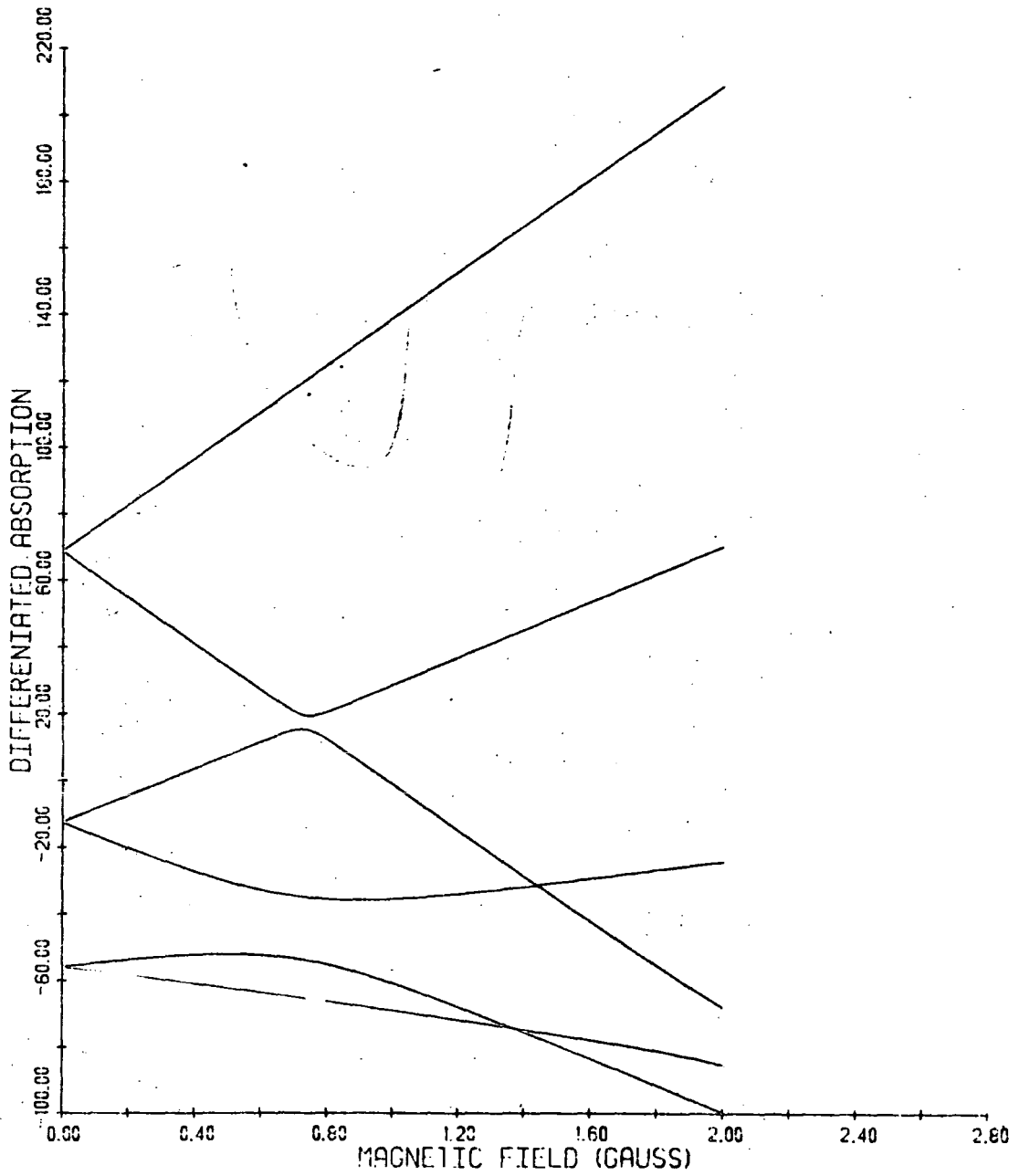Fig 3.1a :   ENERGY LEVELS   H ‖ X

Fig 3.1b : ENERGY LEVELS   H ‖ Y

Fig 3.1c :   ENERGY LEVELS   H∥Z

amplitude of the resonance signal at field H :-

$$S(H) \quad dH \quad = \quad \frac{1}{4\pi} \sum_{m} \int_{H}^{H + dH} \ell_m (\Omega) \quad d\Omega (H_m) \qquad (3.3)$$

Where the equation is integrated over all elements of solid angle, Ω, such that $H < H_m < H + dH$ where H_m satisfies the resonance condition (equation 3.2). $\ell_m (\Omega)$ is the transition probability for the mth component of the spectrum as it is not dependent on Ω ; in this case can be taken out of the integral. The subscript refers to the two separate transitions. S(H) can be calculated numerically and then convoluted with an appropriate single crystal, line broadening function (usually Lorentzian or Gaussian) to be compared with experimental results. (Methods of deriving powder spectra have been described by many authors and some useful papers and review articles are Taylor et al (1973), Pilbrow (1978), Van Vreen (1978) and Aasa and Vanngard (1975).

This results in Fig 3.2(c). Comparison with t./o experimental spectra (Figs 3.2a and b) allow the Fe^{3+} lines to be identified. This has now been extended to Cr^{3+} ions and the results are shown in Fig 3.3.

The features all occur at the same fields as the single crystal resonances when the magnetic field is along one of the principle axes. By calculating these positions we can find where these features should occur but not their shape. However, even the shape can be predicted. For example, if for a transition the principle resonant fields are .1, .2 and .3 tesla, and if the single-crystal linewidth is small compared with the differences between these, which it is, ($\sigma \simeq$ .002 T) then the shapes when differential will be, .1 tesla;a positive spike, .2 tesla;a broad "line" and .3 tesla a negative spike. These shapes can be seen in Fig 3.2c. The exact shape is considered in depth in Chapter 4. For the moment we are
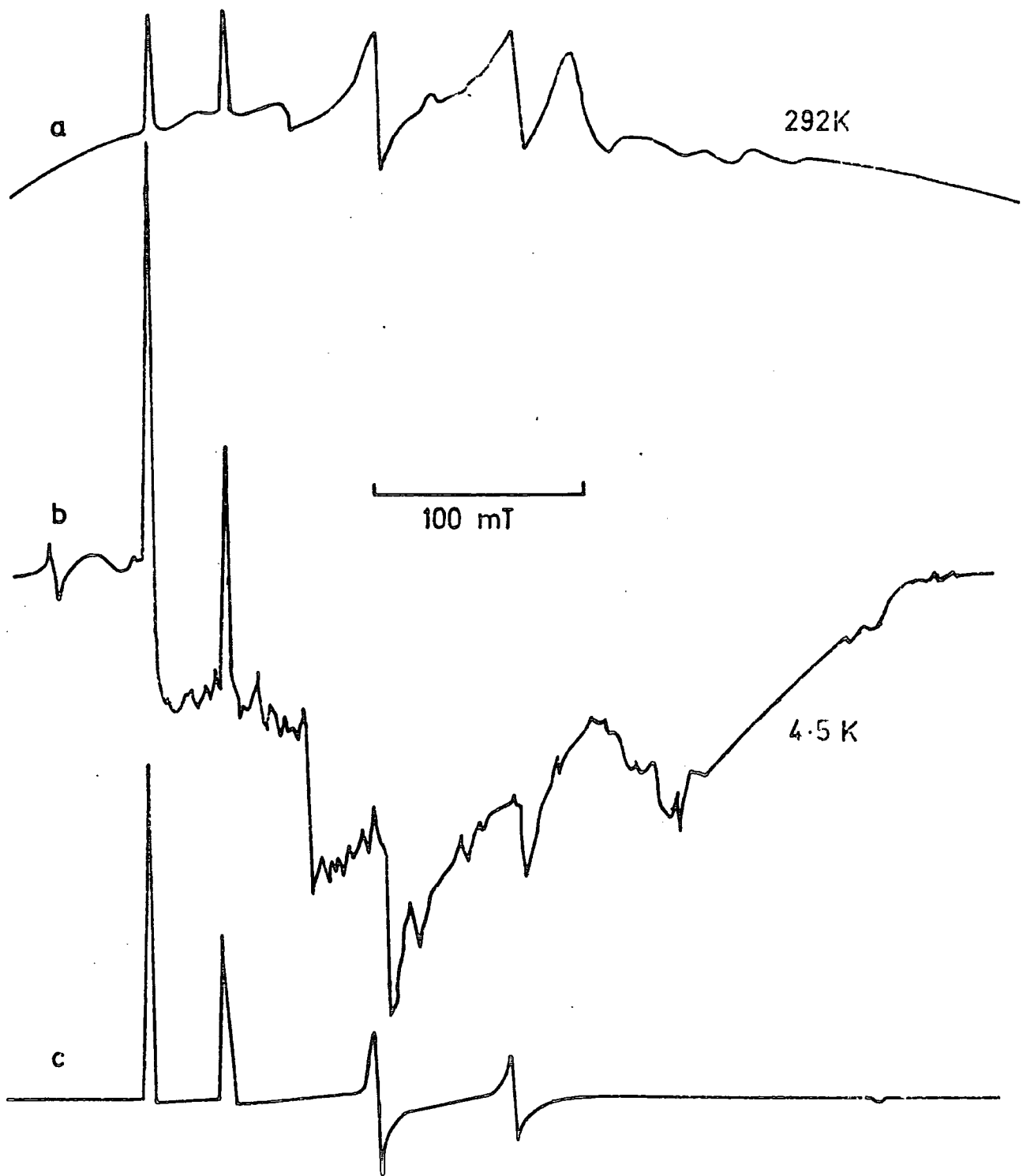
FIG.3·2 POWDER SPECTRA OF IRON DOPED RUTILE;(a) AND (b) EXPERIMENTAL SPECTRA AT 292 K AND 4·5K RESPECTIVLY; (c) COMPUTED SPECTRUM (9·1 GHz)
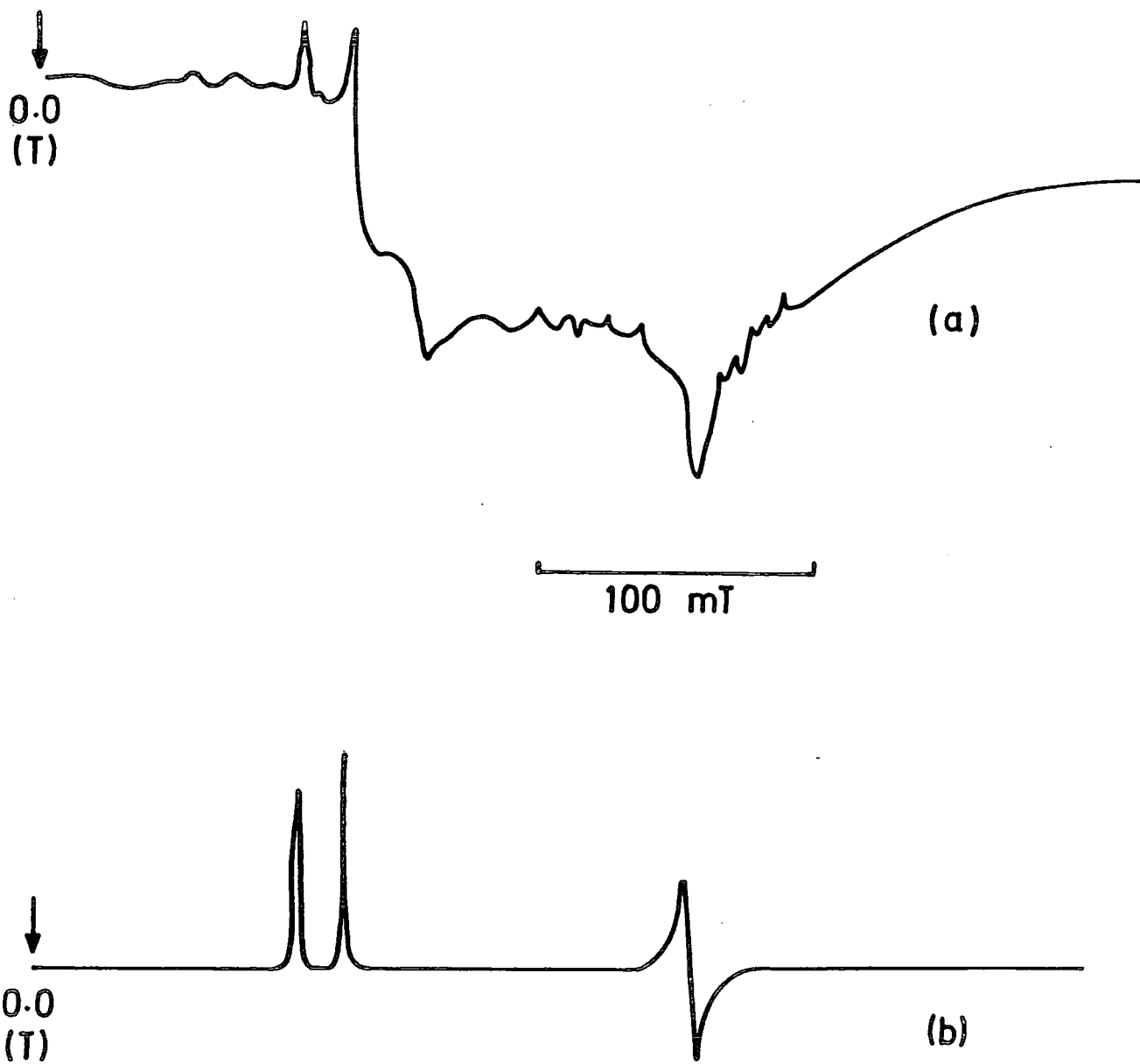
0.0
(T)

(a)

100 mT

0.0
(T)

(b)

FIG.33 POWDER SPECTRA OF CHROMIUM DOPED RUTILE;
(a) EXPERIMENTAL SPECTRUM, 4·2k; (b) COMPUTED
SPECTRUM; (9·102 GHz)

only interested in identification and so this very simple scheme will suffice.

3.2   IRON DOPED RUTILE PIGMENTS

Figs 3.4 - 3.6 show four powders with a range of iron dopant as shown in Table 3.1.

TABLE 3.1 : Date for iron doped pigments.

Figure	Fe concentration ppm		Signal height (arbitary units)		
	as doped	stripped 5%	Fe^{3+} (A)	g = 4.2 (C)	g $\simeq$ 2 (D)
3.3	35	15	O	1.5	6
3.4	70	20	1	4.5	6
3.5	135	125	7	9.5	5
3.6	405	195	9.5	14.5	5.5

Figure 3.7 plots the concentration of each signal as a function of iron concentration. The signal amplitude is proproti nal to the concentration of the ion or site causing that absorbtion if the linewidth is constant.

"Stripped" refers to an analysis performed after the powders where etched in HF so that they lost 5% of their weight. The Fe^{3+} and the g = 4.2 amplitudes are related to the amount of iron present but not the g $\simeq$ 2 signal. Several signals could be seen (Fig 3.8) when the samples were examined in the dark before irradiation. The ch nges and the signals seen on irradiation with optical and U.V.light are discussed later. Features A, B and E correspond to Fe^{3+} in a substitutional site and have already been discussed. As expected, their amplitude (which is proportional to the number of sites) is proportional to the iron concentration.

This is also true of signal C, which has tentatively been identified as Fe^{3+} in another site. This is discussed in the next section.

FIG. 3·4   E.P.R. SPECTRA OF IRON DOPED RUTILE PIGMENTS AT 4·2 K

35 ppm Fe

70 ppm Fe

0·5 T

G

D

Signals

0·0 T
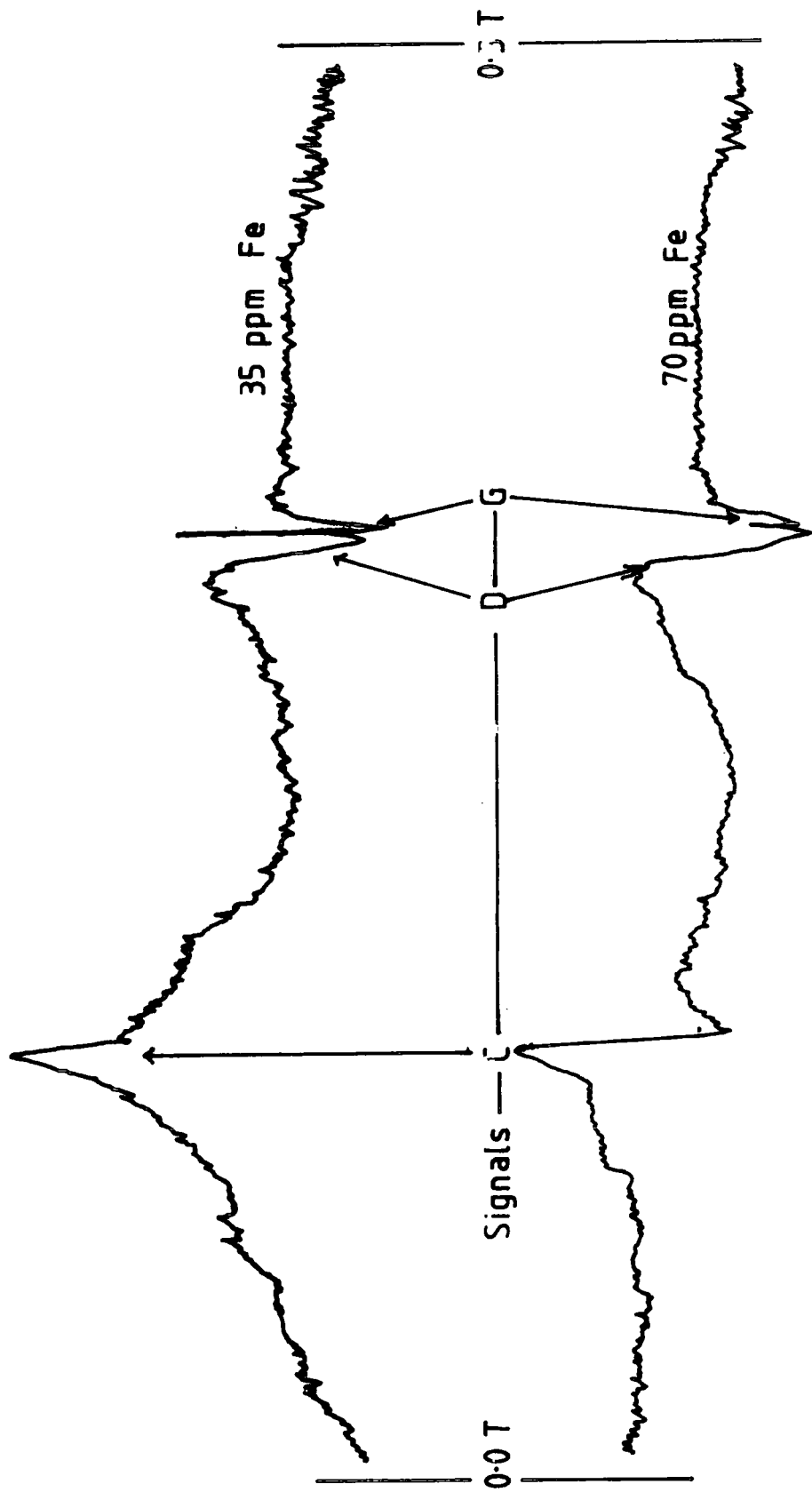
FIG.35.   E.P.R. SPECTRA OF AN IRON DOPED RUTILE PIGMENT AT 4·2 K

135ppm Fe

0·0 T   Signals——A——B——C————D-G   0·5 T
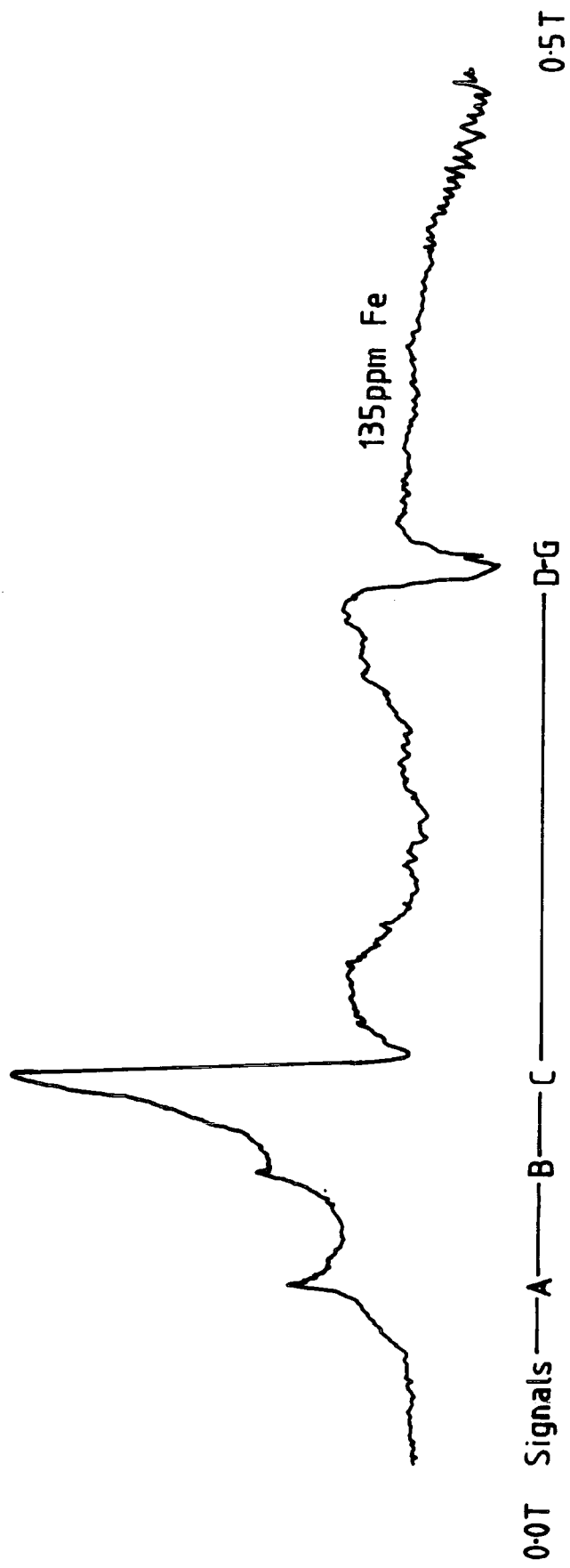
FIG. 3.6   E.P.R. SPECTRA OF AN IRON DOPED RUTILE

PIGMENT AN 4.2 K.
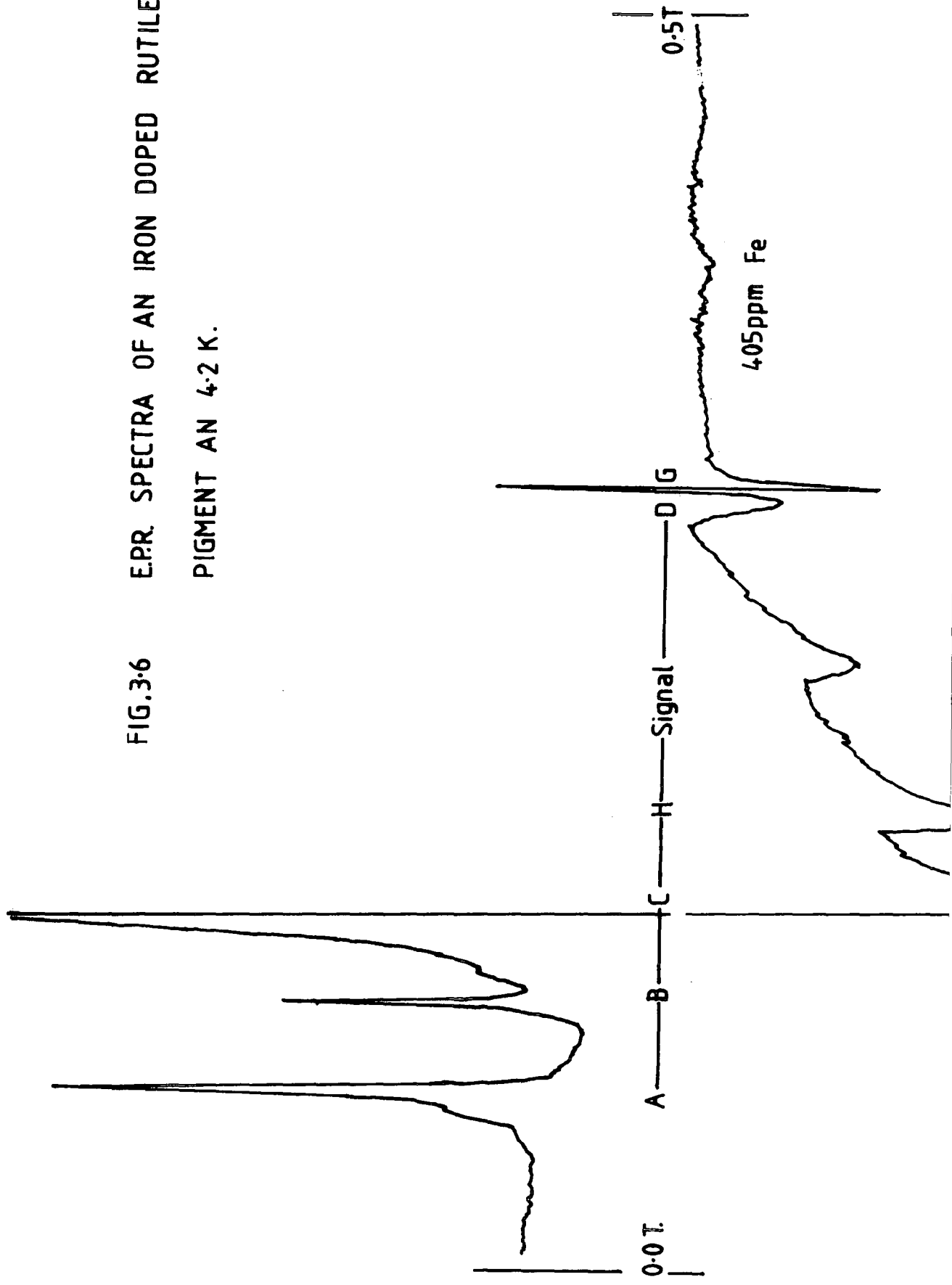
FIG. 3·7   AMPLITUDES OF SIGNALS FROM RUTILE PIGMENTS

X g=4·2

□ g=2

⊙ Substitutional Fe^{3+}

AMPLITUDE
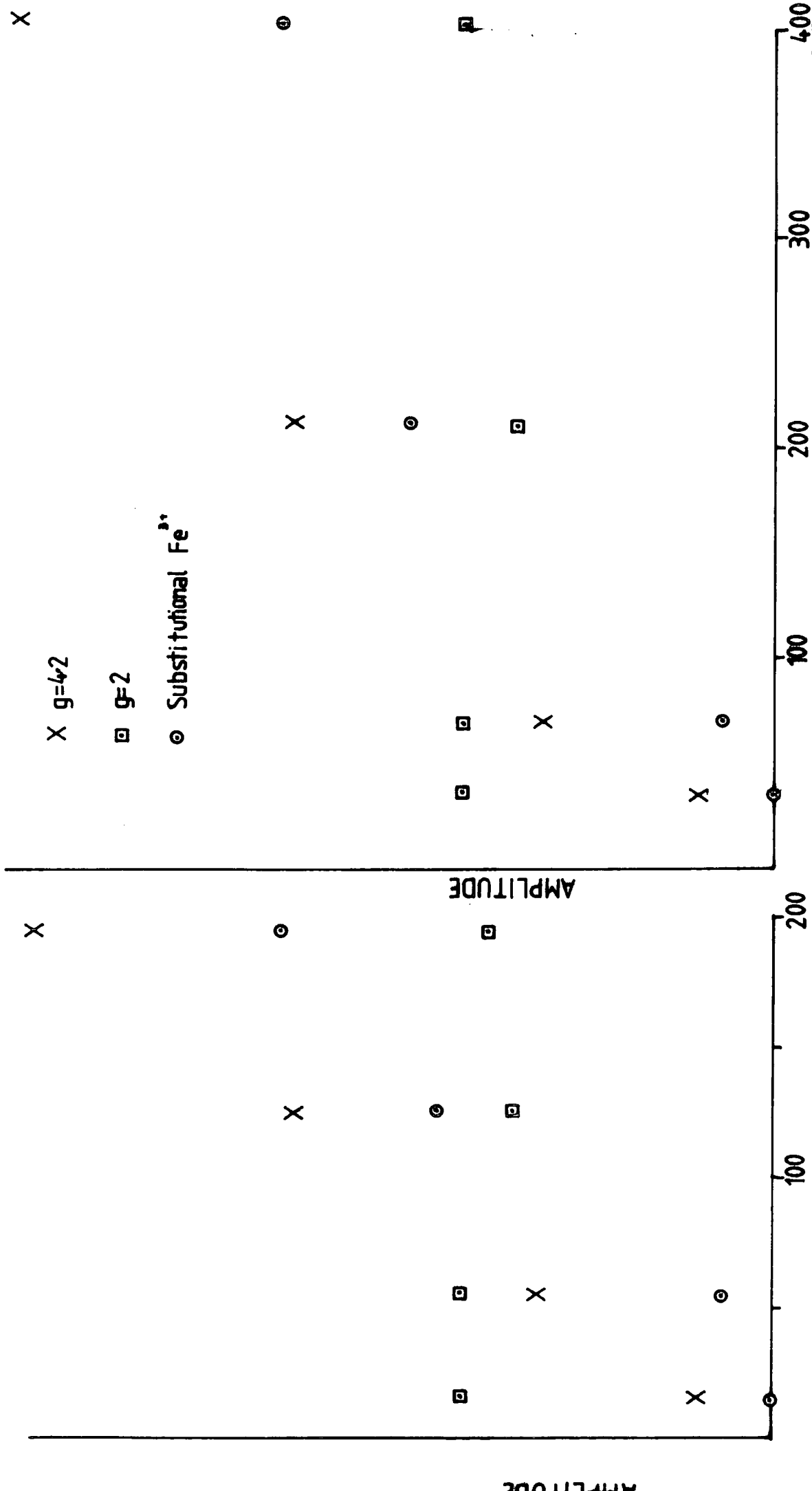
FIG.3·8   E.P.R. SPECTRA OF PIGMENT X11/1000
AT 4·2 K $\nu = 9·110\,GHz$

A,B,E & H are due to substitutional Fe^{2+} and C to Fe^{3+} in a site with rhombic symmety
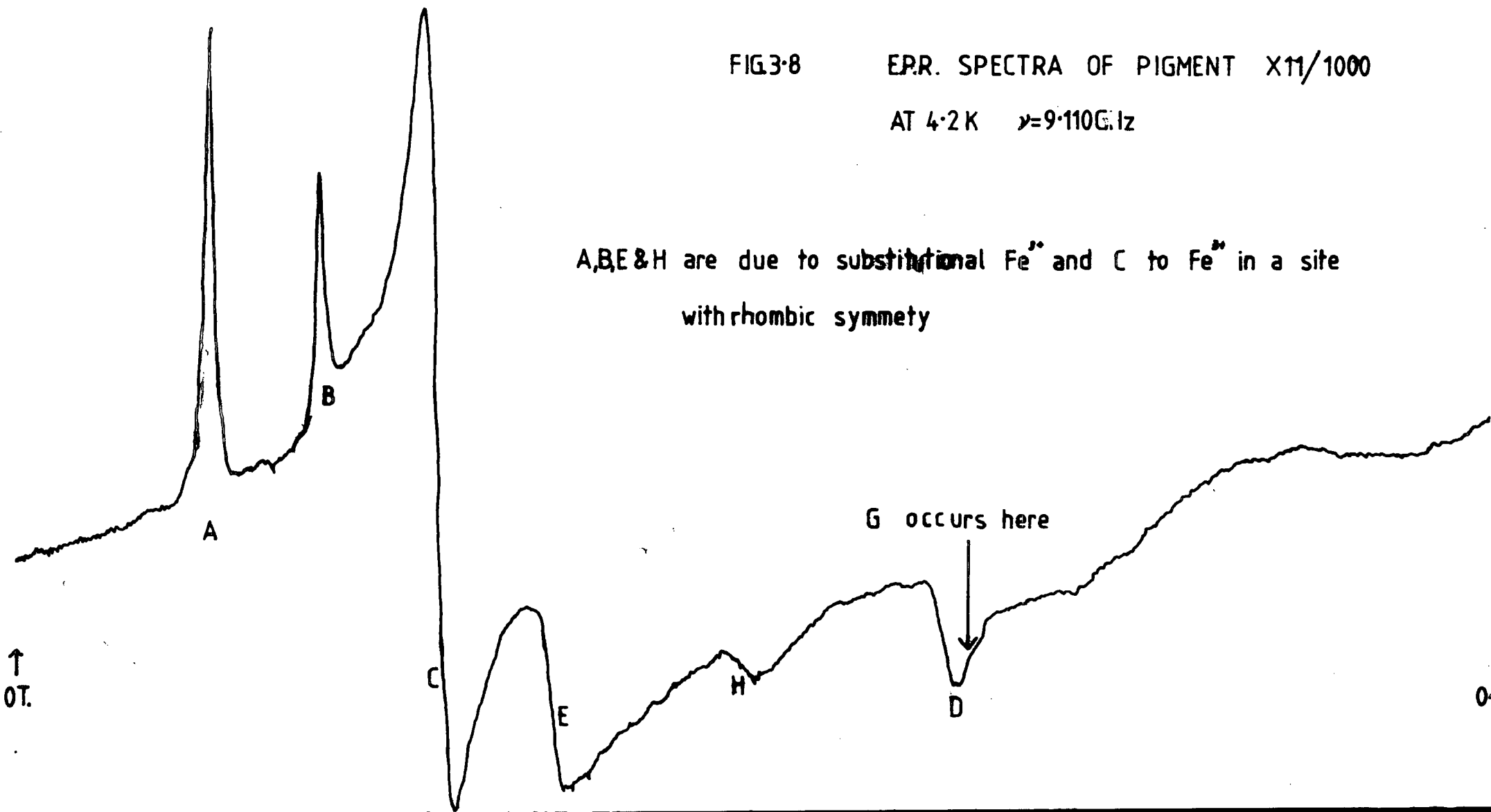
Signal D is not related to iron concentration. As indicated in Table 1.4, there are many different paramagnetic defects which would give rise to spectra in the region $g \simeq 2$. It would be impossible to distinguish between all of them and to say which contribute to this feature. However, this signal does appear to be due to defects, impurities and clusters in the rutile lattice and gives an indication of the purity of the sample. G was very small but its amplitude increased with irradiation to make it the largest signal.

3.3 IDENTIFICATION OF THE g = 4.3 SIGNAL (SPECTRA C) (Fig 3.9a)

In section 3.1 we noted that significant features in the powder spectra occur at the same fields as the single crystal resonances with the magnetic field aligned along the principle magnetic axis of the ion.

We can use this fact to identify powder signals if the single crystal E.P.R. data is known. In the previous section, we saw that the $g = 4.3$ signal was proportional to the iron concentration. Could it be due to iron in some other site than the normal substitutional site ? The iron sites in rutile reported by Anderson and Kollberg (1972) are as given in Table 3.2 below :-

	Spin Hamiltonian Parameters
Fe^{3+} (substitutional for Ti^{4+})	D = 20.35, a = 1.10, F = -0.50, E = 2.21 g = 2.000
Fe^{3+} ion with nearly interstitial proton.	g_x = 1.993, g_y = 2.04 , g_z = 1.998 D = 13.1, E = 2.3, F = 1.9, a = -0.7
Fe^{3+} ion with nearest neighbour O^{2-} vacancy	g_x = 2.001, g_y = 1.993, g_z = 2.001 D = 22.9, E = 2.7, F = -6.3, a = -0.1

TABLE 3.2 : Iron Sites in Rutile

FIG.3.9α SIGNAL C.   E.P.R. Spectra of X11/1000 at

4.2 K.   ν = 9·110 GHz.

175
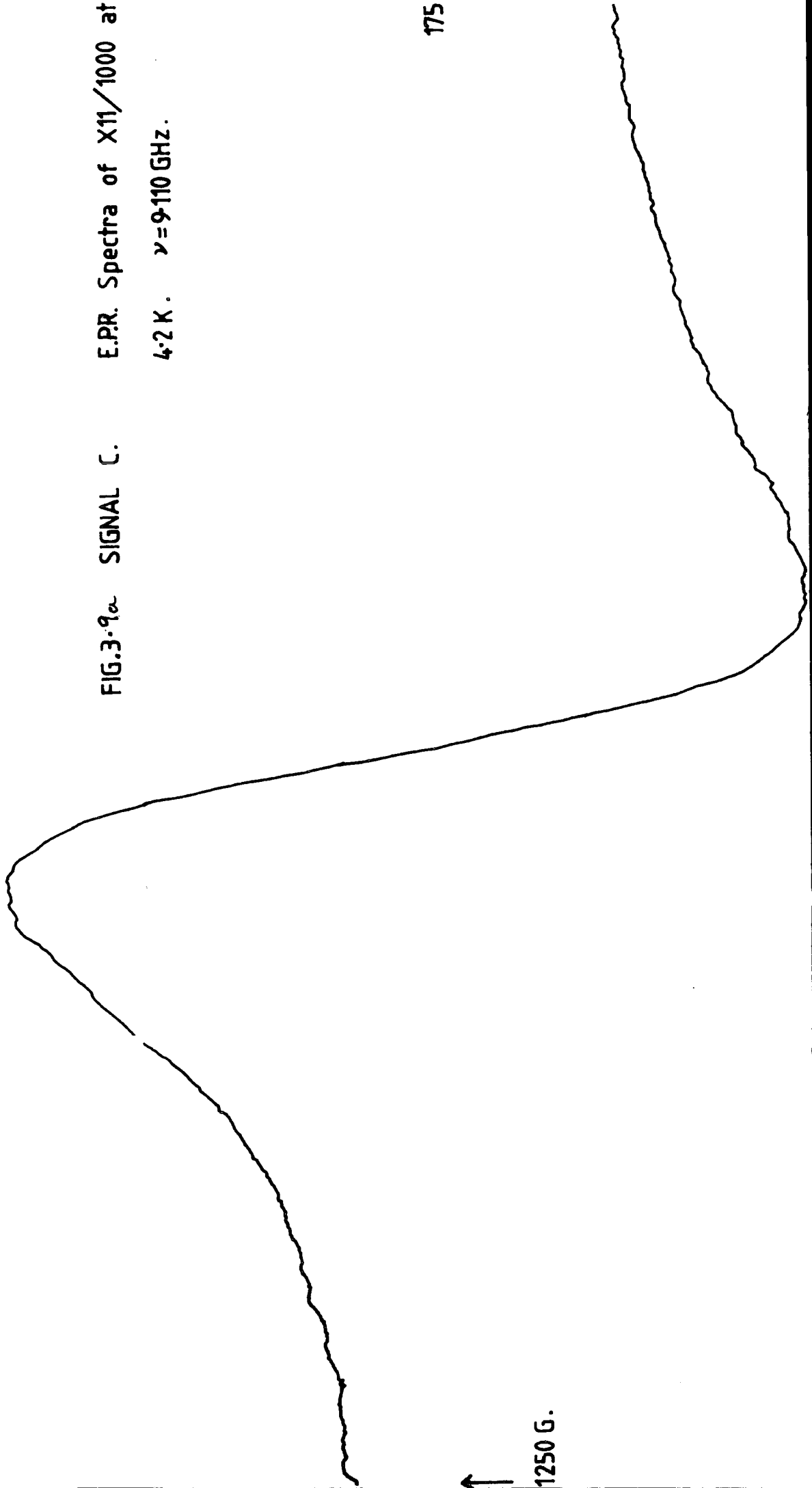
← 1250 G.

A computer program was written in Fortran using subroutines supplied by NAG (Numerised Algorithms Group) to solve the Spin Hamiltonian $\not{\mu}_{i\tau}$. Fe^{3+} ions. The values of g and of D, E, f and a are read into the program and the program gives the values of resonant field for transitions within the doublets (i.e. 1 ↔ 2, 3 ↔ 4 and 5 ↔ 6), for the magnetic field along the x,y and z axis(Fig 10a,b,c). The program also checks whether transitions between the doublets are allowed (i.e. 2 ↔ 3, 4 ↔ 5). The results are shown in Table 3.3 for the Fe^{3+} spectra. No known 'g' values give values for the observed values.

It is well known that iron ions in a rhombic symmetry exhibit, for the 3 ↔ 4 transitions, a nearly isotropic absorption line. This was first pointed out by Castner et al (1960) to explain spectra observed in glasses and has since been observed for other rhombic sites, (Blumberg (1967)).

This isotropic spectrum arises when E/D ≃ 1/3. This represents rhombic symmetry. Fig 3.9b shows the principle values of resonant field for a D = 20 GHz and E varying from 0 to E = D/3. As E approaches D/3 all the transitions 3 ↔ 4 , tend to be the same value with g ≃ 4.28. In the iron pigment we see a wide absorption peak centred at g = 4.3 and this could result from a nearly rhombic site with E = D/3. This would have the effect of broadening the powder spectra. A simulation is shown in Fig 3.11 . The values in the Spin Hamiltonian were chosen as g = 2, isotropic (reasonable for a Fe^{3+} ion) and D = 20 GHz (to coincide with the rutile value) and E = 6 GHz. All other terms are zero. The effect of a and F having non-zero values would be to make the 3 ↔ 4 transition slightly non-isotropic. This would also result in a broadening of the line.

Site		Principle values (Gauss)		
		x	y	z
Fe^{3+}	$1 \leftrightarrow 2$	1998	802	4.27
	$3 \leftrightarrow 4$	2663	> 5000	1175
	$5 \leftrightarrow 6$	75000	> 5000	942

TABLE 3.3 : Principle values of Fe^{3+} : TiO_2

Fig 3.9b : POWDER FEATURES AS A FUNCTION OF E

Axis labels: RESONANT FIELD (TESLA) vs E (GHZ)

Curve labels: $(1\leftrightarrow2)_z$, $(3\leftrightarrow4)_x$, $(1\leftrightarrow2)_x$, $(3\leftrightarrow4)_y$, $(3\leftrightarrow4)_z$, $(5\leftrightarrow6)_z$, $(1\leftrightarrow2)_y$

Fig 3.10a :   ENERGY LEVELS   *H ‖ X*

(y-axis) DIFFERENTIATED ABSORPTION

(x-axis) MAGNETIC FIELD (GAUSS)
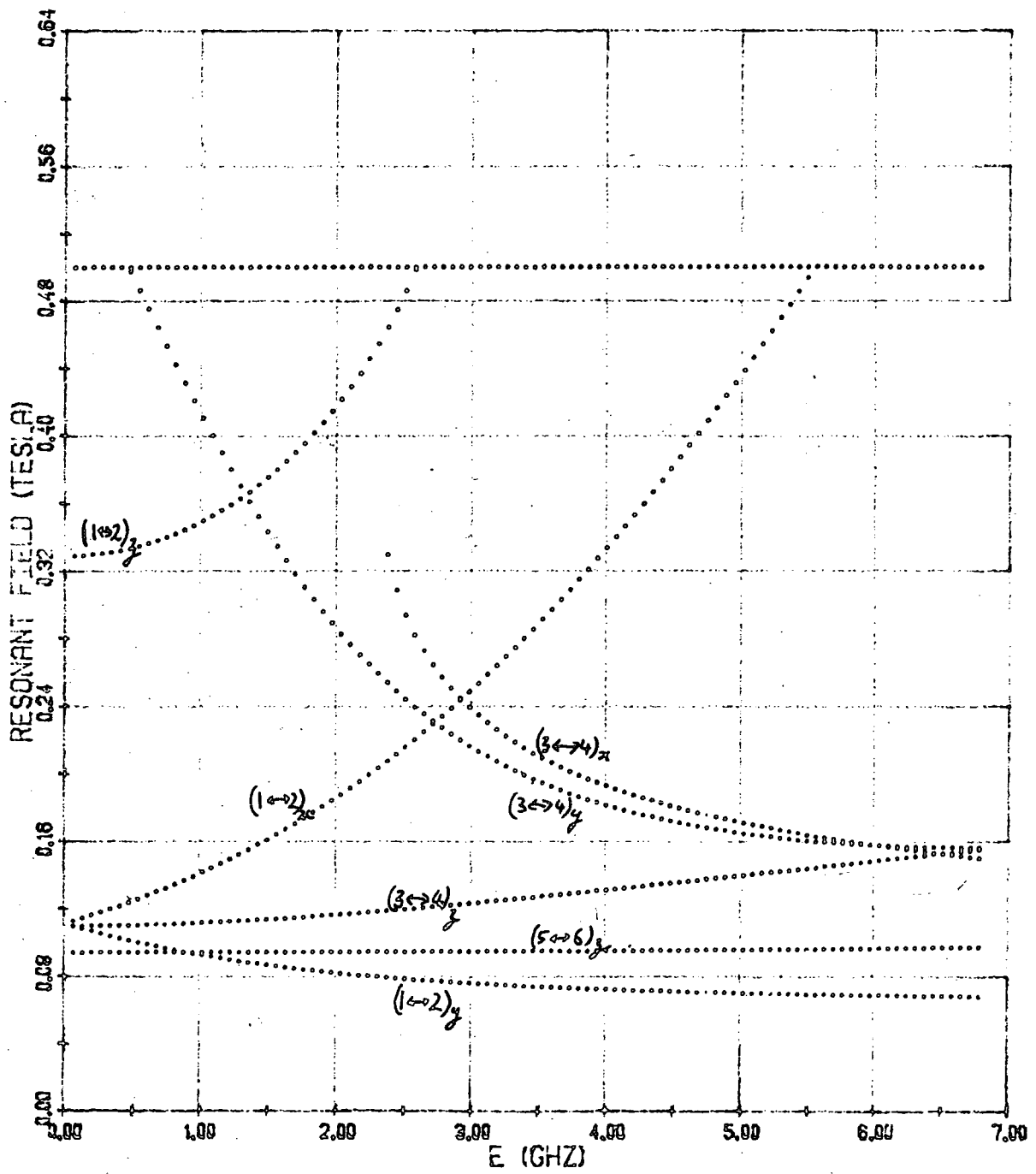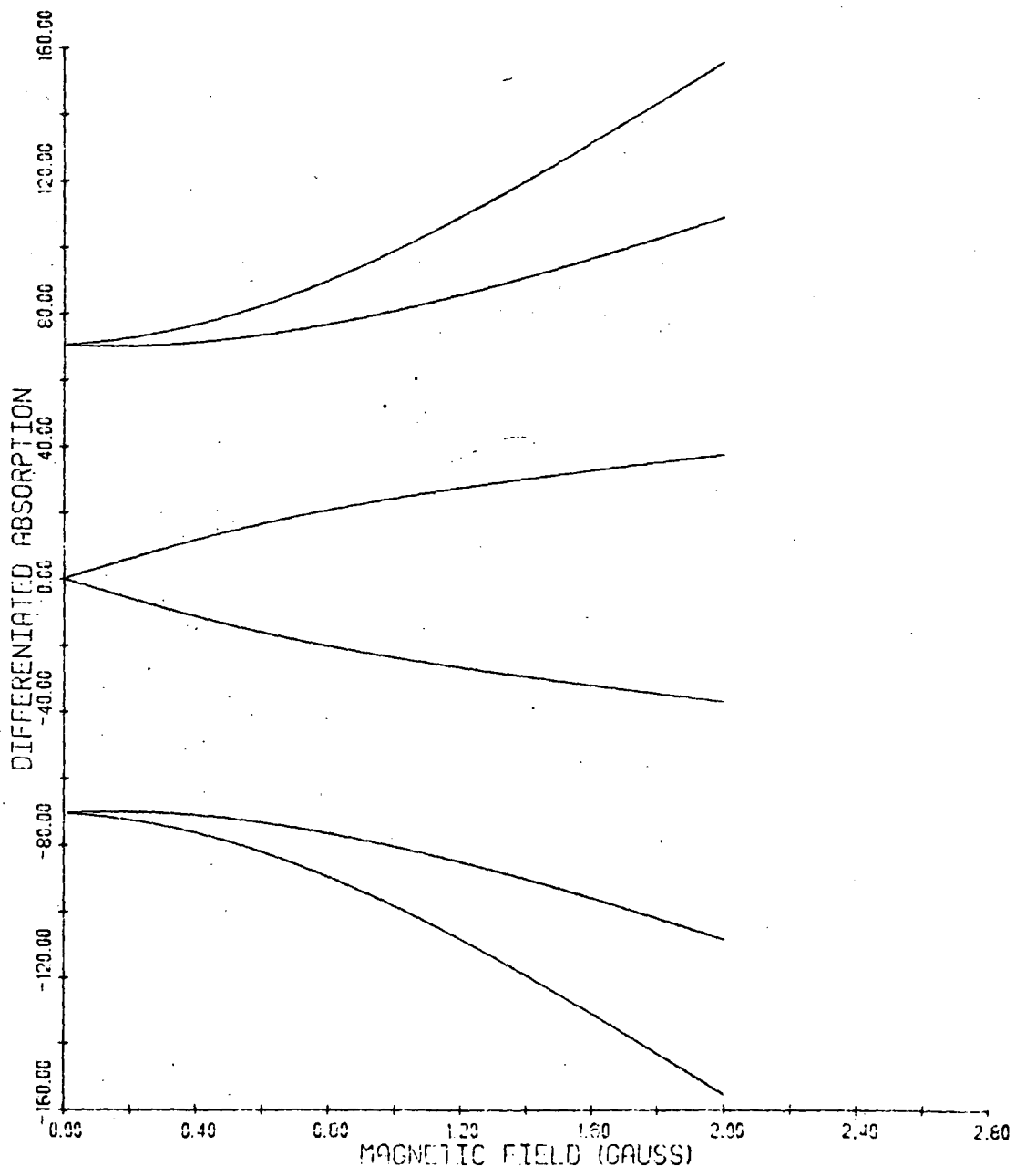
Fig 3.10b : ENERGY LEVELS $H \parallel Y$

DIFFERENTIATED ABSORPTION

MAGNETIC FIELD (GAUSS)

Fig 3.10c :   ENERGY LEVELS   MHZ.

DIFFERENIATED ABSORPTION

MAGNETIC FIELD (GAUSS)
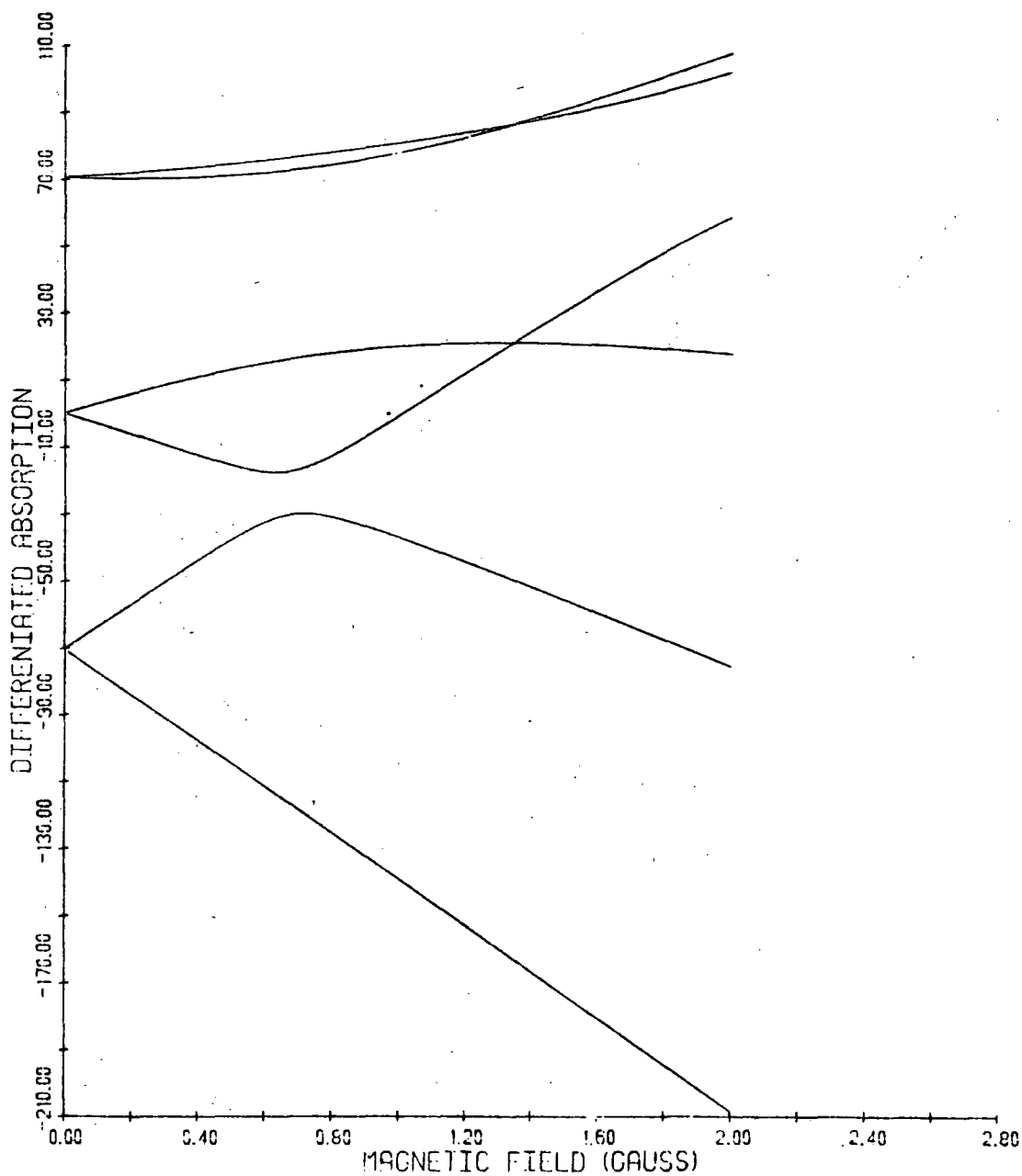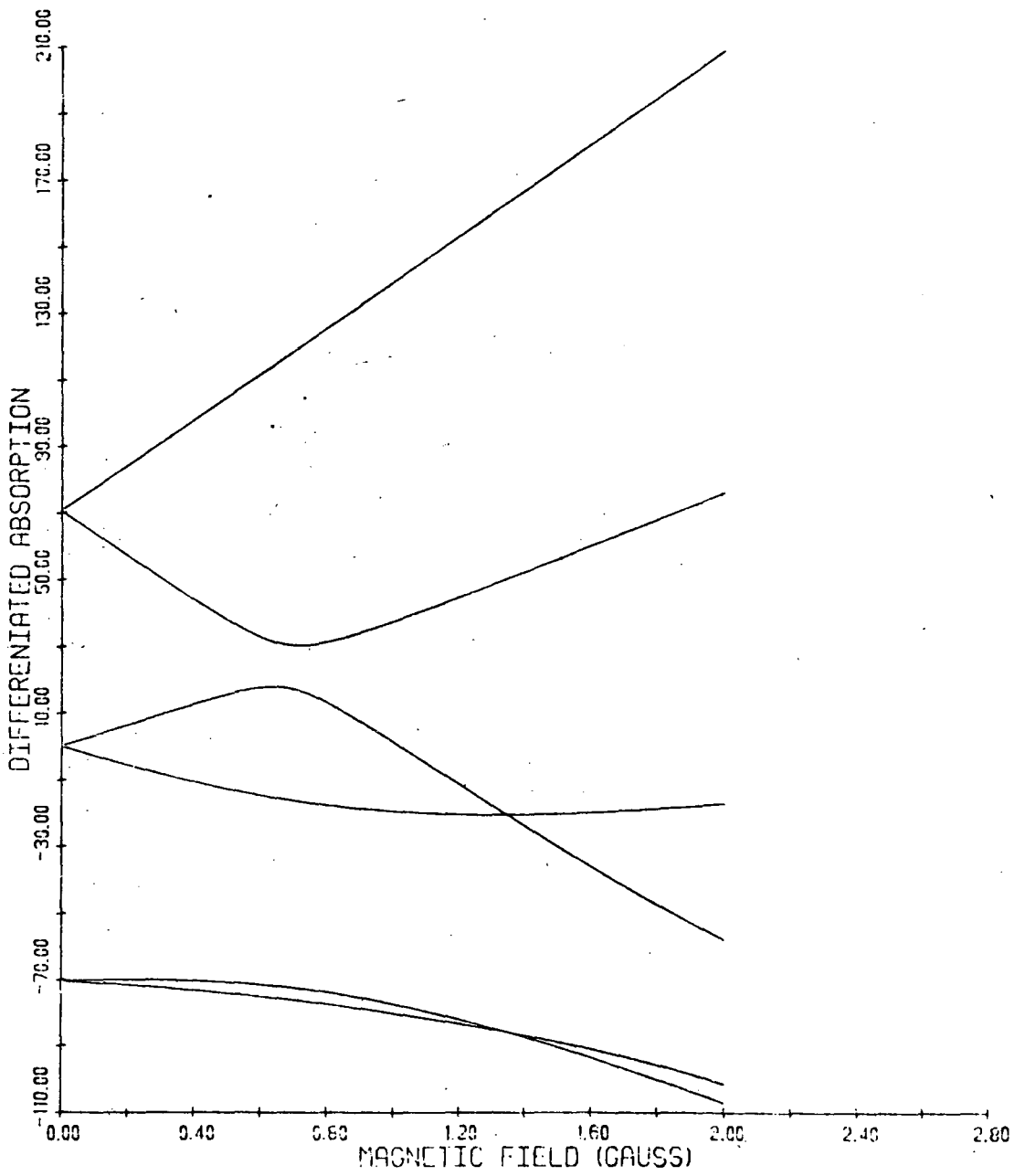
Fig 3.11: POWDER SPECTRA (LORENTZIAN BROADENING)

SIMULATION USED A WIDTH OF 40 G..

DIFFERENIATED ABSORPTION

MAGNETIC FIELD (GAUSS)
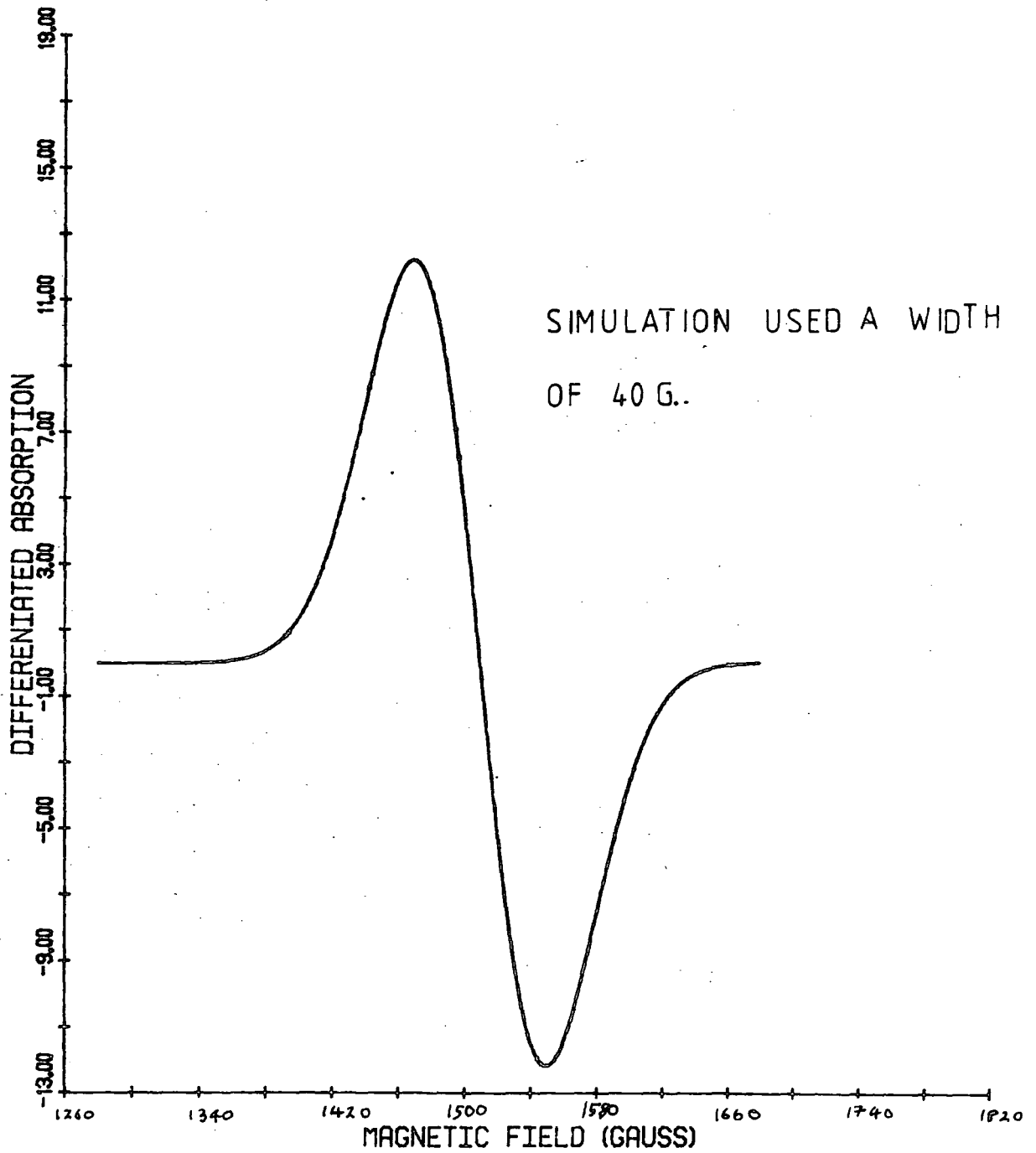
3.4   IDENTIFICATION OF FEATURE,D (Fig 3.12)

This feature was seen in all the pigments. Its shape is a broad

negative peak which implies a step in the absorption. Due to its width and

poor signal to noise ratio it is difficult to assign accurate g values to

this line but it is likely to be due to various native defect sites in the

crystal which are overlapping to produce this feature. From Fig 3.7 it

can be seen to be independent of iron concentration and so it is not

thought to be associated with either iron signal. The peak occurs at

g = 2.03. A broad line with this g value was reported by Hodgskiss (1981)

but was not positively identified further than this.

3.5   IDENTIFICATION OF SIGNAL,F (Figs 3.13-3.14)

After the sample had been evacuated for two days to 10^{-4} Torr

helium was admitted into the tube to see if the specimens could be studied

under the gas rather than the rather cumbersome arrangement required to

evacuate the sample tube. However, a new signal was seen (Fig 3.13 - 3.14).

This has g values of $g_x = g_y = 2.017$ and $g_z = 2.216$. It is thought that

this line results from adsorbed helium on the surface of the crystallites.

The change in shape above 40 K is discussed in Chapter four.

The amplitude of this line was reduced on further evacuation. This

line was only seen in the X11/Blank sample. This was the base material

before doping with iron.

3.6   THE LIGHT SENSITIVE SPECTRA, G. (Fig 3.15)

Several of the lines were affected by light in one way or another

but only one line was actually generated by irradiation. This was the line

at g ≃ 2.01. This line had several features.   The first is that when

the temperature is raised the linewidth narrows. This is described in the

next section. At higher temperatures it can be seen that this line is

characterised by two g values :

$$g_{||} = 2.010$$
$$g_{\perp} = 2.006$$

FIG.3·12   SIGNAL D.   E.P.R Spectra of X11/ Blank .at 4·2K. ν =9·100GHz

2500 G.

Signal
G

3500 G.
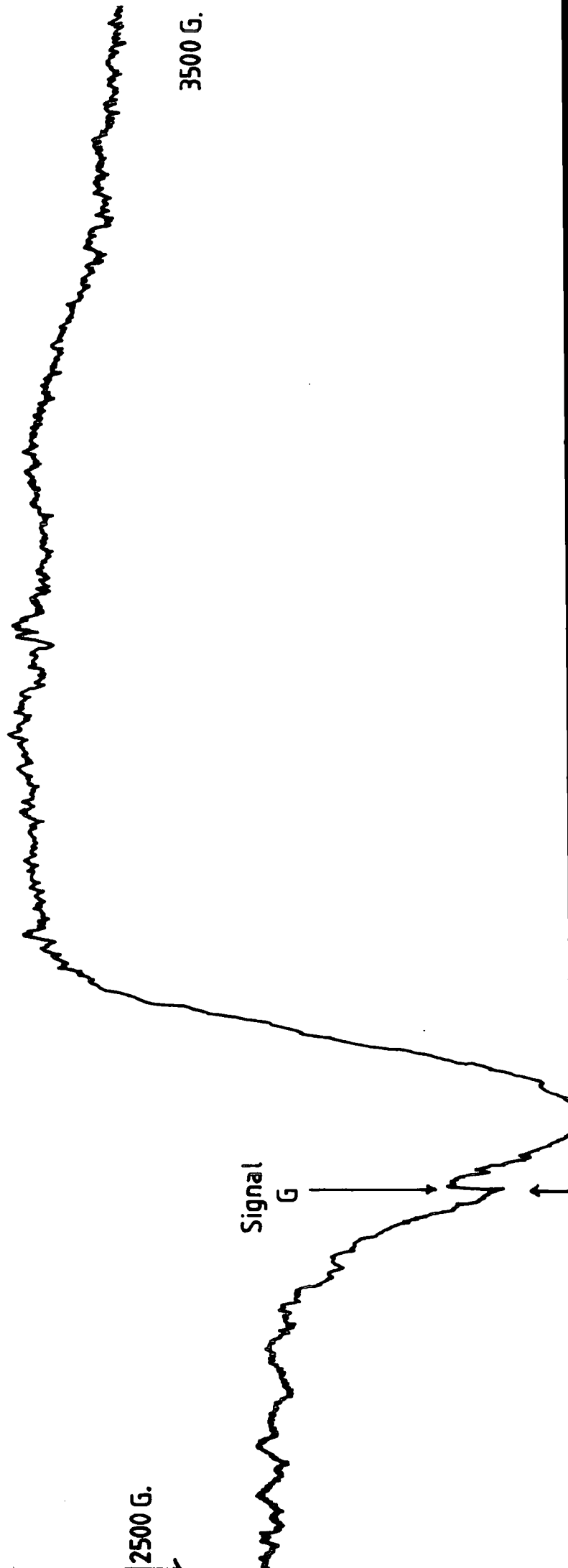
FIG, 3·13   SIGNAL F.

E.P.R. Spectra of sample X11/Blank

$\nu = 9·097$ GHz.

20 Gauss

20K

10·3K

4·0K

g=2·216

g=2·017
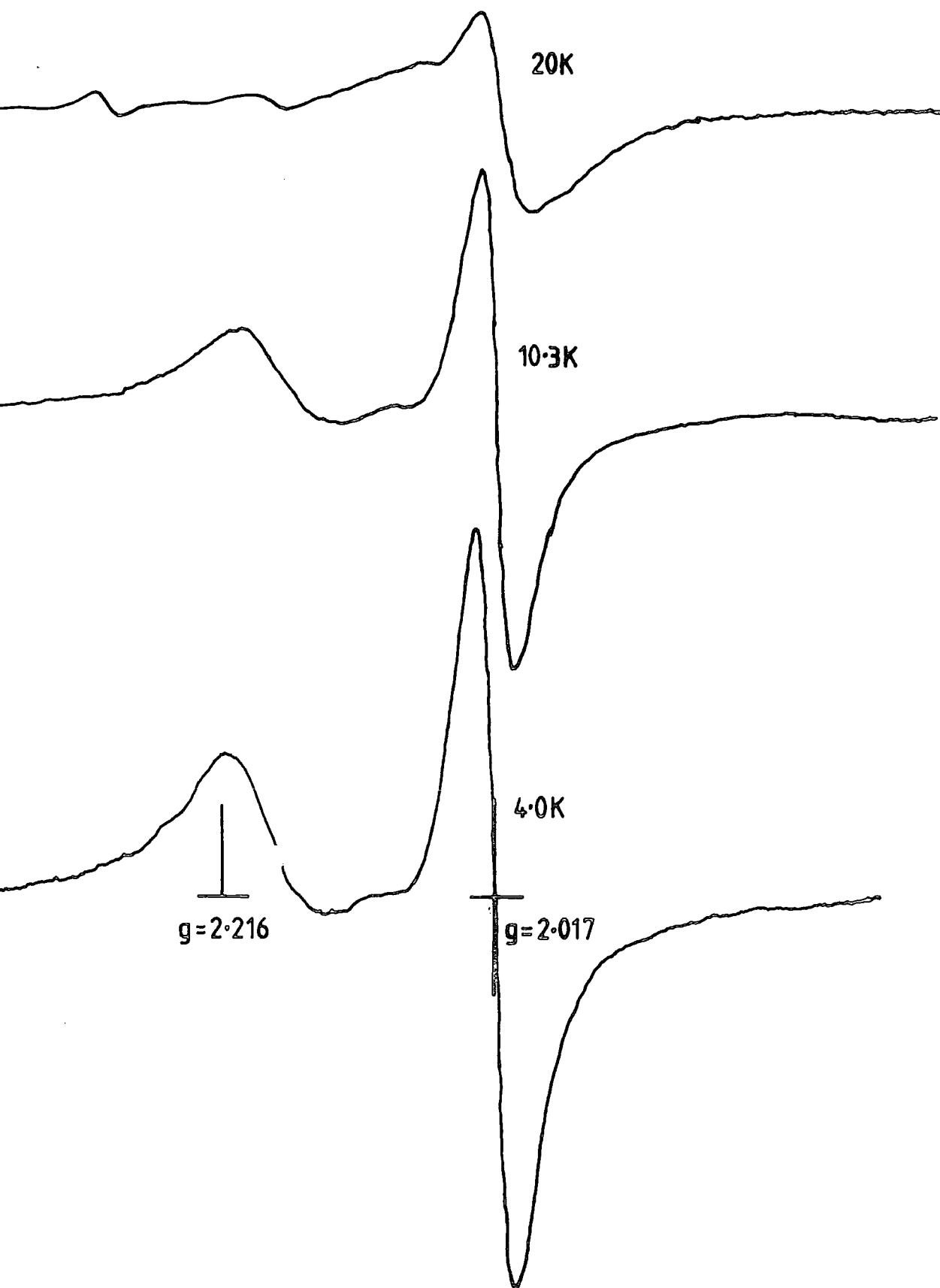
FIG.3·14   SIGNAL F   E.P.R. Spectra or sample X11/Blank

$\nu = 9\cdot097$ GHz.

20Gauss.

100K

60K

40K

g = 2·216

g = 2·017
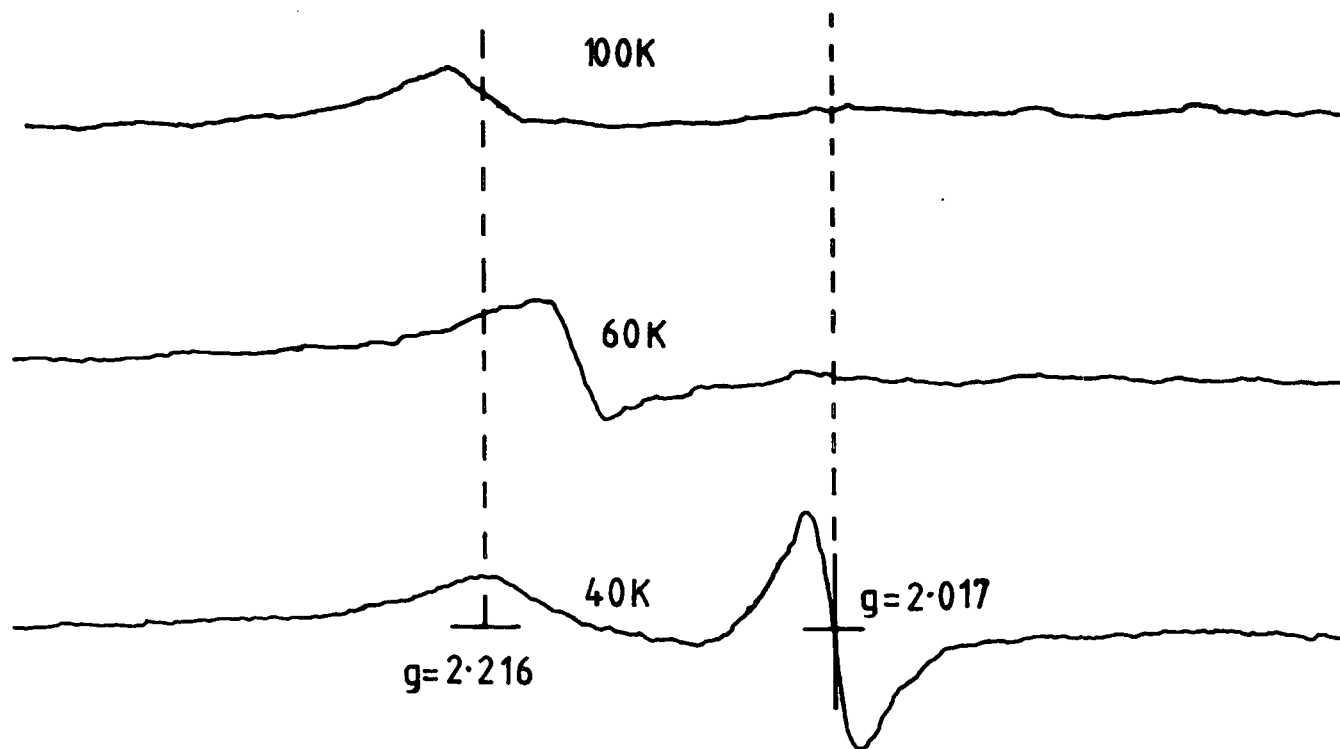
FIG.3·25

THE EFFECT OF CHANGING
THE TEMPERATURE OF
IRRADIATION
ON SIGNAL G

Spectra recorded at the
temperature of illumination.

Sample X11/blank

$\nu = 9\cdot097GHz$

4·2 K

10·3K

20 K

40K

60K

100K

20 Gauss
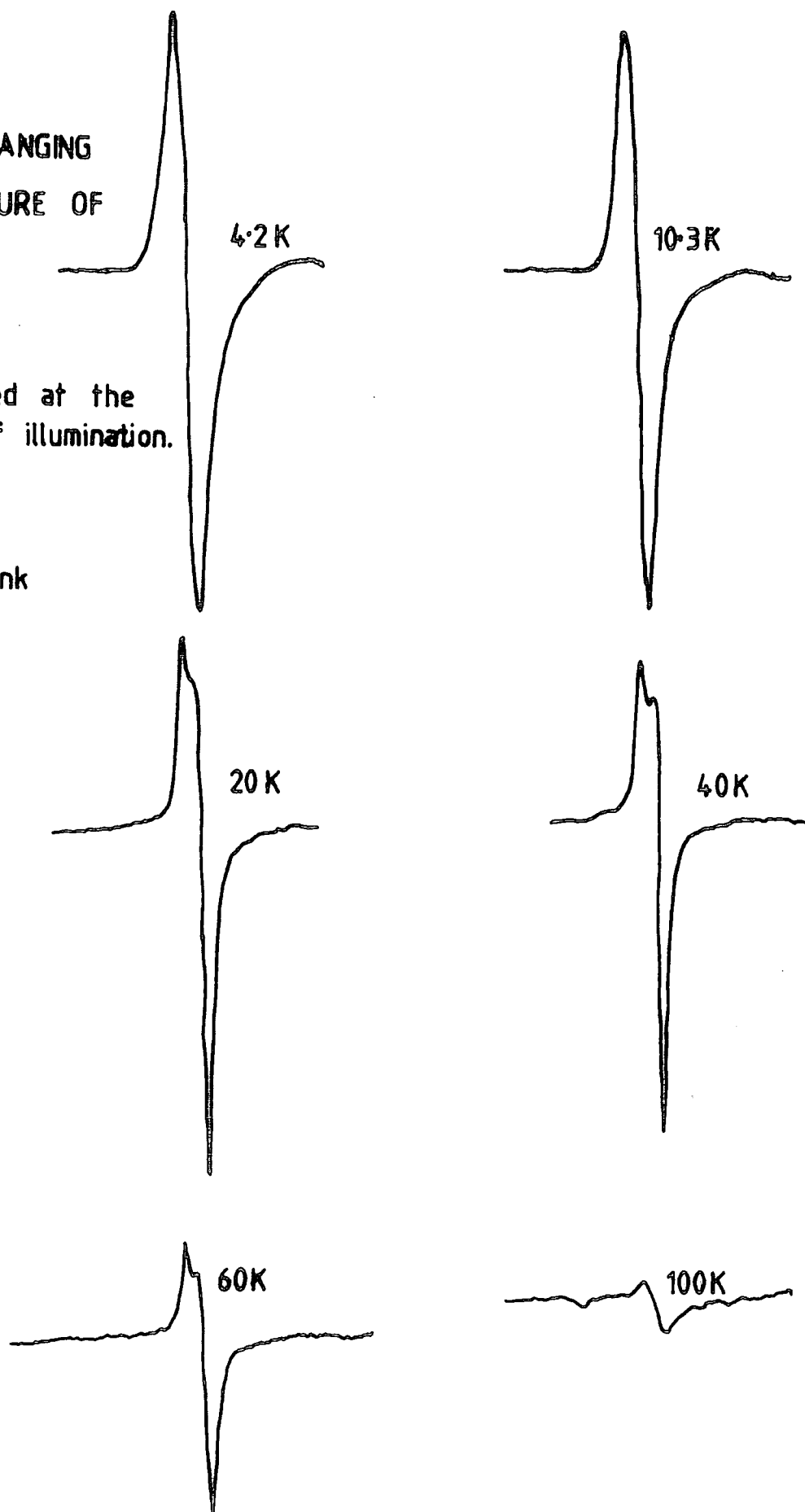
These values do not correspond to any spectra reported for single crystals. When the irradiation is removed the signal amplitude reduces but attains a steady level (Fig. 6.8) and is only removed by heating to about 150 K.

It is thought that this corresponds to a trapped hole because the g value is greater than that for a free electron (g = 2.0023).

Table 3.4 summarises the identifications and g-value estimates for the lines A to G observed in the e.s.r. spectra of these pigments.

Signal	Identification	'g' value	width (mT)	
A)	Fe^{3+})	8.18	~18)	
B)	Substitutional)	5.62	~2)	'Spikes'
E)	)	3.378	4	
C	Fe^{3+} Rhombic ?	~ 4.3	10	Width increases T < 5 K.
D	Bulk defects ?	~ 2	~ 10	
F	Adsorbed He ?	2.017 2.216	2	After evacuation to 10^{-4} Torr for 2 days.
G		2.010 2.006		Greatly enhanced by U.V. irradiation.

TABLE 3.4 :   Signals seen in Rutile Pigments.

CHAPTER 4

LINESHAPES

4.1   INTRODUCTION

In the previous chapter the general features of powder spectra were examined and explained. However, no detailed examination of the observed features was undertaken to see if any further information could be extracted. In particular, the width of the lines was not monitored. This chapter will look at the detailed width and shape of the parts of the powder spectra and relate this to the structure of individual powder particles.

When we talk about linewidths of powder spectra we must be careful to be clear about what we mean. The term linewidth has been used for two different quantities. The first is the total width of the powder spectra, for example for the Fe^{3+} substitutional spectra described in Fig 3 this would be very large ; greater than 0.5 Tesla. This information however does not give us any indication of the interactions between paramagnetic ions or between them and the lattice as it is a result of the effect of the crystal field. The second is as used for single crystal linewidths, and is a result of the relaxation mechanisms of the paramagnetic ion. This is the meaning that is used in this thesis and so for the Fe^{3+} spectra the linewidth is of the order of 1 mT not 1 T. The linewidth of powders arises from the same mechanisms as for single crystals.

4.2   E.P.R. LINEWIDTH AND LINESHAPE - A REVIEW

The width of E.P.R. lines in single crystals can arise from several causes such as magnetic dipole-dipole and exchange interactions, interactions with different paramagnetic ions and with the nucleii of surrounding paramagnetic particles or through spin-lattice relaxation to the surrounding diamagnetic ions. Broadening can also occur through unresolved hyperfine

structure or from the experimental conditions for instance through modulation broadening. If the crystal contains lattice distortions caused by strain or by various defects the Spin Hamiltonian parameters for each individual paramagnetic ion near these defects (or in the strained region) will have slightly different values and will result in a spread of resonant field and a resultant broadening of the linewidth.

It is usual to consider moments of the lines, particularly the second and fourth moments. The nth moment of a line is :-

$$M_N = \int_0^\infty (\nu - \nu_0)^n \, f(\nu) \, d\nu. \tag{4.1}$$

where ν_0 is the peak of the line and $f(\nu)$ is the lineshape normalized so that

$$\int_0^\infty f(\nu) \, d\nu = 1 \tag{4.2}$$

If $u = \nu - \nu_0$, $g(\nu) \equiv g(\nu_0 + u) \equiv \bar{g}(u)$.

Then

$$M_k = \int_{-\nu_0}^\infty u^k \, \bar{g}(u) \, du \tag{4.3}$$

or for narrow lines :

$$M_k = \int_{-\infty}^\infty u^k \, \bar{g}(u) \, du \tag{4.4}$$

It can be seen that for symmetrical lines the odd moments vanish. There are two different line functions usually taken as typical. They are Lorentzian and Gaussian. Lorentzian lines result from spin-lattice relaxation while

Gaussian are typical of spin-spin interactions. The true lineshape is usually in between these two extremes. The Voigt line edge is arrived at by taking a convolution of these two functions. The functions are :-

$$\text{Gaussian } \bar{g}_G(u) = \frac{1}{\sigma \sqrt{2\pi}} \quad e^{-\frac{u^2}{2\sigma 2}} \tag{4.5}$$

$$\text{Lorentzian } \bar{g}_G(u) = \frac{\Delta}{2\pi} \quad \frac{1}{u^2 + \frac{1}{4}\Delta^2} \tag{4.6}$$

The linewidth Δ or σ is calculated from

$$\bar{g}\left(u = \frac{\Delta\nu}{2}\right) = \frac{1}{2}\bar{g}(o)$$

and is given by $\Delta\nu = 2\sigma \sqrt{2 \ln 2} = 2.35 \sigma$

for Gaussian and

$$\Delta\nu = \Delta$$

for Lorentzian lineshapes.

Now for the Gaussian line the even moments are

$$M_2 = \sigma^2$$

$$M_4 = 3\sigma^4 \tag{4.7}$$

$$M_{2n} = 1.3.5.....(2n-1)\sigma^{2n}$$

and for the Lorentzian line the line must be truncated at $\nu = \nu_o \pm \alpha$ where $\alpha \gg \nu_o$ to ensure that the line has a finite area ; the moments are :

$$M_2 = \frac{\alpha\Delta}{\pi}$$

$$M_4 = \frac{\alpha 3 \Delta}{\pi} \tag{4.8}$$

$$M_{2n} = \frac{\Delta}{\pi} \frac{\alpha^{2n-1}}{2n-1}$$

In order to examine the similarity between a given shape and either of these we only need to calculate M_4/M_2^2.

For a Gaussian this is

$$\frac{M_4}{M_2^2} = 3$$

and for a Lorentzian line $\quad \frac{M_4}{M_2^2} = \frac{\alpha \pi}{3} \gg 1 \qquad\qquad (4.9)$

while for a rectangle $\quad \frac{M_4}{M_2^2} = 1 \qquad\qquad (4.10)$

4.2.1 Spin-Spin Interaction

Van Vleck (1948) considered the dipole-dipole interaction in a crystal with one type of paramagnetic centre and calculated the second and fourth moments. He used a Hamiltonian of the form :—

$$\mathscr{H} = Hg\beta \sum_i S_{zi} + \sum_{k>j} \tilde{A}_{jk} S_j S_k + g^2 \beta^2 \sum_{k>j} \left[r_{jk}^{-3} (S_j \cdot S_k) - 3r_{jk}^{-5} (r_{jk} S_j)(r_{jk} \cdot S_k) \right]$$

$$(4.11)$$

Where the first, second and third terms represent the Zeeman, exchange and dipolar energies respectively. $\tilde{A}_j$ is related to the normal exchange integral by $\tilde{A}_{jk} = 2 z^2 J_{jk}$.

From this it can be derived that the second moment is given by :-

$$\langle \Delta \nu^2 \rangle = \frac{1}{3} S(S + 1) h^{-2} \sum_k B_{jk}^2 \qquad\qquad (4.12)$$

where $\quad B_{jk} = -3 g^2 \beta^2 r_{jk}^{-3} (\frac{3}{2} \gamma_{jk}^2 - \frac{1}{2})$

γ_{jk} is the direction cosine of r_{jk} with the electric field.

r_{jd} is the distance between the jth and kth atoms.

The fourth moment is :

$$h^4 < \Delta_\nu^{\,4} > = N^{-1} \sum_{jkl \neq} \left[3B_{jk}^2 B_{jl} + 2A_{jk}^2 (B_{jl} - B_{kl})^2 + 2A_{jk}A_{kl}(B_{jl} - B_{jk}) \times \right.$$

$$\left. (B_{jl} - B_{kl}) + 2 A_{jk}B_{jk}(B_{jl} - B_{kl}) \right] \left[\frac{1}{3} S(S+1) \right]^2$$

$$+ 2N^{-1} \sum_{k>j} \left\{ B_{jk} \frac{1}{5} \left[S^2(S+1)^2 - \frac{1}{3} S(S+1) \right] \right.$$

$$+ 2B_{jk}^3 A_{jk} \frac{1}{5} \left[\frac{2}{3} S(S+1)^2 - \frac{1}{2} S(S+1) \right]$$

$$\left. + B_{jk}^2 A_{jk} \left[\frac{4}{5} S^2(S+1)^2 - \frac{3}{5} S(S+1) \right] \right\} \tag{4.13}$$

$$\text{where} \quad A_{jk} = \tilde{A}_{jk} + g^2 \beta r_{jk}^{-3} \left[\frac{3}{2} \gamma_{jk}^2 - \frac{1}{2} \right] \tag{4.14}$$

This can be thought of by considering each paramagnetic particle in an extended field H_o and subject to a local field H_{loc} (Al'tshuler & Kozyres (1974)). Now because of the random orientaion of the magnetic moments H_{loc} will vary from site to site. With $H = H_o + H_{loc}$ in $g \beta H = h\nu$, the resonance condition will be fulfilled for different values of H_o depending on H_{loc}.

The order of magnitude of $H_{loc} \sim \beta/r^3$ where r is the separation of the particles. So $\Delta \nu \sim \frac{\beta^2}{hr^3}$. Van Vleck made the following assumptions to arrive at his formula.

(1) The paramagnetism is purely spin in nature, so both initial splittings and g-value anisotropy are absent.

(2) The Zeeman energy is larger than the dipole-dipole interaction.

(3) The temperature is high enough so that the populations of both levels can be considered equal.

Now in rutile the Fe^{3+} ion has no orbital momentum and so the above assumptions are reasonable but as there are two sites (rotated at 90° with respect to each other) the interactions between these two different sites needs to be considered as well. This adds a second term as shown below. The two sites have spins S and S' and g-values g and g'. The unprimed values relate to the site which is causing the resonance. (These equations are only valid when g and g' are dissimilar enough so that their respective absorptions do not overlap).

$$<\Delta\nu^2> = \frac{5}{3}(S+1)h^{-2}\sum_k B_{jk}^2 + \frac{1}{3}S'(S'+1)h^{-2}\sum_{k'}C_{jk'}^2 \quad (4.15)$$

where $\quad C_{jk} = A_{jk'} + \frac{gg'\beta^2}{r_{jk'}^3}(1 - 3\gamma_{jk'})$

and the fourth moment is :-

$$h^4 \quad >= h^4\left[<\Delta\nu^4>\right]_0 + N^{-1}\left[\frac{1}{3}S(S+1)\right]\left[\frac{1}{3}S'(S'+1)\right]$$

$$\sum_{l'}\sum_{k\ j}\left\{6B_{jk}^2(C_{j1'}^2 + C_{k1'}^2) + 2A_{jk}^2(C_{j1'})^2 + 4B_{jk}A_{jk}\ x \right.$$

$$\left. (C_{j1'}-C_{k1'})^2\right\} +$$

$$N^{-1}\sum_j\sum_{l'>k'}\left[2A_{k'1'}(C_{jk'}-C_{j1'})^2 + 6C_{jk'}^2C_{j1'}^2\right]\left[\frac{1}{3}S'(S'+1)\right]^2 +$$

$$N^{-1}\sum_{j_1 k'}C_{jk'}^4\frac{1}{5}\left[S'(S'+1)-\frac{1}{3}\right]S'(S'+1) \quad (4.16)$$

However Van Vleck's argument considered a regular array of para-magnetic ions for instance the copper ion in $Cu_2SO_4 \cdot 4\ H_2O$ crystals. Kittel and Abrahams (1953) have considered the effect of dipolar broadening in magnetically dilute crystals. Their approach is one extension of Van Vleck's method. If f is the probability that a lattice site is occupied by a para-magnetic ion, the number of sites k, at a displacement r_{jk} from the occupied

site j, is N f , (summing over j), as N sites j are occupied and f is the probability that any other site is occupied, so the sum Σ_{jk} is just N f Σ_k where we sum over __all__ sites k whether or not occupied. Consequently, equation (4.13) becomes,

$$\langle \Delta v^2 \rangle = \left[S(S+1)/3h^2 \right] \; f \sum_k B_{jk}^2 \qquad (4.17)$$

and the fourth moment becomes (Al'tshuler and Kozyres (1974))

$$h^4 \langle \Delta v^4 \rangle = \left\{ f^2 \left[3 \left(\sum_k B_{jk}^2 \right)^2 - \frac{1}{3} N^{-1} \sum_{j \neq k \neq 1} B_{jk}^2 (B_{j1} - B_{k1})^2 \right] + \right.$$

$$\left. f \left[\left(1.4 - \frac{0.3}{S(S+1)} \right) \sum_k B_{jk}^4 \right] \right\} \left[\frac{1}{3} S(S+1) \right]^2 \qquad (4.18)$$

For small values of f the term in f^2 can be ignored and so

$$\frac{\langle \Delta v^4 \rangle}{\langle \Delta v^2 \rangle^2} \sim \frac{1}{f} \frac{\sum_k B_{jk}^4}{\left(\sum_k B_{jk}^2 \right)^2} \quad > 1 \qquad (4.19)$$

and from (4.11) the line is Lorentzian.

From equation (4.9) we can write that the Lorentzian linewidth Δ (the width at half height) is

$$\Delta = \frac{\pi}{\sqrt{3}} \frac{\langle \Delta v^2 \rangle^{3/2}}{\langle \Delta v^4 \rangle^{1/2}} \qquad (4.20)$$

$$= \frac{\pi}{3} f \frac{\left(\sum_k B_{jk}^2 \right)^{3/2}}{\left(\sum_k B_{jk}^4 \right)^{1/2}} \left[\frac{S(S+1)}{1.4 - \frac{0.3}{S(S+1)}} \right]^{1/2} \qquad (4.21)$$

This means that the second moment is always proportional to the concentration. When Kittel and Abrams considered the fourth moment they concluded that for f > 0.1 the line is Gaussian while for f < 0.01 the line is approximately Lorentzian as the fourth moment increases as the square of the second moment. In rutile, with the magnetic field along the 'c' axis the two sites of Fe^{3+} substitutional ions become equivalent and give rise to a signal with a g value of 8.18. In this case equation (4.20) is appropriate and can be evaluated using a computer. The program sums the contributions of all the ions in a cube 10 x 10 x 10 unit cells. This means that interactions from up to 5 ions nearest neighbour away are included. It was found that increasing the size of the cube did not appreciably alter the result. A method which enables an exact answer to equation (4.20) has been used by some authors for sites of higher symmetry. This involves expressing B_{ij} in terms of spherical harmonics and examining the terms. However, for rutile this would be very complex and would have no real advantage over the simple, direct computation used.

4.2.2 Spin-Lattice Interactions

The establishment of a thermal equilibrium is determined by relaxation processes caused by interactions between paramagnetic particle spins and lattice vibrations (phonons).

If the two levels are labelled j and k with energies E_j and E_k, containing N_j^O and N_k^O particles per unit volume in equilibrium. Assuming Boltzmann statistics we have

$$\frac{N_k^O}{N_j^O} = \exp\left[-\frac{(E_k - E_j)}{kT}\right]$$

(4.22)

If probability of a transition from level j to level k is P_{jk} under

thermal equilibrium we have

$$N_k^O \, P_{kj} \;=\; N_j^O \, P_{jk} \qquad\qquad (4.23)$$

and from (4.21) we find

$$P_{jk} \;=\; P_{kj} \, \exp\left[-\frac{(E_k - E_j)}{kT} \right] \qquad\qquad (4.24)$$

and if $E_k > E_j$ then $P_{kj} > P_{jk}$ so the probability of transitions from upper

levels to lower levels is greater than the reverse. Thus during paramagnetic

resonance the R.F. field transfers particles from lower to higher levels and

lattice vibrations give rise to transitions mainly in the opposite direction ;

the R.F. energy is transformed into heat.

By shortening the lifetime of paramagnetic ions this interaction

causes broadening of the levels and so of the E.P.R. lines. The temperature

dependence of the linewidths can be used to determine whether this inter-

action contributes substantially to the width. If the line is related to two

levels E_i and E_k the width of the line is given by

$$2\pi\Delta\nu \;=\; \sum_{m \neq j} P_{jm} \;+\; \sum_{n \neq k} P_{kn} \qquad\qquad (4.25)$$

for $S = \dfrac{1}{2}$

$$2\pi\Delta\nu \;=\; P_{12} \;+\; P_{21} \;=\; 1/\tau \qquad\qquad (4.26)$$

There are two main processes, the direct and the Raman processes.

In the direct process a phonon of frequency ν is created according to $E_k - E_j = h\nu$.

This process is typified by the fact that the relaxation rate is proportional

to temperature. The Raman process involves two phonons. A phonon of frequency

ν, is absorbed and one frequency ν_L is emitted according to $E_k - E_j = h\nu_L - h\nu_1$.

(The transition involving the creation of two phonons, i.e. $E_k - E_j = h\nu_2 + h\nu_1$ is not very efficient). The temperature dependence of the relaxation time T_1 is $T_1 \alpha T^{-7}$ for $S = \frac{1}{2}$. For various processes and temperatures $T_2 \alpha T^{-2}$ or T^{-5} or T^{-9} for various situations has been predicted (Standley & Vaughan, 1969). For a Kramers ion whose ground state is a spin doublet $T_1 \alpha T^{-9}$ is expected. According to Orback and Stapleton (1972) in a multilevel system a Raman process which has a T^{-5} dependence would be expected.

In experimental measurement of T_1 in Fe^{3+} doped rutile, Carter and Okaya (1960) thought that the dominant process was the direct process even at 78° K. Manenkov et al (1962) and Madon (1964) found that $T_1 \alpha T^{-1}$. Recent measurements by Tanaka et al (1980) say that the direct process is important below 15° K and above that a Raman process with $T_1 \alpha T^{-7}$ dominates.

4.2.3 The Effect of Lattice Defects and Distortions

Lattice imperfections can arise from a variety of causes, for example dislocations, point defects, such as vacancies and interstitial ions, and planar defects such as stacking faults and the crystallographic shear planes found in slightly reduced rutile. They result in a strain field which depends upon position according to the random spread of the defects. The typical features of strain broadening are that the lines are broader than expected from spin-spin interactions and are independent of spin concentration. (Also for ions with nuclear spin the different hyperfine lines have different widths).

Strains will alter the local crystal field around the paramagnetic site and so alter the resonant field. For a distribution of strains we will have a distribution of resonant fields and hence the absorption line will be broadened. If the E.P.R. transition has an energy h_o in an unstrained crystal the transition energy of one of the centres responsible for this line is altered by the local strain field to (Stoneham, 1966) :-

$$h\nu_o = h\nu_o + h\nu_1 \left(\sum_{ij} a_{ij} e_{ij} \right) + h\nu_2 \left(\sum_{ijkl} b_{ijkl} e_{ij} e_{kl} \right) + \ldots \qquad (4.27)$$

where e_{ij} is a component of the strain tensor. In many cases the quadratic term is negligible and can be ignored. The problem can then be reduced to calculating the probability that the scalar

$$\epsilon = \sum_{ij} a_{ij} e_{ij} \qquad (4.28)$$

lies between ϵ and $\epsilon + d$. ϵ is the linear combination of strain components which describe the particular strain distribution being considered. Stoneham (1968) has considered the case where the linear term vanishes and the quadratic term must be considered. He shows that for a homogeneous distribution of dislocations the lineshape is nearly Gaussian with a width proportional to the dislocation density while for a similar distribution of point defects we would expect a Lorentzian shape and a linear dependence of the width of defect concentration (Stoneham, 1957).

4.2.4 Experimental Effects

When the power incident on the sample is increased the amplitude of the absorption line first increases and then decreases. This decrease is marked by a broadening of the line. This is referred to as saturation broadening. It is necessary to use power levels well below that needed to saturate the system in order to observe an unbroadened and undistorted lineshape. At low temperatures saturation can occur at quite low levels and care must be taken to avoid distorting the lineshape.

Another effect is modulation broadening. If the amplitude of the modulation field is of a comparable size to the width of the absorption line the recorded amplitude of the line will diminish and the lineshape will be distorted with a larger linewidth. So the amplitude of the modulation field H_{mod} should be kept well below the width of the line ΔH. As the amplitude of the line increases with H_{mod} until broadening occurs a practical condition is

$$H_{mod} \leq \frac{\Delta H}{5} \qquad (4.29)$$

Another effect is that caused by the frequency of the modulation field f_{mod} which must be less than the linewidth. ΔH expressed in frequency units, i.e.

$$f_m \quad << \quad \frac{g\beta}{h} \quad \Delta H \tag{4.30}$$

So for 100 kHz linewidths as small as 0.1 Gauss can be recorded.

4.3   EXPERIMENTAL RESULTS

The linewidth of powder spectra can be deduced by assuming a particular lineshape function and then simulating the spectra. The simulation can be adjusted by altering the linewidth of the line broadening function until the simulation and experimental results are similar. If the original assumption of the broadening function is correct then we should have good agreement between the two.

Typical results are shown in Figure 4.1 and Figure 4.2 for the peak due to Fe^{3+} in a substitutional site. Figure 4.1 shows the simulation for a range of Gaussian broadening functions and Figure 4.2 of the same peak but assuming a similar range of Lorentzian functions. It should be noted that for a given linewidth the peak is broader for the Gaussian function.

This peak was considered because the rest of the spectra could yield little lineshape information. The lines at $g \approx 4.3$ and $g \approx 2.0$ have a width that is largely a function of the pigment because the absorbtion peak they represent is due to the smearing of the spectra caused by having a set of randomly orientated crystallites.

4.3.1 The Fe^{3+} Substitutional Ion

Figure 4.3 is derived from Figs 4.1 and 4.2. Here the width of the line at half height ΔH is related to the width of the line broadening function. While different line broadening functions have different relationships for

Fig 4.1a : POWDER SPECTRA (GAUSSIAN BROADENING)
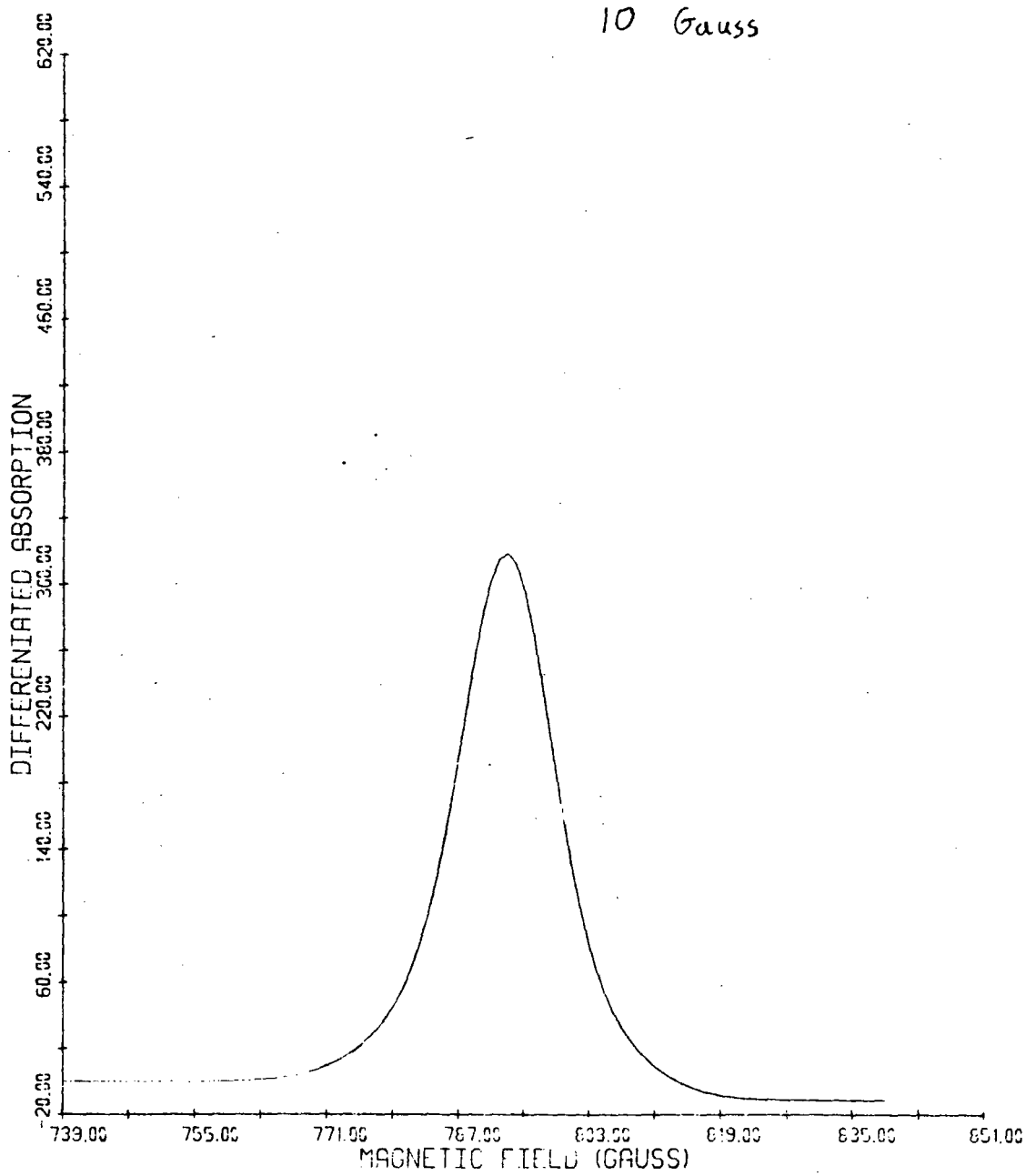
Fig 4.1b: POWDER SPECTRA (GAUSSIAN BROADENING)
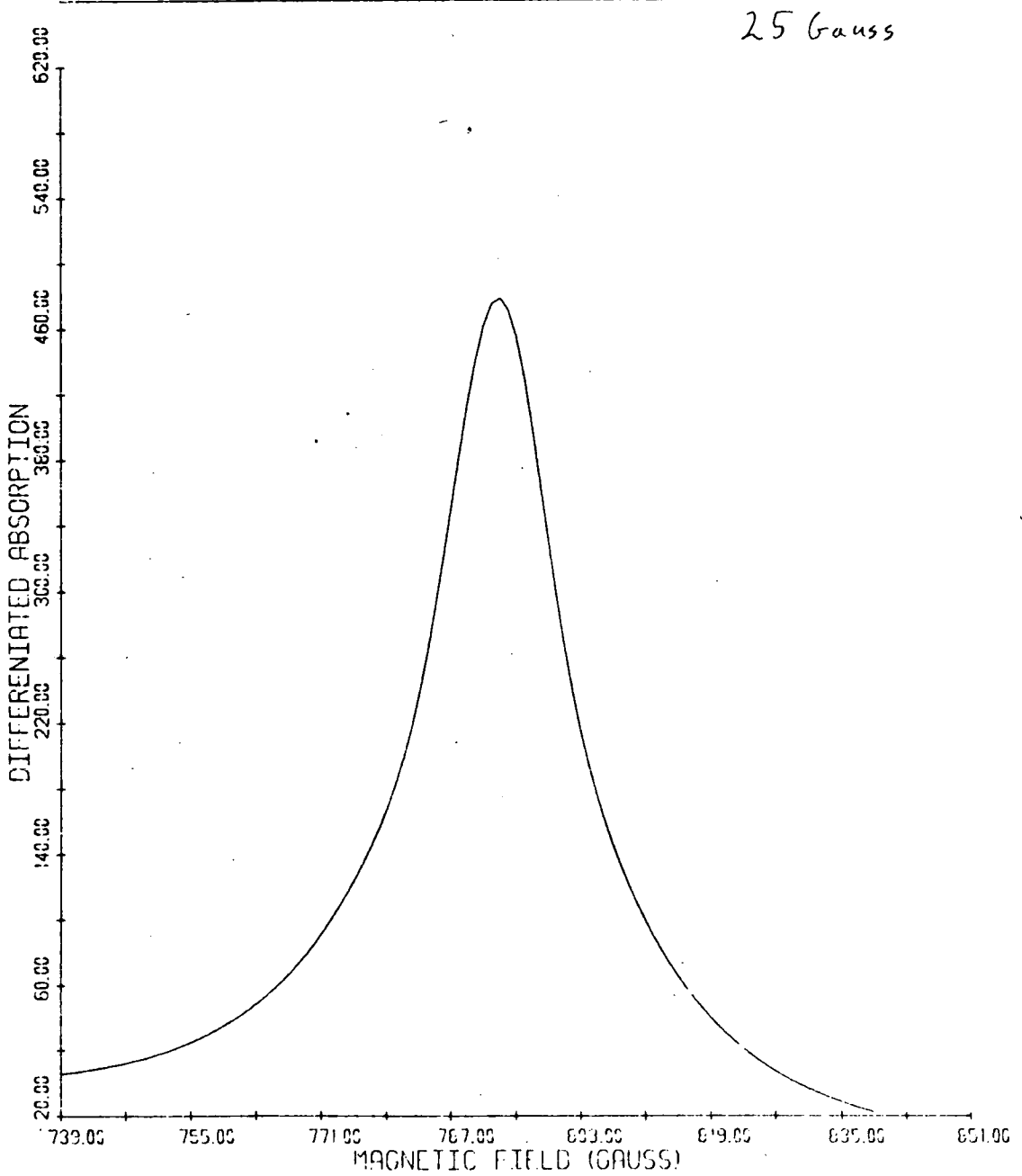
25 Gauss

Fig 4.1c : POWDER SPECTRA (GAUSSIAN BROADENING)

45 Gauss
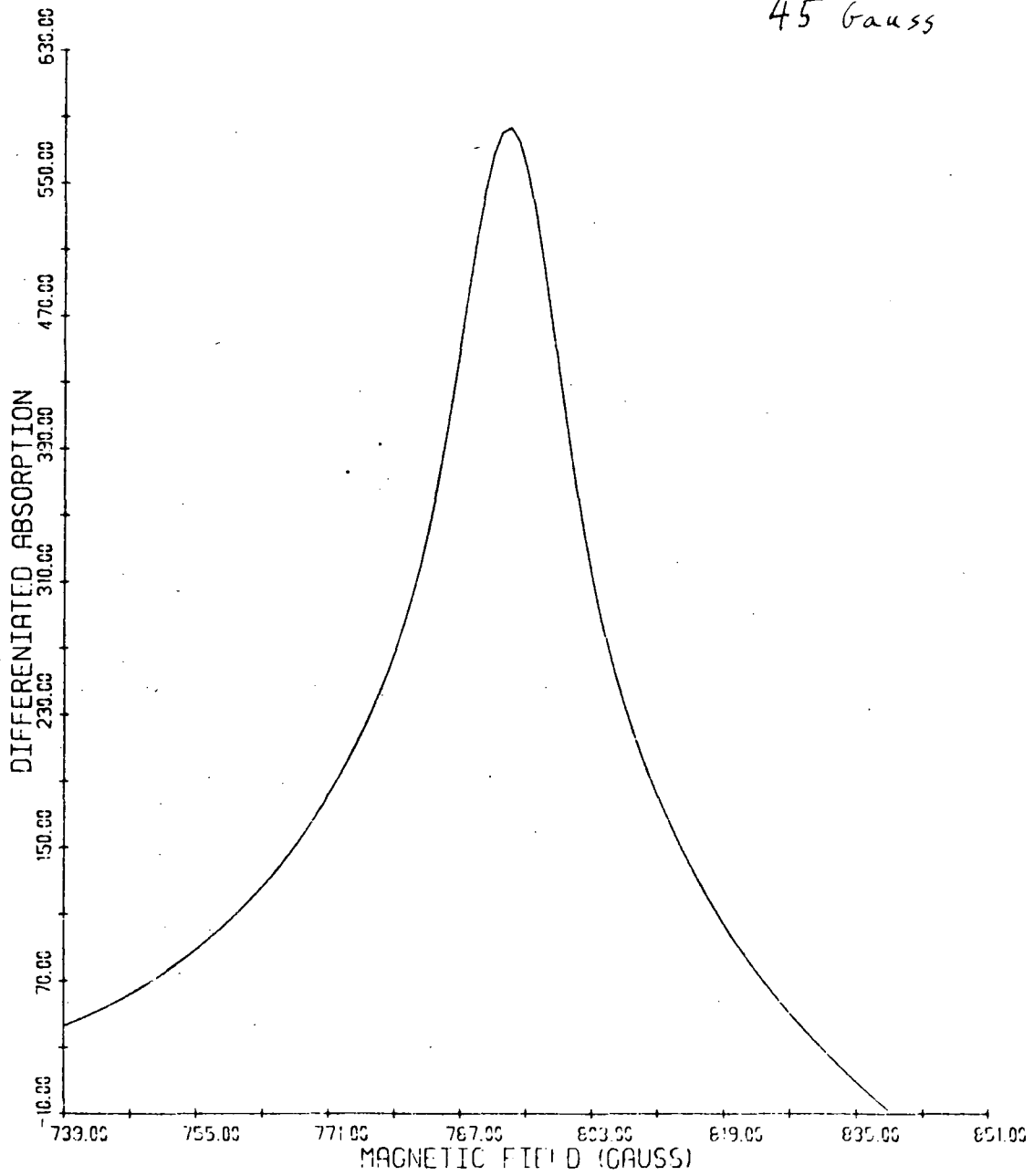
Fig 4.2a : POWDER SPECTRA (LORENTZIAN BROADENING)
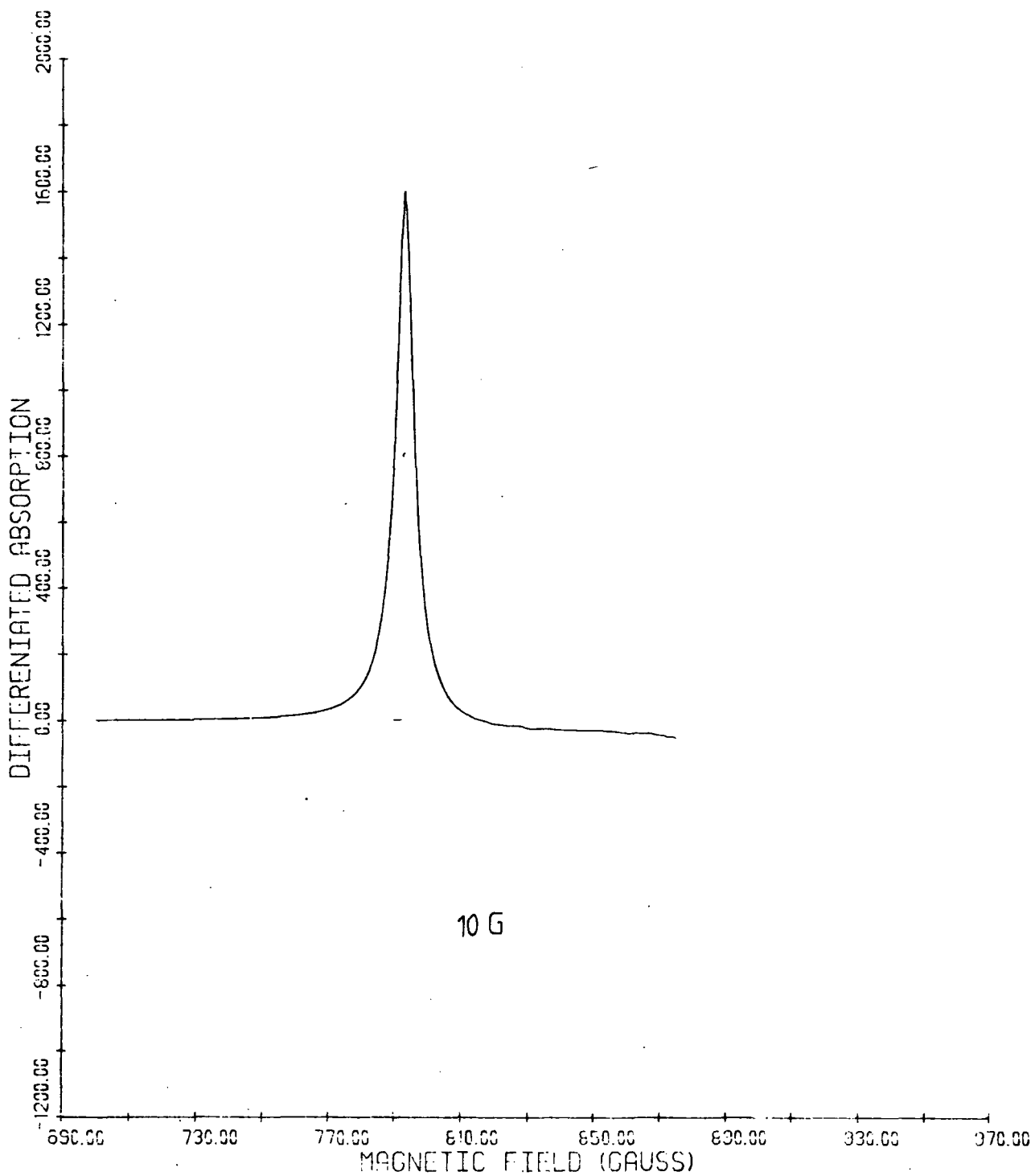
Fig 4.2b: POWDER SPECTRA (LORENTZIAN BROADENING)

25 G

MAGNETIC FIELD (GAUSS)

DIFFERENTIATED ABSORPTION
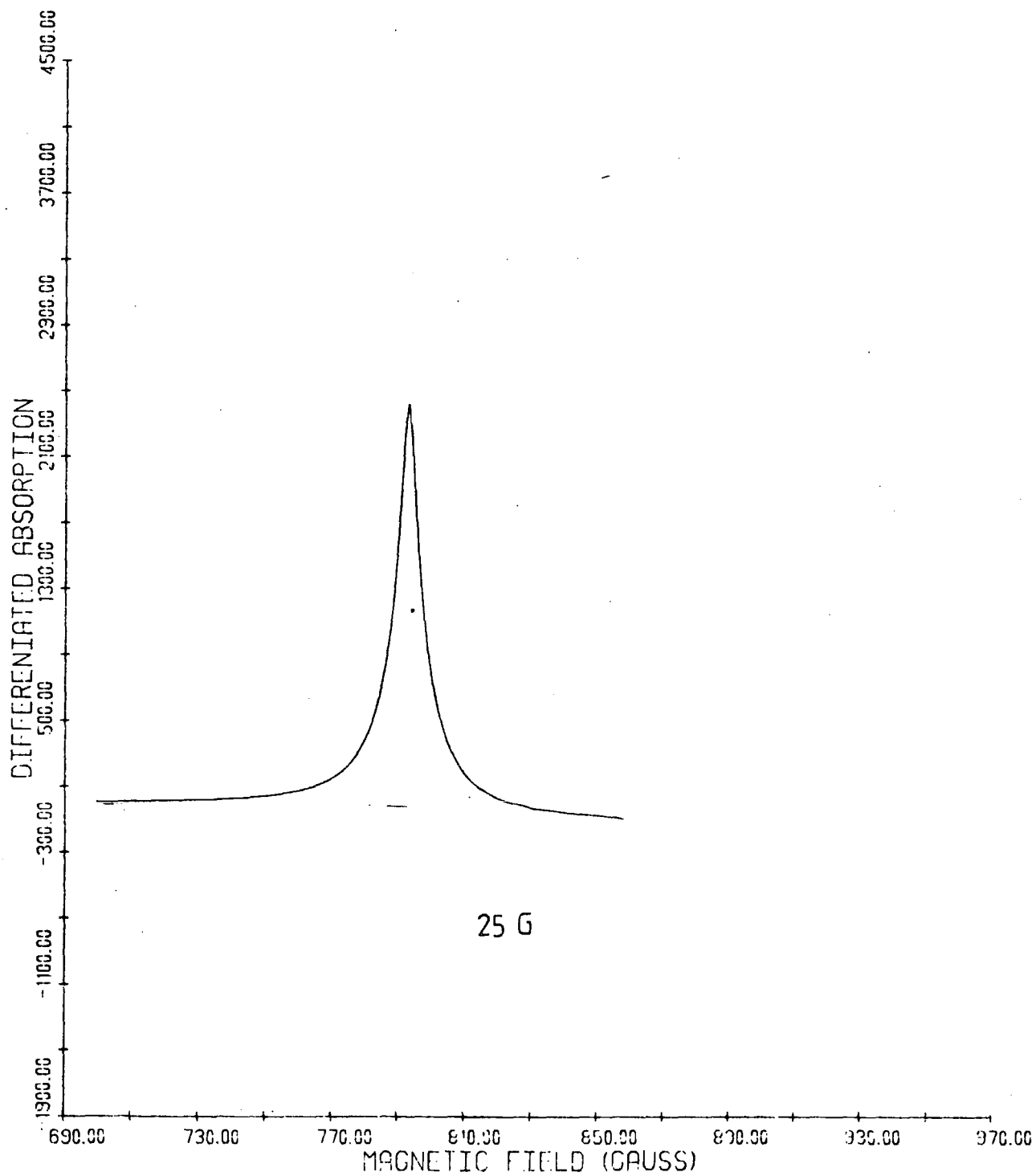
Fig 4.2c : POWDER SPECTRA (LORENTZIAN BROADENING)
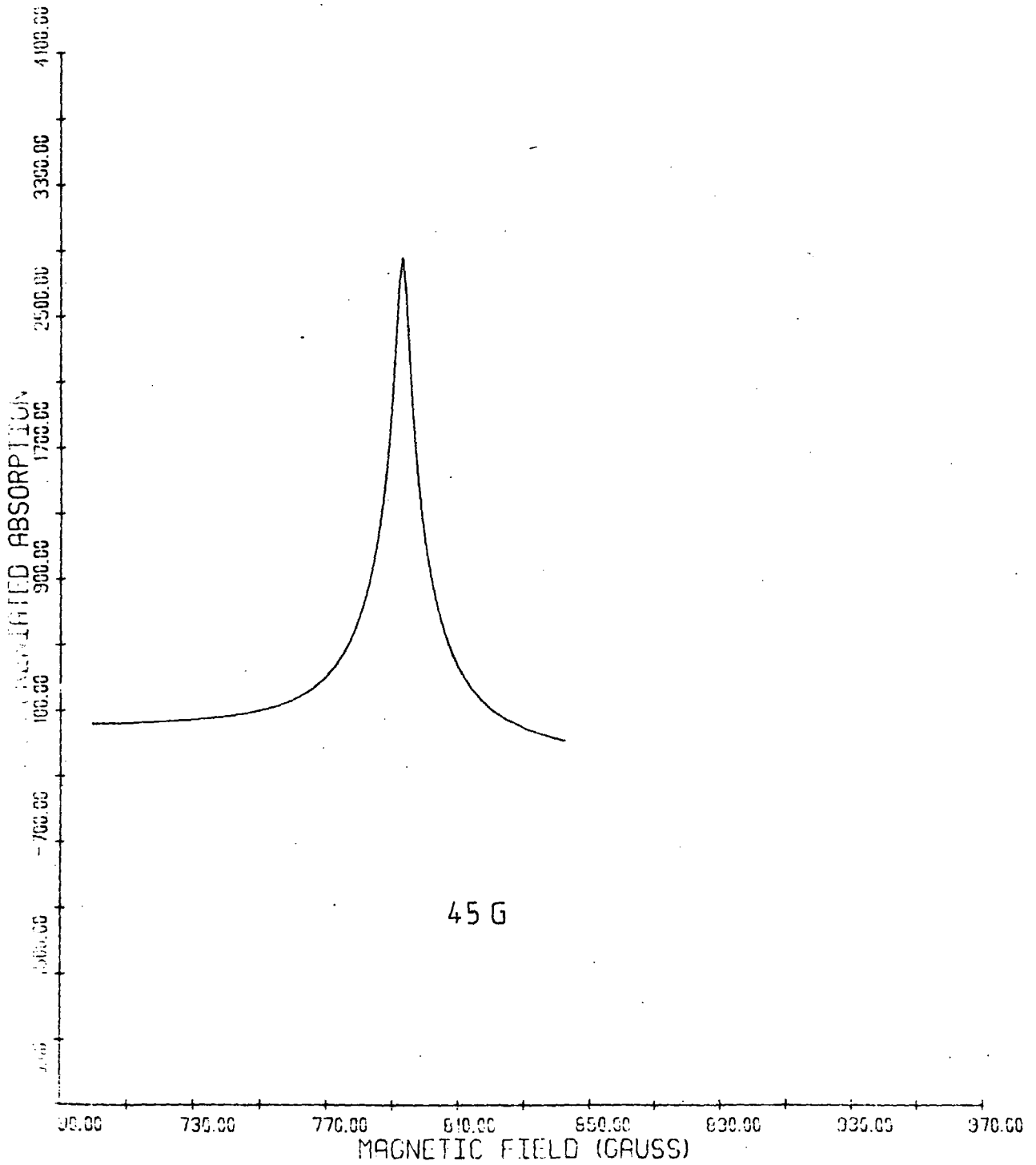
FIG 4·3   PREDICTED HALFWIDTH OF SIGNAL A AS A FUNCTION OF SINGAL CRYSTAL LINEWIDTH
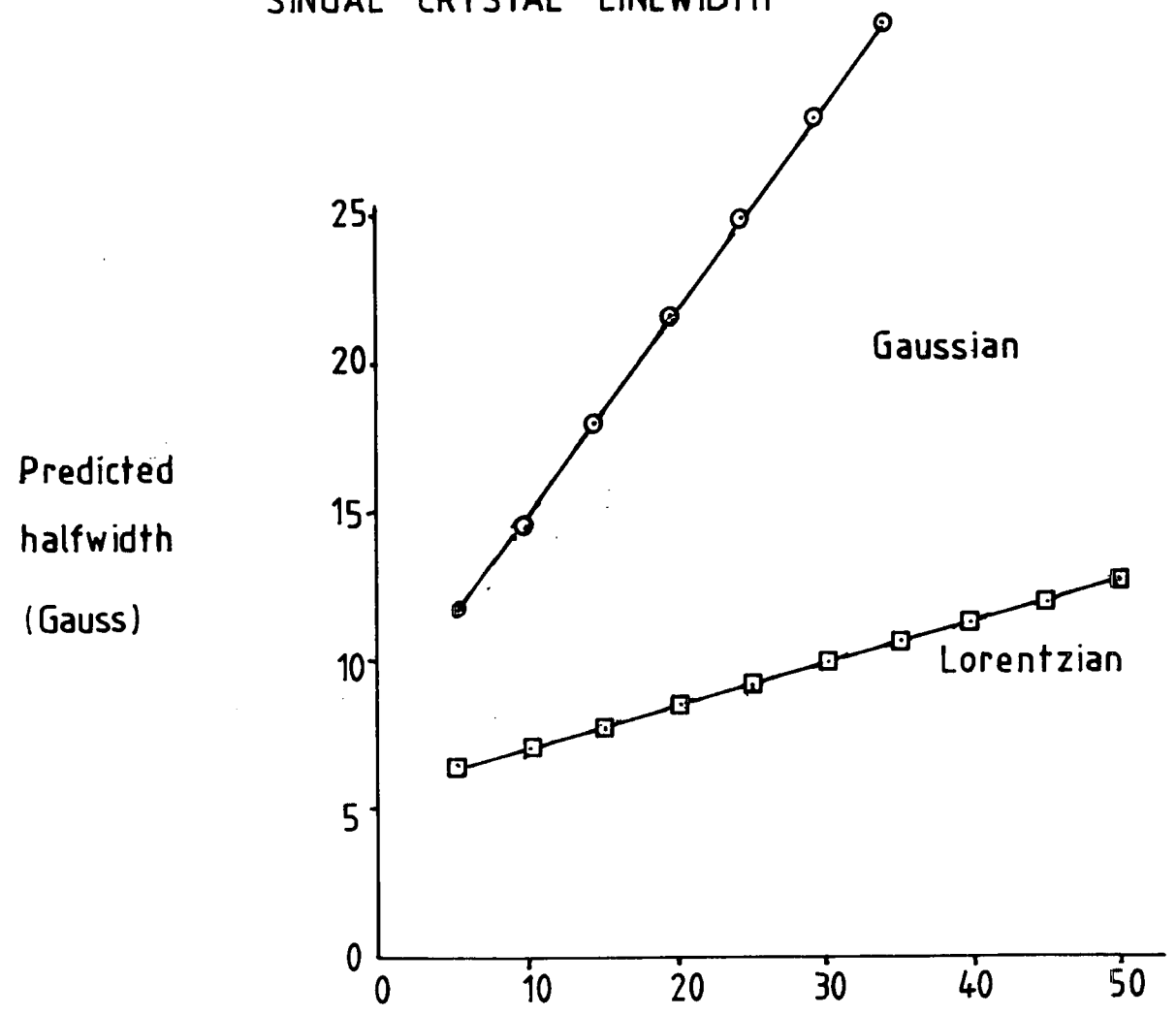
FIG.44 HALFWIDTH OF g=8.18 FEATURE OF Fe^{3+} SUBSTITUTIONAL SPECTRA.
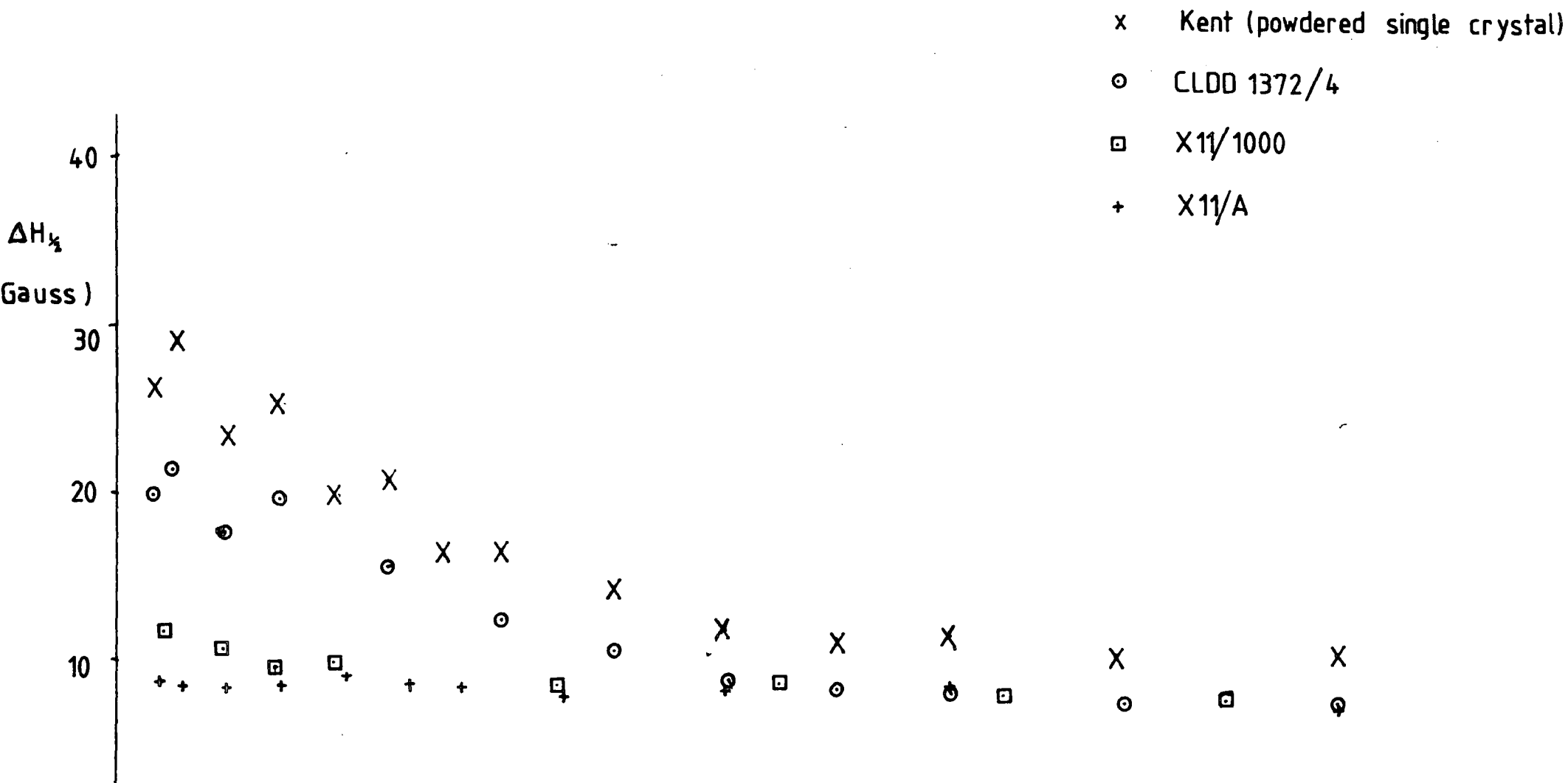
FIG.45.EFFECT OF CONCENTRATION ON WIDTH OF SIGNAL A
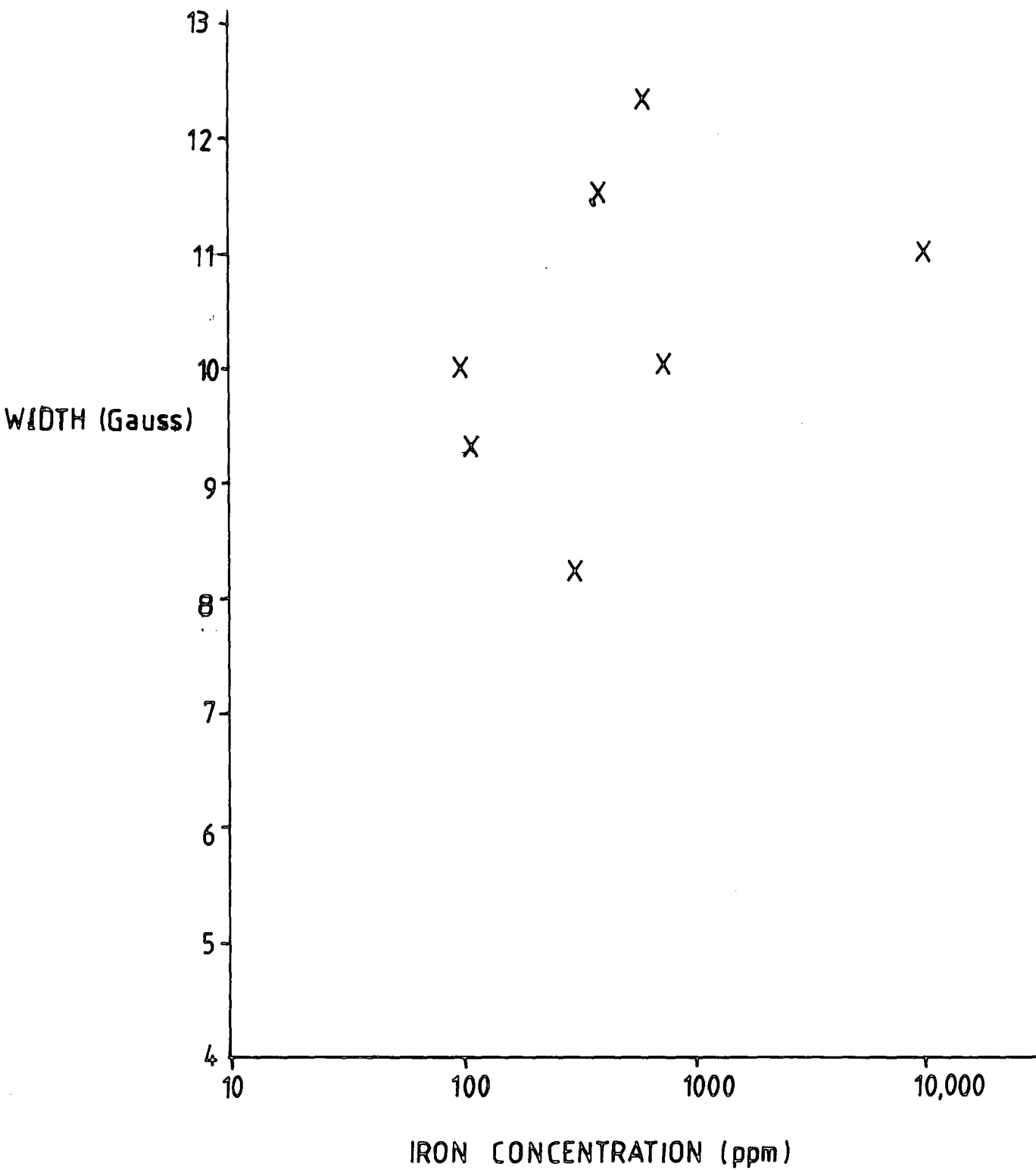
both Gaussian and Lorentzian functions ΔH is proportional to σ the width

of the line broadening function.   For each function Figure 4.4 shows how

ΔH varies for a range of samples as a function of temperature and Fig 4.5

shows ΔH as a function of iron concentration.   Apart from a rise in ΔH for

temperatures below about 40 K for some of the pigments all have $\Delta H \simeq 9$ Gauss.

The Kent sample, a crushed single crystal exhibited a decreasing linewidth

ΔH which although about twice the size of the pigments appeared to behave

similarly;by the time room temperature was reached even this sample had a line-

width of 11 Gauss and the pigment linewidths were beginning to rise.

The calculation referred to in section 4.2.1 to find the dipolar line-

width was performed for $g = 8.18$ on the Fe^{3+} ion and gave the following

results :-

$$\sum_k B_{jk}^2 = 9.38 \times 10^{-52}$$

$$\sum_k B_{jk}^4 = 85.9 \times 10^{-11}$$

Which means that

$$\frac{\sum_k B_{jk}^4}{f\left(\sum_k B_{jk}^2\right)^2} \gg 1$$

(for 100 ppm Fe)

So the line is Lorentzian with   (from eqn 4.24)

$$\Delta = 1.7 \text{ G (for 100 ppm Fe)}$$

From Fig 4.3 this would imply a peak at $g = 8.18$ and would have a

width ΔH of 1.0 Gauss considerably less than that observed.   Also, Fig 4.5

clearly shows that the ΔH does not depend on f, the concentration, so the

line broadening mechanism is not due to dipolar interactions.

The temperature dependence of H also rules out the spin lattice interactions as the width for most of the range examined (for some samples all temperatures looked at) does not change while as explained in section 4.2.2 the width should change as a T^n where n can be as large as 9 or higher depending on the particular process involved. Care was taken during the experiments to ensure that modulation and saturation effects did not contribute but there is still strain broadening to consider. This is quite likely because the pigments are made at a high temperature and then cooled rapidly.

Figs 4.6 to 4.9 show experimental and theoretical fits of the Fe^{3+} peak. These results are typical of the lineshape at all the temperatures. In the range with the temperature above about 40 K the line is best fitted by a Lorentzian with a width of about 20 Gauss (for pigments ; 45 Gauss) for the crushed single crystal). Where the half-width increases below 40 K the lineshape tends towards a Gaussian lineshape with for the sample CLDD1372/4 a width of 10 Gauss. The Kent sample has a width of 20 Gauss, so while the half-width increases with decreasing temperature the linewidth actually decreases as shown in Figure 4.6 because the lineshape below 40 K becomes more and more Guassian. Thus the increase of ΔH with decreasing temperature is due to a lineshape change from Lorentzian to Gaussian and not an increase in the linewidth.

A decreasing linewidth at low temperatures is usually associated with spin-lattice broadening (except in the case where kT $\lesssim$ hν where the distribution of electrons changes and the Boltzman equations must be used to calculate the population of the Zeeman levels. In this case the dipolar linewidths can be temperature dependent. For ν = 9 GHz this means T $\lesssim$ 0.65 K). However spin-lattice broadening usually gives a Lorentzian lineshape.

FIG, 4·6   FITTED LINEWIDTHS OBTAINED FROM FEATURE A

(Signals which are not clearly gaussian or lorentzian

have been omitted because of the ambiguity in

determining the linewidth)
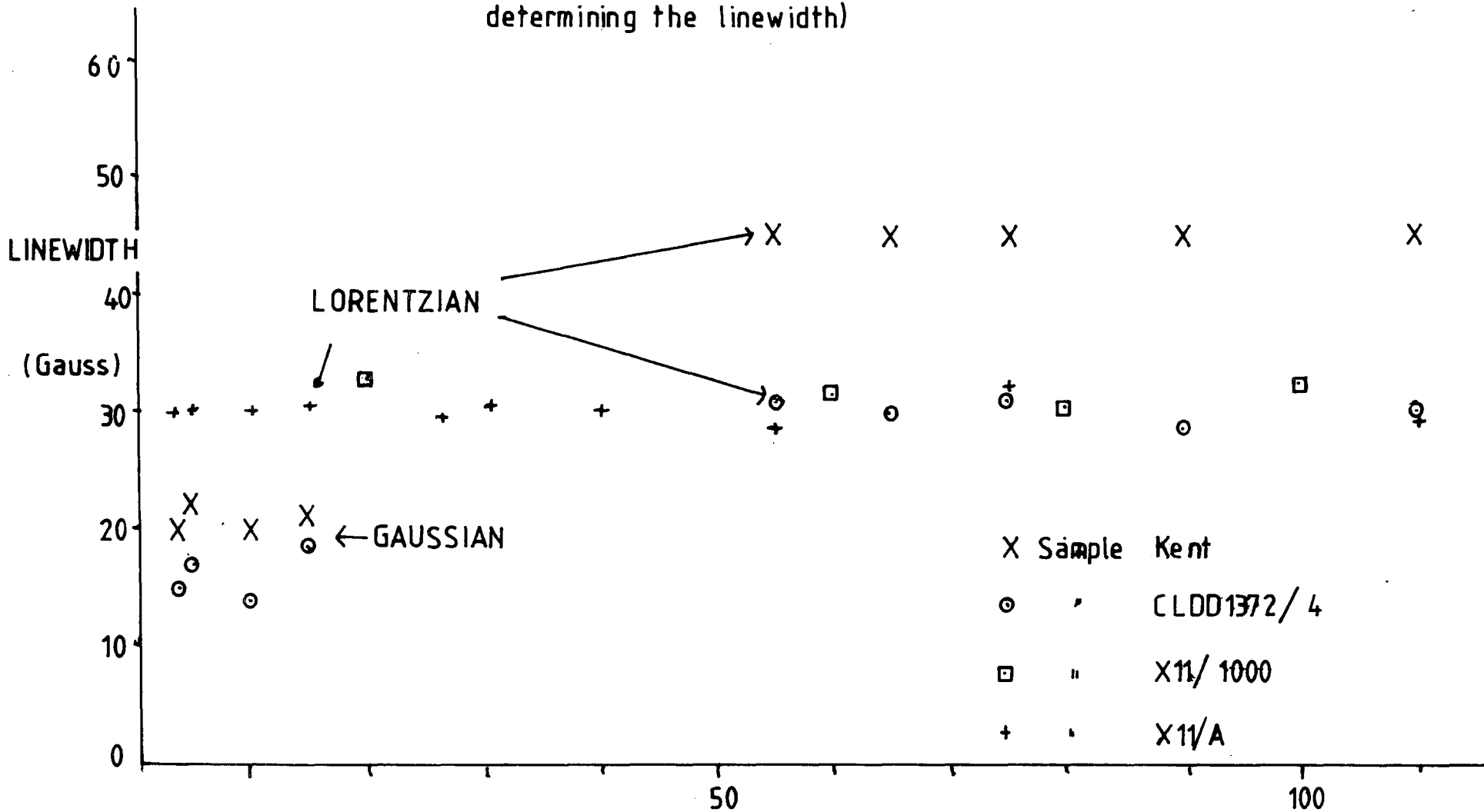
Fig 4.7 : POWDER SPECTRA (GAUSSIAN BROADENING)
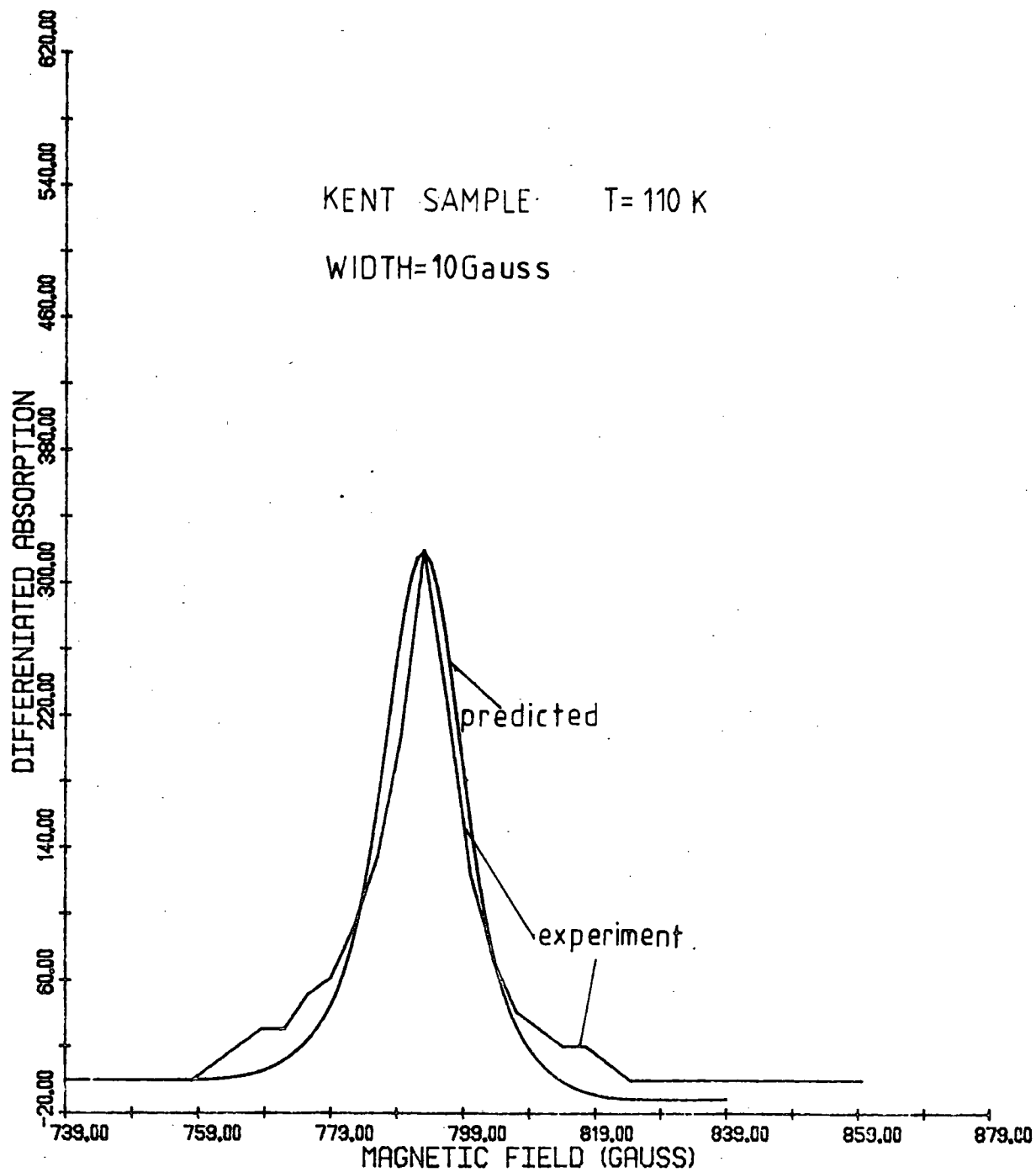
KENT SAMPLE   T= 110 K

WIDTH=10Gauss

predicted

experiment

DIFFERENIATED ABSORPTION

MAGNETIC FIELD (GAUSS)

Fig 4.8 : POWDER SPECTRA (LORENTZIAN BROADENING)

KENT SAMPLE   T = 110 K

WIDTH = 30 Gauss

experiment

prediction

DIFFERENIATED ABSORPTION

MAGNETIC FIELD (GAUSS)

Fig 4.9 : POWDER SPECTRA (GAUSSIAN BROADENING)

KENT SAMPLE   T= 4·3 K

WIDTH= 20 G.

Prediction

Experiment

DIFFERENIATED ABSORPTION

MAGNETIC FIELD (GAUSS)
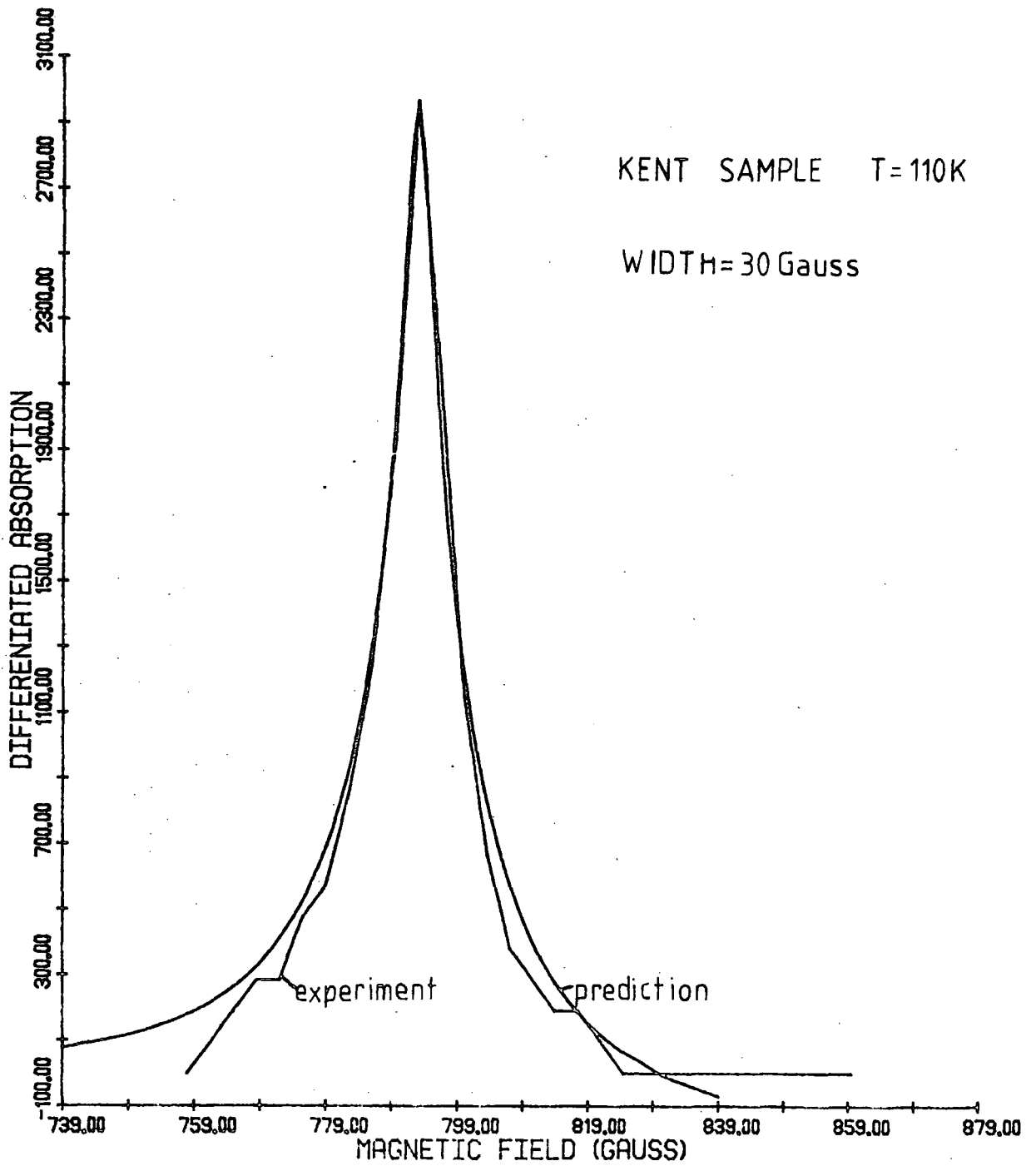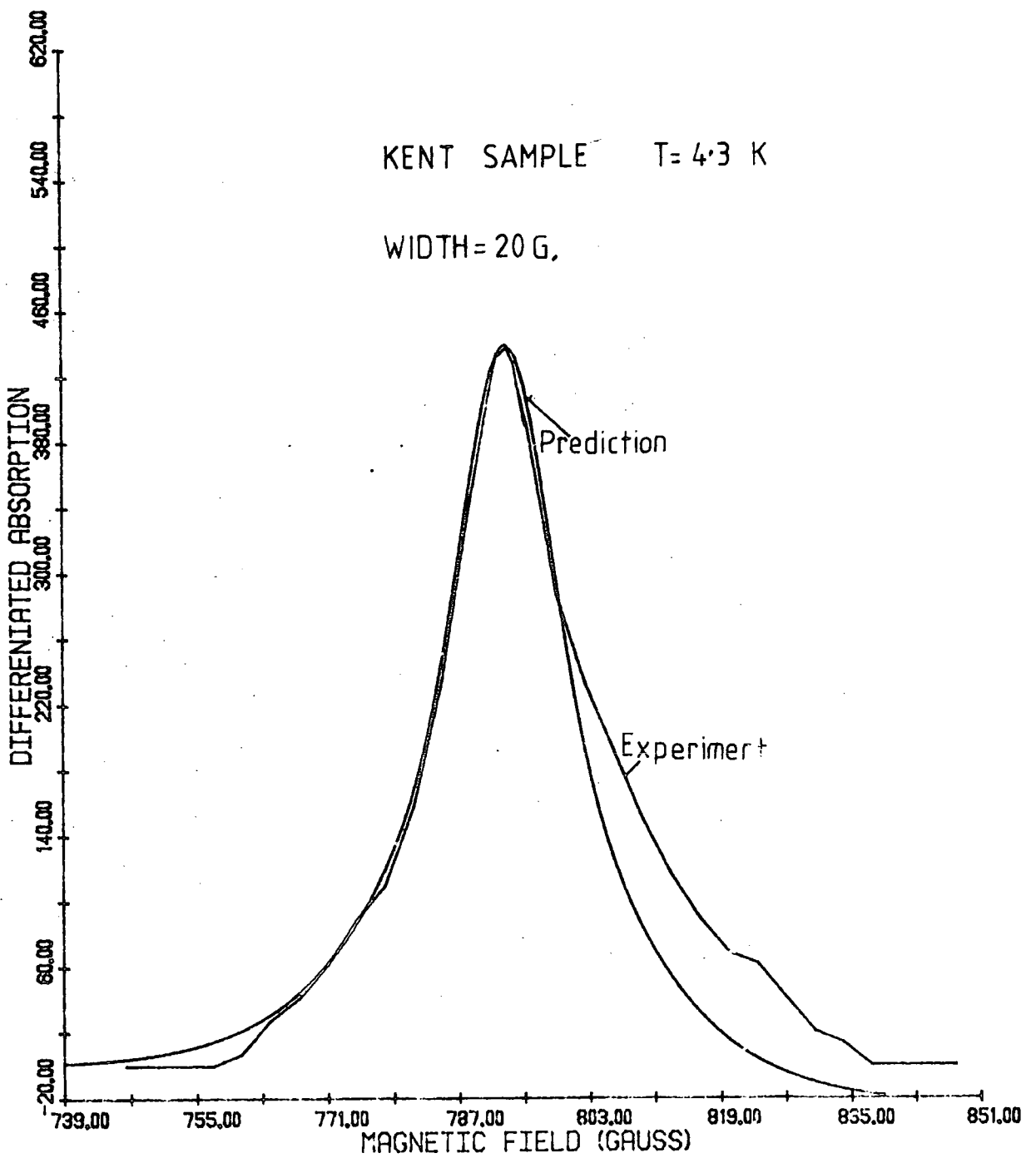
In the region T > 40 K it seems likely that the observed linewidth is due to strain broadening. Stoneham(1976)shows that a Lorentzian lineshape would be expected for a homogeneous distribution of point defects. From Fig 4. it can be seen that at the fringe of the feature it diverges from a Lorentzian in fact tending towards a Gaussian in the tails so the lineshape cannot be due entirely to point defects although they would appear to be the dominant cause.

At lower temperatures some of the pigments show a Gaussian lineshape with a narrower linewidth. There are several factors to be taken into account. Firstly there will still be strain broadening effects present. Secondly there will be spin lattice broadening and these two should be represented by two lineshape functions which should be convoluted together to give the final lineshape. No account was made in the computations for the anisotropy of T_1 (and hence the spin lattice linewidth) of the strain effects. Tanaka et al (1980) describe both these effects but offer no explanation for the size of the anisotropy.

Several authors (Poole and Farach (1971,1972) and Abragam and Bleaney (1970) give examples) show that a Gaussian line can result from inhomogeneous broadening of a homogeneously broadened Lorentzian lineshape.

According to Tanaka et al (1980) T_1 for Fe^{3+} ion in rutile is of the order of 1 msec for a temperature of 5 to 10 K. From Poole and Farach (1972) for a Lorentzian line :-

$$T_1 = \frac{1}{\pi 3^{\frac{1}{2}} \gamma \Delta H_{pp}}$$

where ΔH_{pp} (the peak-peak distance of the differentiated Lorentzian line) $= \Delta H/3^{\frac{1}{2}}$.

and $\Delta \nu = \gamma \Delta H$.

$$i.e. \ T_1 \ = \ -\frac{1}{\pi \Delta H} \cdot \frac{h}{g\beta}$$

$$so \ \Delta H \ = \ \frac{h}{g \ \beta \ \pi \ T_1}$$

and for $T_1 \simeq 1$ msec $\quad \Delta H = 8.7 \times 10^{-9}$ T, i.e. 8.7×10^{-5} G - far too small to explain the observed line and so no firm statement can be made about which process causes this change.

Not all of the samples showed this rise. In fact the X11 and X5 pigment showed little or no change with temperature and so it is possible that some form of cross-relaxation with another impurity or defect site causes relaxation mechanism that dominates at low temperatures.

4.3.2 Fe^{3+} in Rhombic Symmetry (Spectrum C)

Figure 3.12 shows this line. The width is about 70 Gauss. No attempt was made to simulate this line exactly becasue the width is likely to be caused by two very different effects. The first is that while, as explained in Chapter 3, the line results from an isotropic $3 \leftrightarrow 4$ transition, this transition is unlikely to be exactly isotropic and so the variations in g value will contribute to the width of the line. The second is that all the broadening mechanisms discussed earlier are likely to occur especially the strain broadening because the rutile lattice must be particularly deformed in a local region around the ion to allow it to have rhombic symmetry. It would be impossible to separate these effects.

4.3.3 The g = 2.0 line (Spectrum F)

This line is shown in Fig 3.14 and simulations are shown in Figs 4.10 and 4.11. The lineshape changes as a function of temperature and the results are indicated on the diagrams. At 20 K the line was best simulated with a Lorentzian line broadening function with a width of $\approx$ 20 Gauss. This line was thought to be due to adsorbed He and only occurred on one sample.

Fig 4.10 : POWDER SPECTRA G.

gaussian linewidth 30G

DIFFERENIATED ABSORPTION

MAGNETIC FIELD (TESLA)
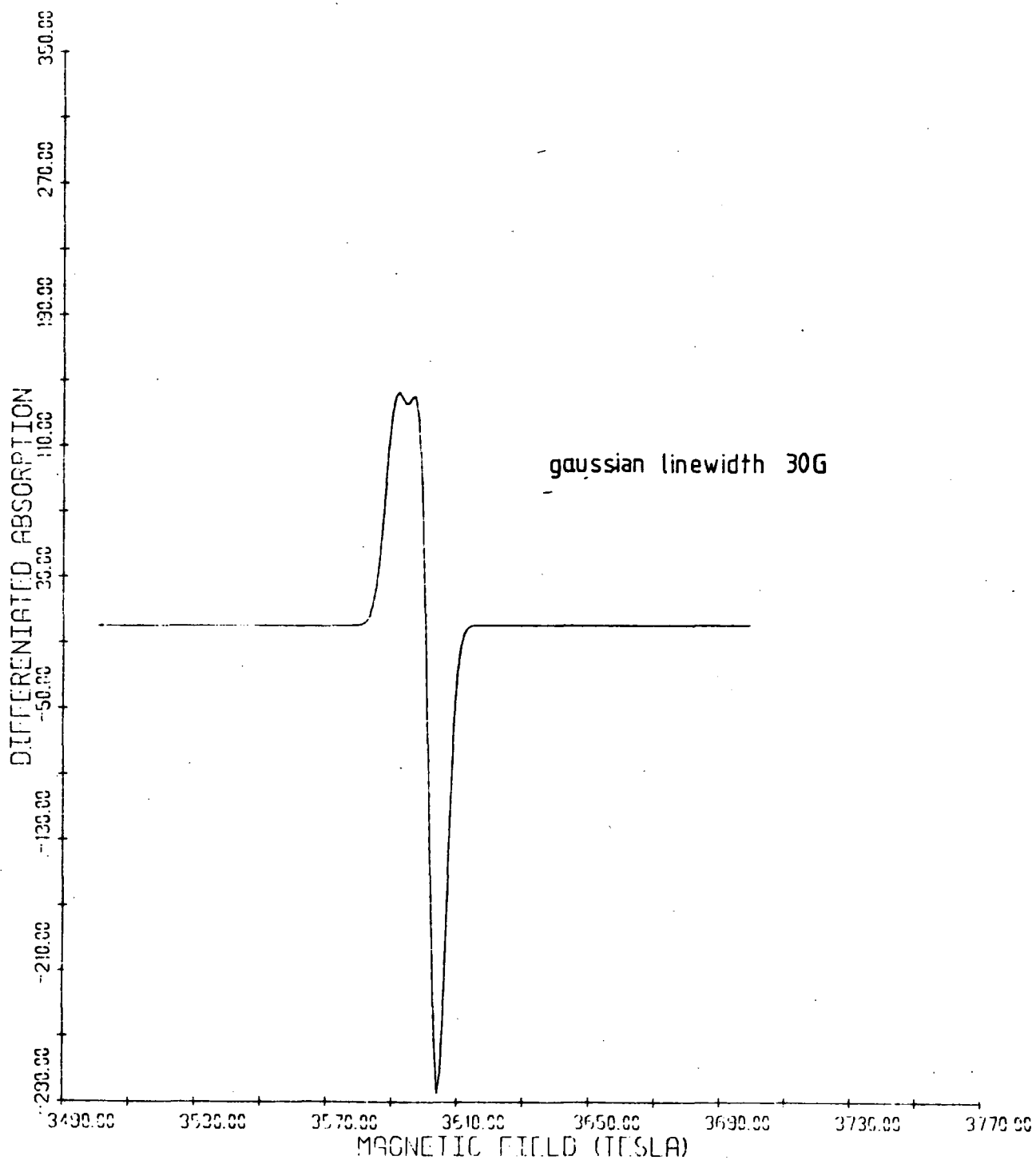
FIG.4.11. SIMULATION OF SPECTRUM F 4.0 K

Prediction

g = 2.017

g = 2.216

Experiment

20 G
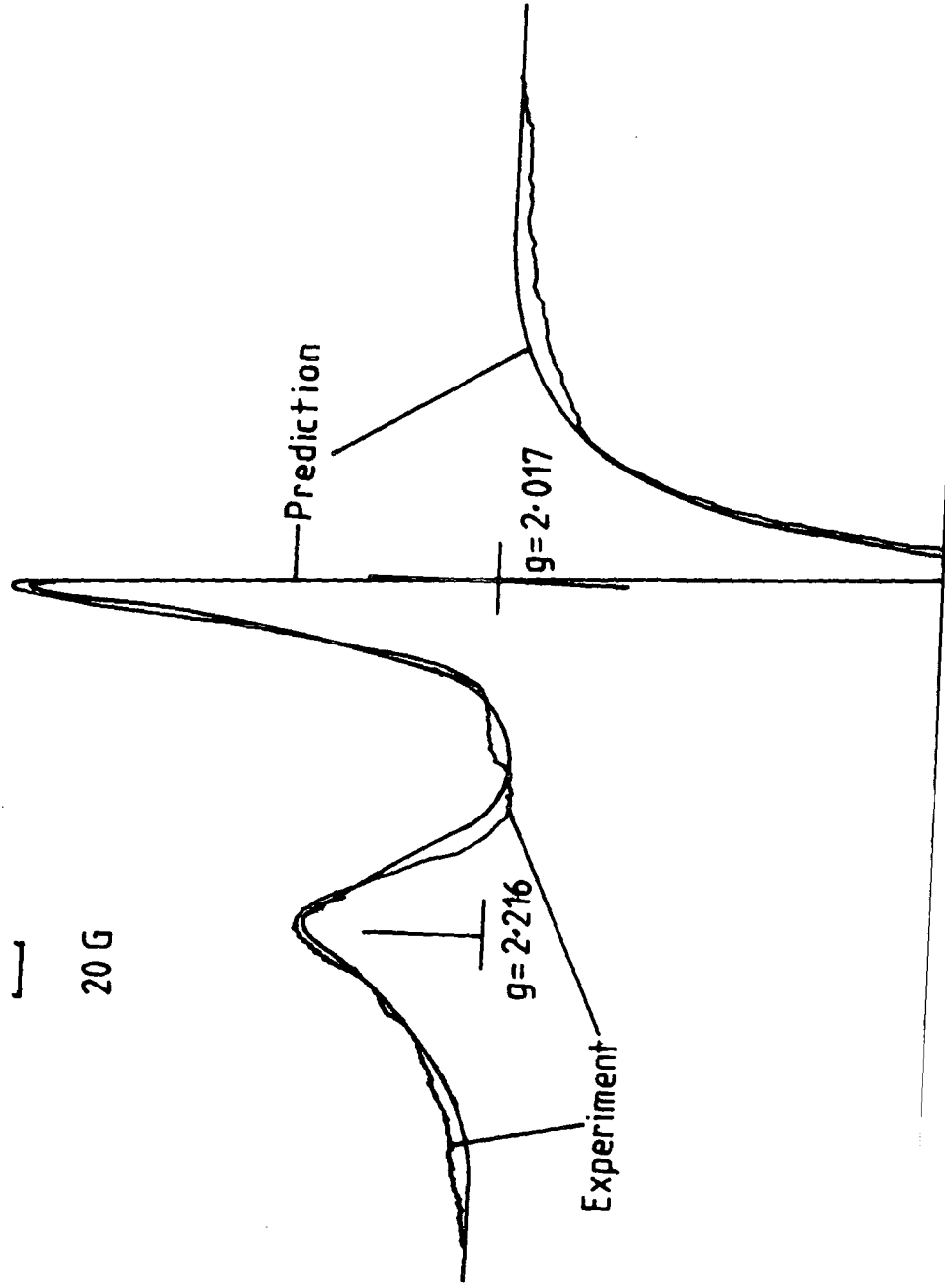
4.3.4 The Light-Induced Line (Spectrum G)

This line was simulated by a site with axial symmetry. The results are shown in Fig 4.10 and the linewidth appears to broaden at the lowest temperatures so that the axial nature of the site was not resolved. The simulated linewidths are shown in Table 4.1 below :

TABLE 4.1 :   Linewidth of the Light Induced Line

Temperature (K)	Width (G) (Lorentzian)
4.2	18
10.3	12
20	8
40	6
60	6
100	∿ 10

4.3.5 Other Features

The large feature near g = 2, signal $\emptyset$ was probably due to several defects (see Chapter 5) and so no simulation of its shape was possible as no detailed information about what was causing the feature could be obtained. There was little change in these features except for a gradual elimination with increasing temperature until it could not be at 77 K.

The other Fe^{3+} substitutional ion features observed (in fact parts of one continuous spectrum underlying the whole range observed) were not examined in detail because they were small with respect to the noise.

4.4   CONCLUSIONS

The shape of the Fe^{3+} spectra was the only one that could be examined in detail and that gave a Lorentzian of width 10 Gauss for temperatures above 40 K. This is probably due to strain broadening caused by, mainly point defects. Below 40 K some samples showed change in lineshape to Gaussian and with a decreased linewidth. This is possibly partially due to some form of spin-lattice effect dominating perhaps a cross-relaxation phenomena.

The light induced line had a width of 8 Gauss and a Lorentzian line-shape. This showed a broadening at lower temperature.

The adsorbed He line had a width of about 10 Gauss and again a Lorentzian lineshape.

CHAPTER 5

5.1 INTRODUCTION

Several investigations into the nature and perfection of the crystallites making up the pigment specimens were made. Each pigment comprises of small particles about $0.5\ \mu m$ in diameter and this means that each gram of pigment has a surface area of about 7 m^2. It has been noted by Tioxide International Limited, who made the pigments, that the composition as deduced from the mass spectroscopic analysis changes quite radically when the samples are etched with hydrofluoric acid. For example, an undoped specimen of sample XII gives a concentration of 1.80% Al_2O_3 before etching and after 5% of the mass has been removed the concentration of Al_2O_3 is 1.07%, so what is the alumina concentration of the etched 5% ? If 1 gram of powder has 1.8% Al_2O_3, that is 0.018 grams Al_2O_3. After etching we have 0.95 grams of Powder with 1.07% Al_2O_3, i.e. 0.0107 grams Al_2O_3 so 0.0078 grams have been lost which means that the concentration of Al_2O_3 is :-

$$\frac{0.0075}{0.05}\ \times 100\% \ \equiv 15.7\%$$

So the material lost by the etching contains about 16% Al_2O_3. Other samples yield higher amounts up to about 18% for XII samples and for X5 samples which have less alumina the figure is about 8% when the concentration measured before etching is approximately 0.6%.

Similarly for iron although the iron was added as a dopant later. For sample X11/500 the total iron concentration decreases from 290 to 150 ppm. Following a similar line of reasoning we can calculate that the material removed by etching had a concentration of about 3000 ppm. (It will be shown later that there is no similar concentration of the two Fe^{3+} ion sites detected by E.P.R. at the surface).

It should be remembered that removal of 5% of the mass of a particle is a small amount which will not appreciably change the size of that particle. This can be demonstrated by some simple calculations. If we assume the particle is a sphere of radius R and mass M and density ρ

$$M = \frac{4}{3} \pi R^3 \rho$$

If the original particle has mass M_1 and radius R_1 and after etching radius M_2 and R_2,

$$\frac{M_1}{M_2} = \frac{R_1^3}{R_2^3}$$

and if $M_2 = .95\ M_1$ and $R_1 = 1 \times 10^{-6}$ m

$$R_2^3 = .95\ (1 \times 10^{-6})^3$$

$$R_2 = 0.983 \times 10^{-6}$$

so the radius has been reduced by about 170 $\overset{o}{A}$.

5.2 INFRA-RED ABSORPTION

A standard method of examining powders was used. Some of the pigment was mixed with K Br (which is transparent to 1.R) and this mixture was then squeezed in a press to form a solid disc. The reason for adding K Br is that there must be sufficient material to make the disc mechanically sound but that would involve using so much TiO_2 that no light would get through the sample and so the TiO_2 is diluted with KBr. A conventional double beam instrument was used and the results are shown in Figures 5.1 - 5.3.

One spectra (Fig 5.3) is not of a pigment but of a sample of pure TiO_2 (Matthey "Specpure" from Johnson Matthey & Co.Ltd, London). The vertical

WAVELENGTH (Microns)

0·61% Al_2O_3

1·56% Al_2O_3

3·28% Al_2O_3

FIG. 5·1   INFRARED ABSORPTION OF UNTREATED RUTILE PIGMENTS.

% Transmittance

WAVELENGTH (Microns)

0·61% Al₂O₃

1·56% Al₂O₃

3·28% Al₂O₃
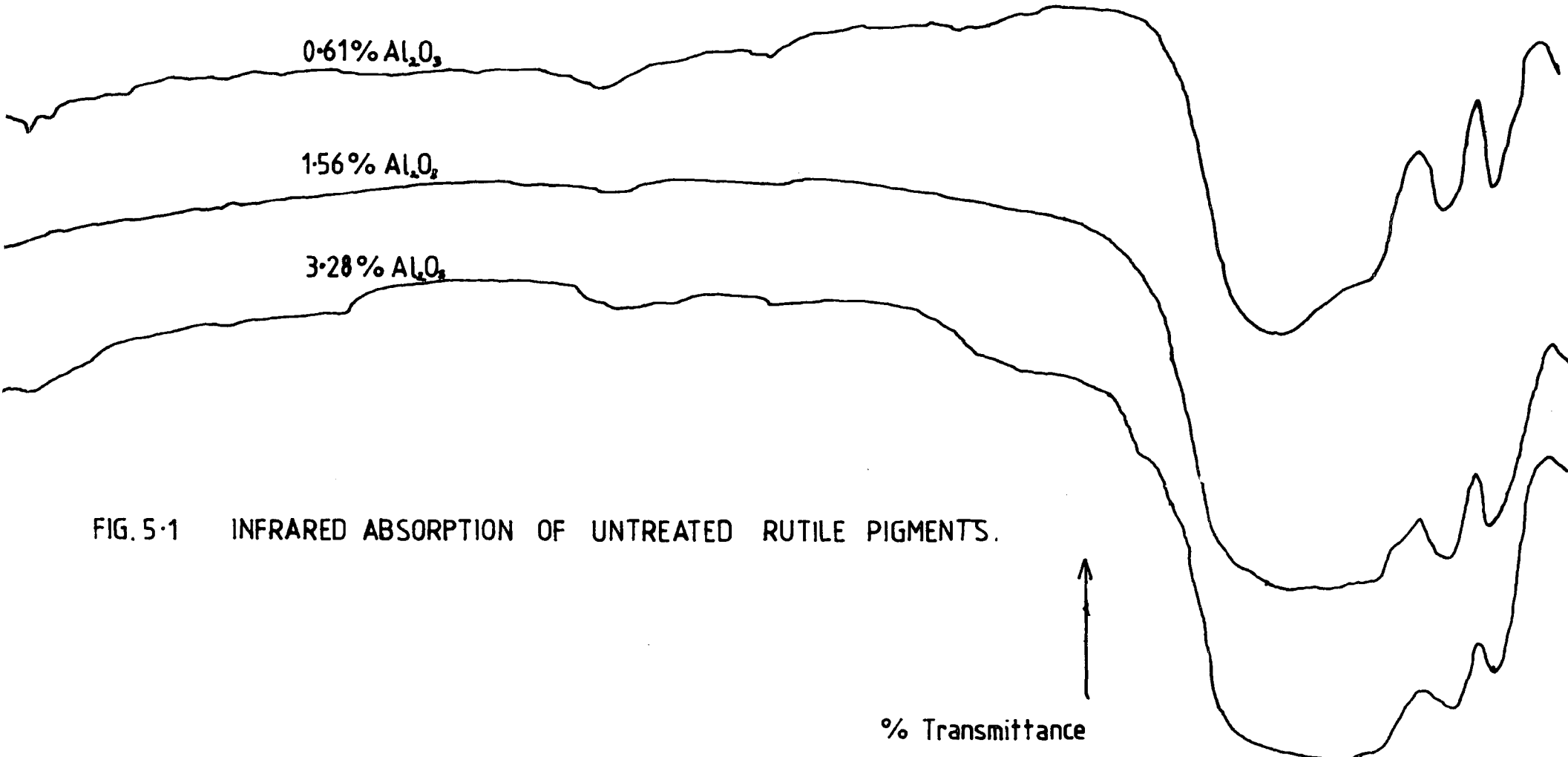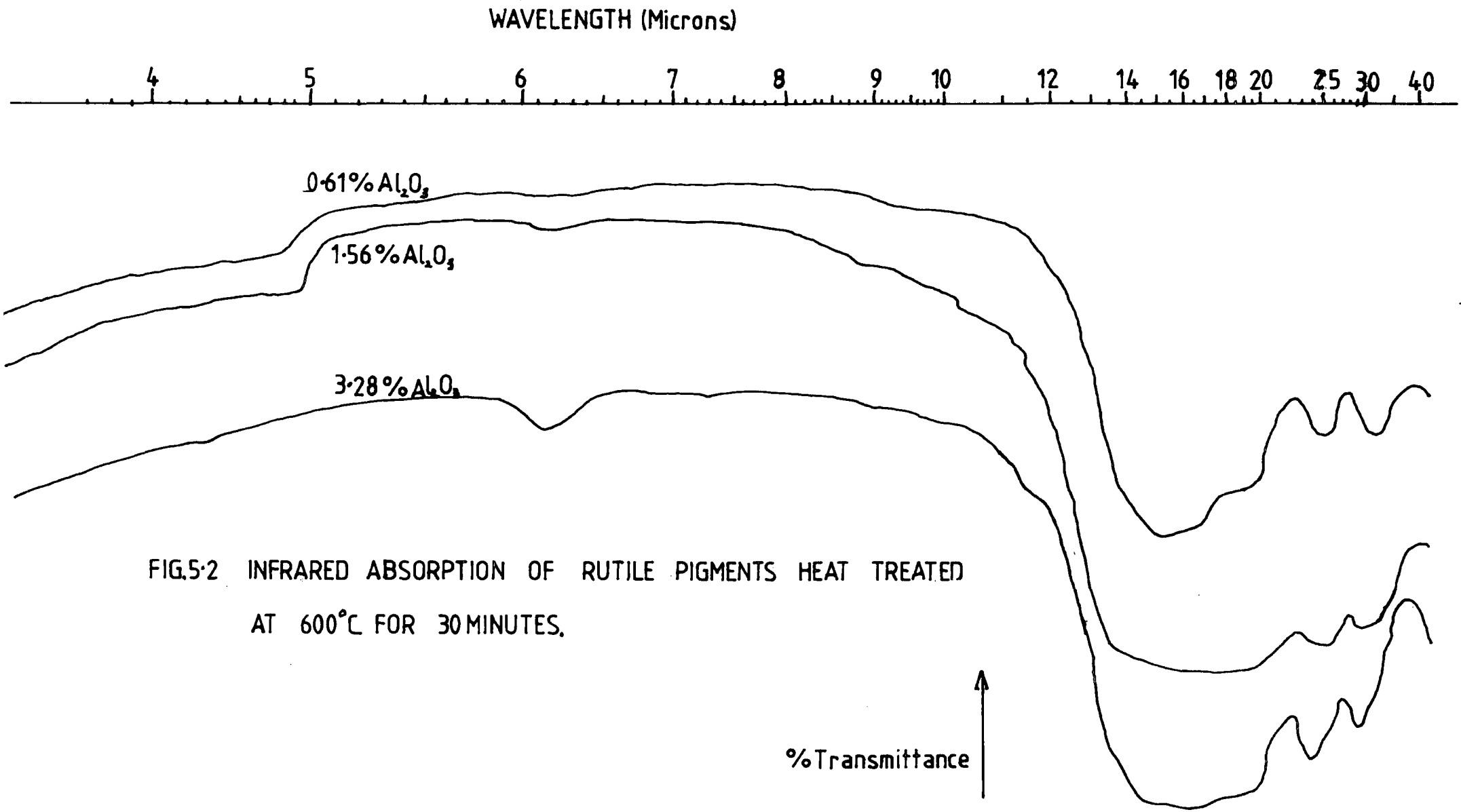
FIG.5·2 INFRARED ABSORPTION OF RUTILE PIGMENTS HEAT TREATED
AT 600°C FOR 30 MINUTES.

% Transmittance

WAVELENGTH (Microns)

4   5   6   7   8   9   10   12   14   16   18   20   25   30   35   40
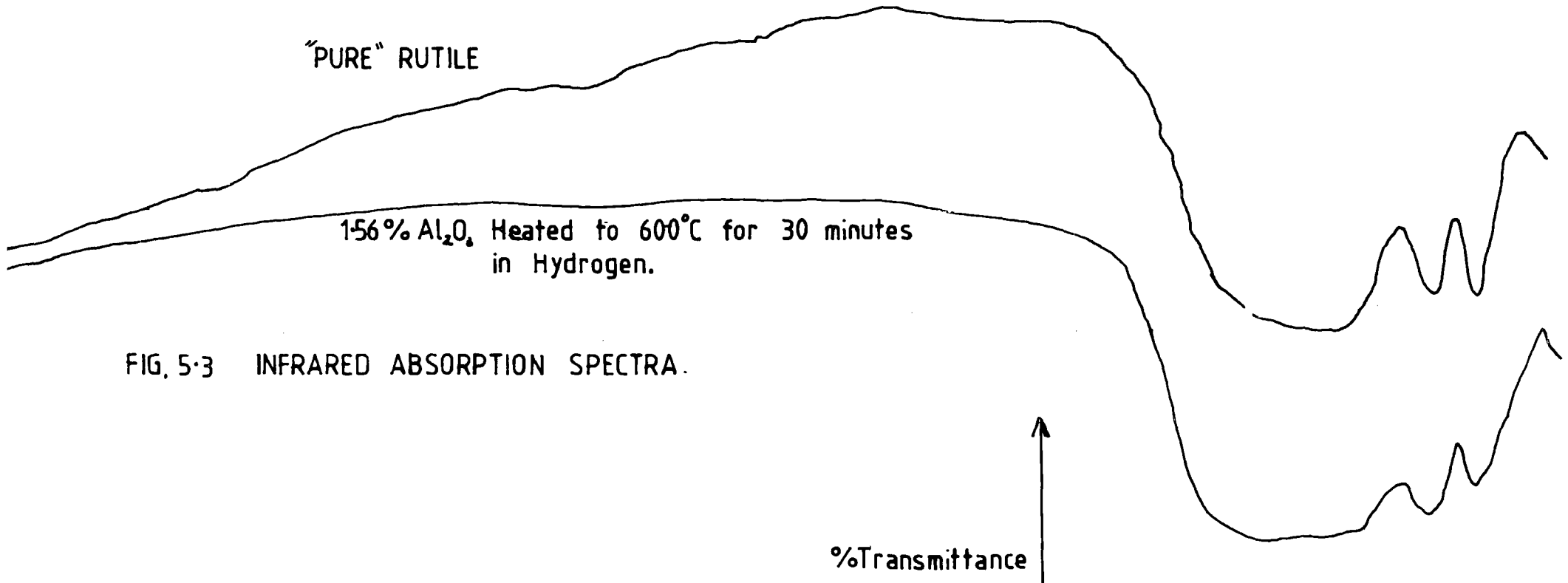
"PURE" RUTILE

1·56% Al_2O_3 Heated to 600°C for 30 minutes in Hydrogen.

FIG. 5·3   INFRARED ABSORPTION SPECTRA.

%Transmittance

scale is in percentage transmittance and so absorption peaks are downward pointing dips. There is a steady rise in transmittance from a wavelength of 2.5 microns to 10 microns. Then there are three absorption peaks at 25, 29.5 microns and a broad peak in the region 18-2c microns. In some of the pigments this broad line is resolved more clearly and can be seen to comprise two peaks one at 15.2 microns and the other at 18.5 microns. There is little variation between the pigments only the fact that in some of the pigments the lines are broader than in others. Table 5.1 lists the pigments used and the Al_2O_3 content in them. They were not doped with iron.

TABLE 5.1 : I.R. Absorption Samples

Pigment	Al_2O_3 Concentration	Notes	Fig No.
A	0.61 %	-	5.1
B	0.61 %	Heated 600°C for 30 mins. in air	5.2
C	3.1 %	-	5.1
D	3.1 %	Heated 600°C for 30 mins. in air	5.2
E	1.6 %	-	5.1
F	1.6 %	Heated 600°C for 30 mins. in air	5.2
G	1.6 %	H4ated for 600°C for 30 mins in Hydrogen.	5.3

A test run made with a disc of Potassium Bromide without any TiO_2 added; showed no dips and as it had a much larger amount of material than the discs containing TiO_2 there is no doubt that the peaks are due to TiO_2. The data is summarised in Table 5.2.

The absorption peaks occur at 345, 420, 520 and 645 cm^{-1} which would be expected by consulting the existing literature. There have been several

studies of the I.R. spectra of single crystal rutile. For instance the authors

Narganson (1950 and 1953), McDevitt and Baun(1964), Matossi (1951) who

also calculated the spectra and Von Hippel et al (1962) and Spitzer et al

(1951) who published reflectance spectra compares well $_\wedge$ $with$ the results described

here. In fact the latters' results show the broad peak at about 600 cm^{-1}

splitting into two poorly resolved peaks. There should be four optically

active modes, one in the c-axis direction corresponding to a displacement

of the cation against the anion sublattice (A_{2u}) and three double degenerate

modes (E_u) normal to the optic axis. One of these is at 130 cm^{-1} outside

the range of the instrument. The additional maxima (the one at 420 cm^{-1} has

not been explained). So to conclude this section, the I.R. absorption

spectrum is what would be expected from well known single crystal results

and the only effect of the varying amount of Al_2O_3 and heat treatment was

to vary the width of the lines. However, this broadening did not have any

obvious relationship to the treatment or composition except that the sample

with least Al_2O_3 appeared to have the narrowest lines.

5.3   X-RAY INVESTIGATIONS

The first step in this investigation was to take X-ray powder

photographs. Copper K_α radiation was used. A set of samples was looked

at with a range of Al_2O_3 and iron concentrations but no difference between

any of the samples was noticed. The photographs gave unit cell parameters

of :-

a = 4.593 $\pm$ 0.005 $\overset{o}{A}$

c = 2.955 $\pm$ 0.005 $\overset{o}{A}$

which agree with the published dimension of a = 4.5937 $\overset{o}{A}$ and c = 2.9581 $\overset{o}{A}$.

(Blanchin et al (1981)).

Care had to be taken to filter the fluorescent radiation from the

rutile as the titanium ions would fluoresce in Cu K_α X-ray radiation.

TABLE 5.2 :   I.R. Absorption of Rutile Pigments

Sample	Peaks (microns)			
A	15.5	18.8	24.0	29
B	16.0	18.8	25.0	30.2
C	15 - 19		24.0	30.
D	15 - 19		23.5	29
E	15 - 19		24.0	28.5
F	15 - 20		24 - 26	31
G	15 - 20		24	28.5
"Pure"	15 - 20		25	29.5

Note : As the peaks are all relatively broad and overlap the peak

position tends to move as the linewidth changes and so the above figures

are only approximate.

Next an X-ray diffractometer was used. Again Cu Kα radiation was
used with a nickel filter. The counter was a sealed proportional type and
was moved at a rate of 1^O of 2θ per minute. The results are shown in
Fig. 5. 4. The first four pigments gave the same result (a). These are
as follows :-

TABLE 5.3

Sample	Composition		
X5/BK	0.57	% Al_2O_3 ;	10 ppm Fe
X5/1000	0.57	% Al_2O_3 ;	620 ppm Fe
X11/BK	1.81	% Al_2O_3 ;	10 ppm Fe
X11/1000	1.81	% Al_2O_3 ;	670 ppm Fe
Kent	0.002	% Al_2O_3 ;	1.0 % Fe

Note : The two pigments with low iron concentrations, X5/BK and
X11/BK were not doped with iron although they were treated
the same as the other pigments. The iron was present when the
pigments were made. The Kent sample is a crushed single crystal.

The X-ray diffractograms of the pigments are all the same and show all the
expected lines. These have been labelled with the corresponding crystallo-
graphic planes. They confirm the previous results using X-ray powder photo-
graphs and I.R. absorption measurements that the pigments are composed of
rutile crystal particles and that there is no sign of other phases occurring.
The width of the lines indicates that the crystallites have a good crystal
structure even though we know from E.P.R. measurements that there is strain
present in them. This must be true as if their structure was grossly distorted
than the E.P.R. spectra of the Fe^{3+} substitutional ions would not occur or

KENT SAMPLE

X 5 / BLANK SAMPLE

330 410 400 212 202 311 301 221 002 220 211 210 111 200 101 110
222 321 112 310
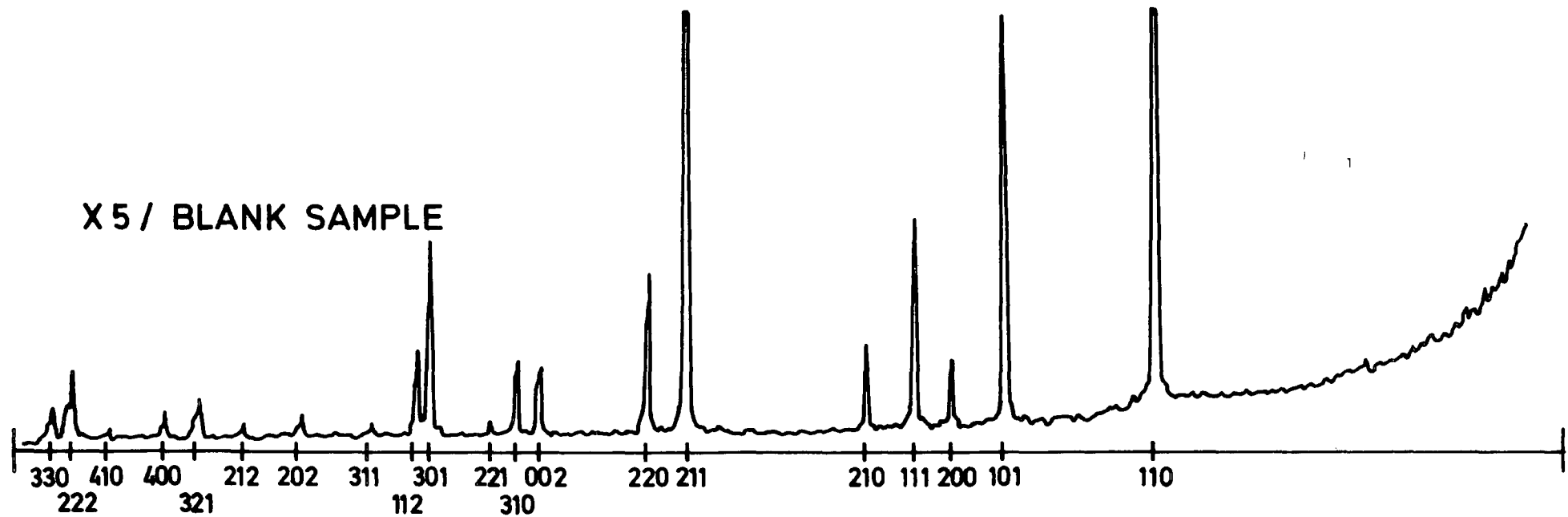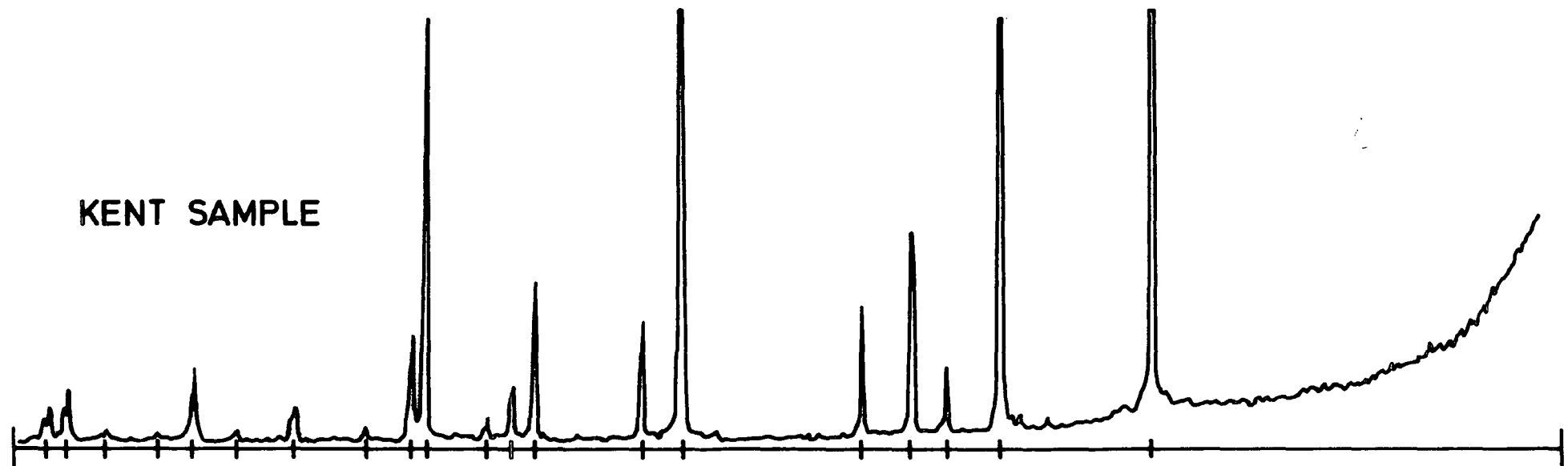
X-RAY DIFFRACTOMETER RESULTS

would be shifted to other g values, however we just observe the effect of strain through line broadening.

However, the diffractogram from the Kent sample (Fig 5.4b),which was a heavily doped single crystal,which had been crushed to a powder,was different. Although all the lines were present they had considerably different amplitudes. For example, the 002 and 310 lines in the pigments have about the same amplitude, while the 221 line next to them can just be seen. In the spectrum of the Kent crystal the 002 line is over twice the amplitude of the 310 line. Also the 301 line is considerably larger than would be expected. This line also shows a double peak although this could be the $K\alpha_1$ and $K\alpha_2$ lines being resolved. The doubling of all the high theta line is due to the resolution improving at this end of the spectra.

We would expect this sample to have a poor crystal structure because the concentration of 1% iron is at the limit of the solid solution of iron in rutile and the crystal had the characteristic red colouration of iron precipitates in rutile.

5.4   S.E.M. OF DOPED RUTILE PIGMENTS

The samples were prepared by placing some of the powder on an adhesive tape on a metal mount. It was found that charging effects caused by the electron beam hitting the insulating pigment particles caused the image to be distorted so a layer of gold was sputtered onto the samples to conduct this charge away. This was done at a low temperature to ensure that the pigment was not affected in any way.

S.E.M. pictures of doped and etched rutile pigments were taken. The results are shown in Figs 5.5 to 5.8. These pictures all show a very interesting feature that the doped pigments all show large lumps (about 100μ wide) and all the etched samples similar but smaller lumps (about 20μ wide). It is thought that each "lump" is a piece of partially sintered powder which can be seen to consist of submicron sized pieces of powder.

FIG 5.5   S.E.M. PHOTOGRAPHS

X11/A

100μ

FIG 5.5   S.E.M. PHOTOGRAPHS

4μ

X11/A

X11/ B

4μ

X11/C

4μ

FIG 5·7   S.E.M.   PHOTOGRAPHS

X11/D

2μ
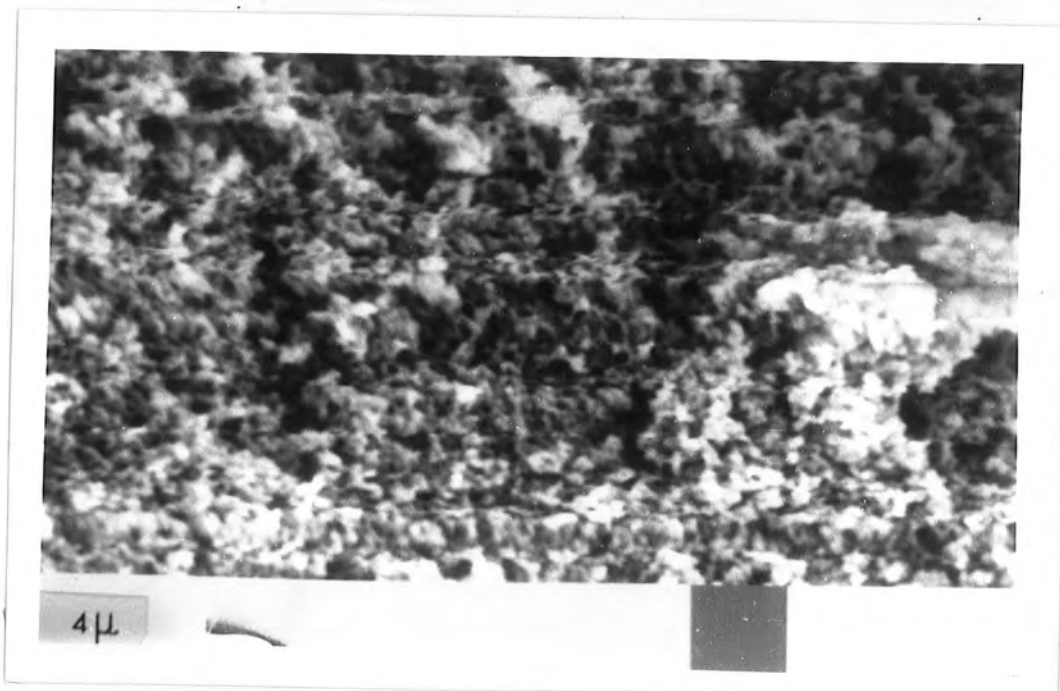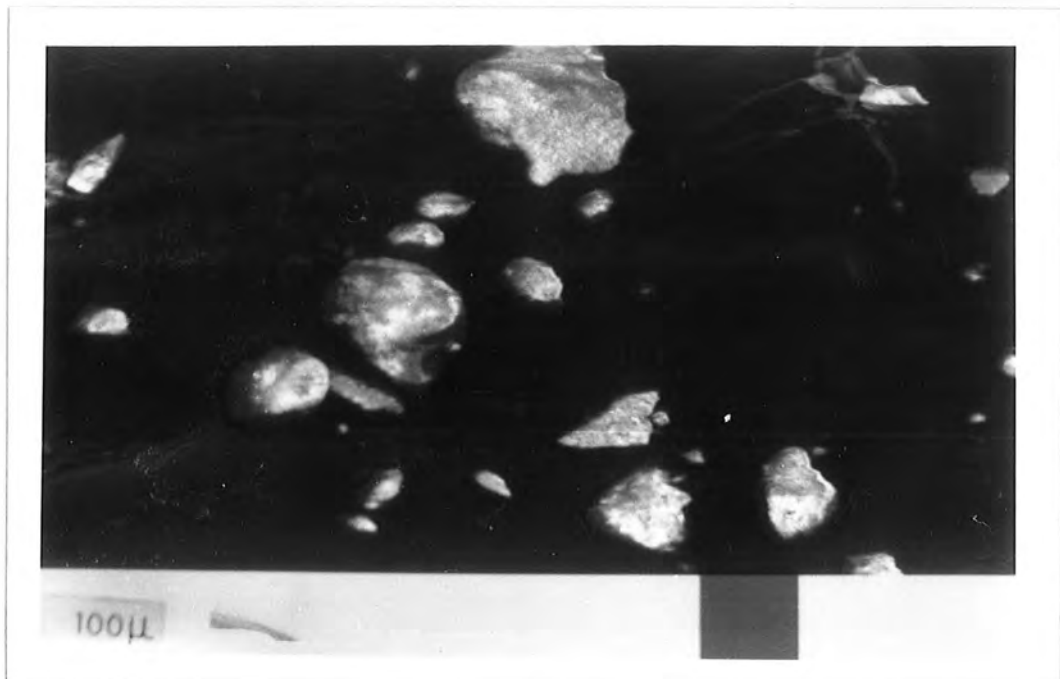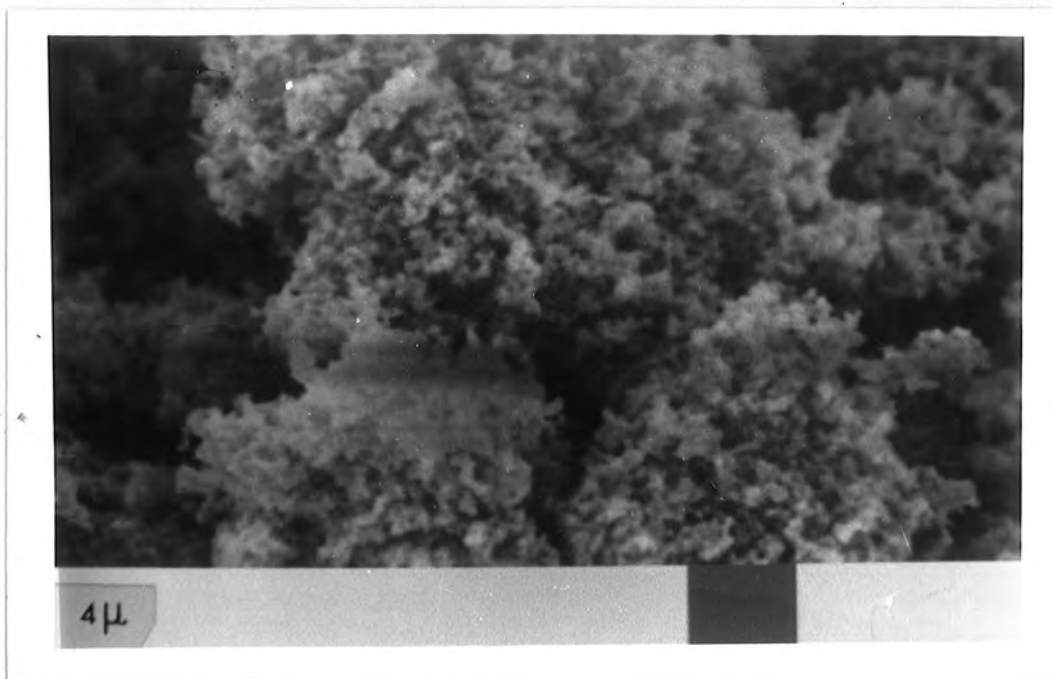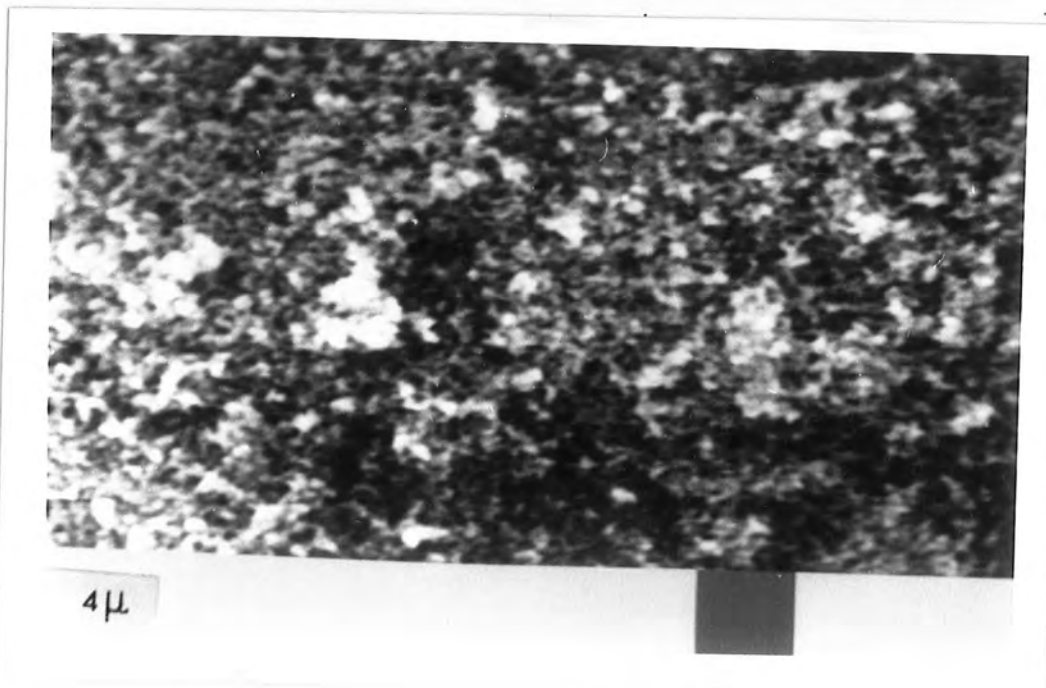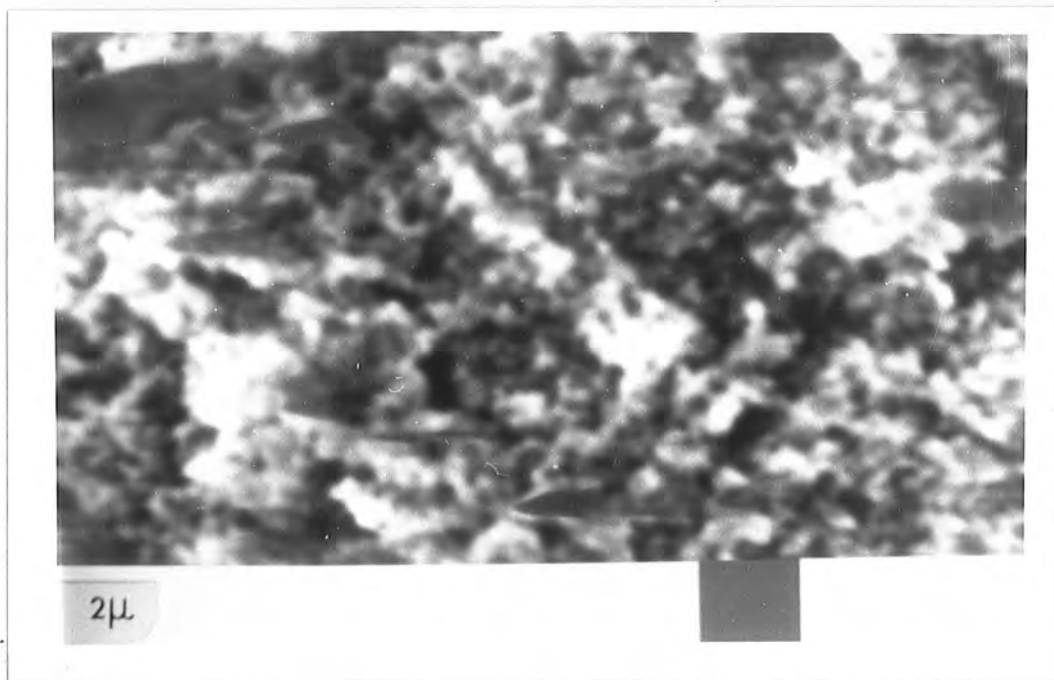
(Note bluring and distortion caused by charging of crystalites.)

20μ

FIG 5·8   S.E.M.   PHOTOGRAPHS
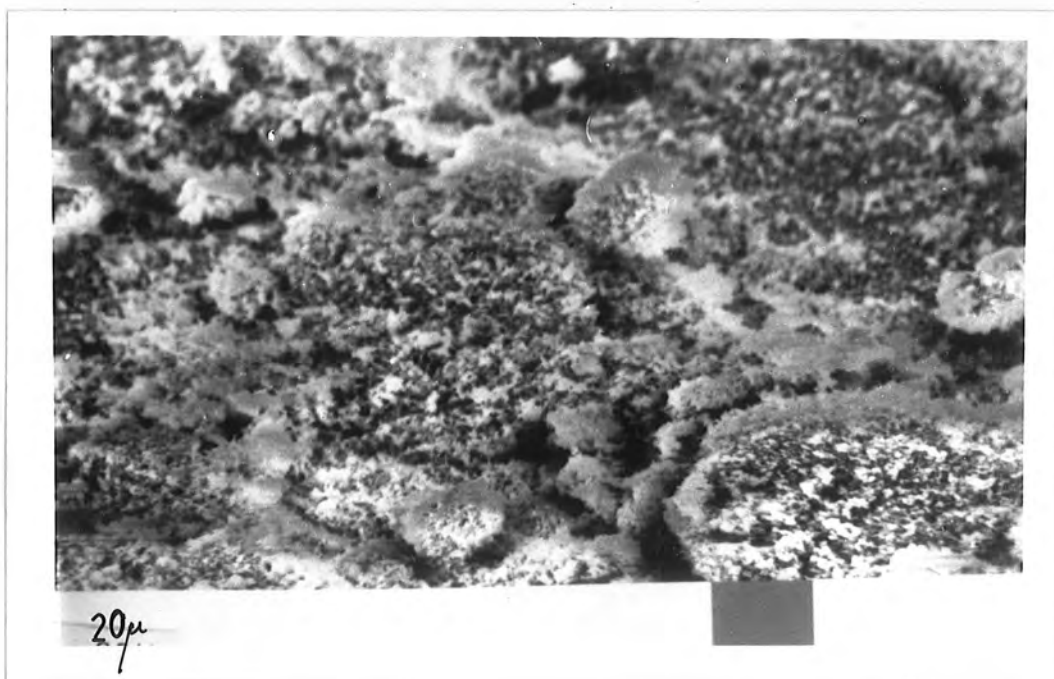
X11/E
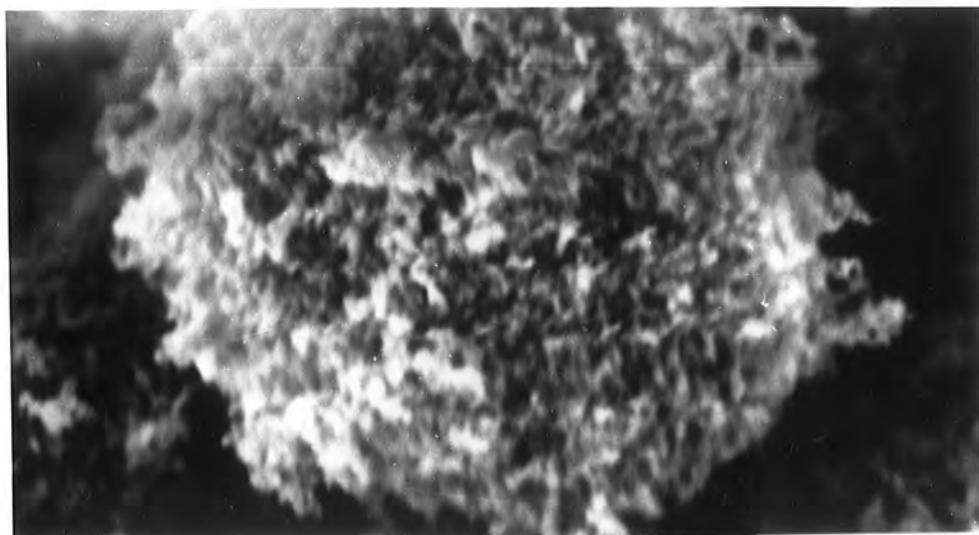
4μ
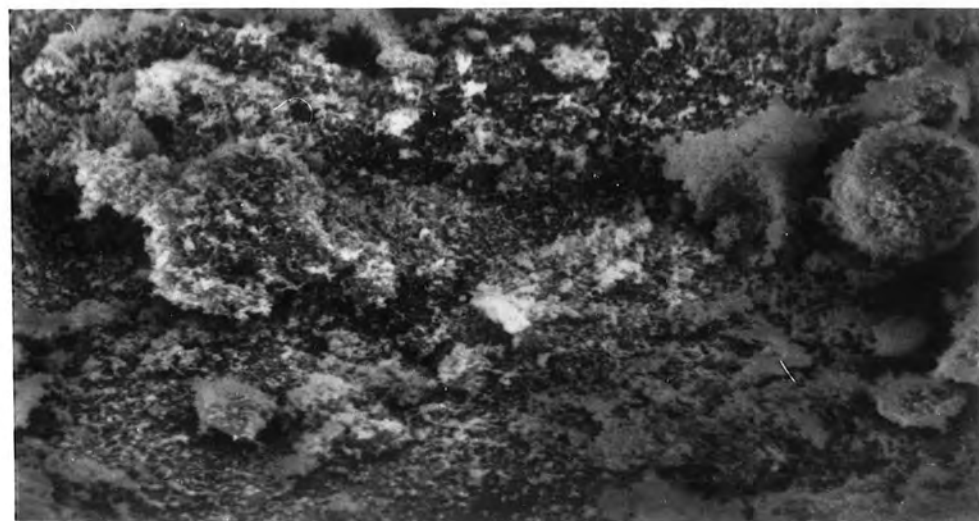
20μ

These would be the individual crystallites of the pigment.

There is no real variation that can be detected between the etched and unetched samples. The undoped pigment shows no agglomeration into larger particles while a sample that was treated the same as the doped samples but without the addition of iron did show the sintering. So this is thought to be a result of the doping procedure.

5.5 E.P.R. OBSERVATIONS OF ETCHED PIGMENTS

Each of the etched samples X11/A to X11/E was examined and the amplitude of each line and feature monitored. A similar amount of pigment was examined in each case, 0.1 grams, and so the amplitude was directly proportional to the concentration of the corresponding site. Fig 5.9 shows the amplitude of each line plotted against the mass lost by stripping. This shows that only one site was affected by the process that of signal D which was thought to be due to defect sites with 'g' values around g = 2.
Fig 5.10 shows how the amounts of iron vary through this etching process. Until approximately 10% of the mass of the pigment is lost the iron concentration drops sharply. (This concentration is the total amount of iron in the pigment as determined by mass spectroscopy). However, from Fig 5.9 we can see that the amount of Fe^{3+} substitutional ions and the Fe^{3+} in rhombic symmetry do not change throughout this etching process so the etched material must contain iron in some other state or site. The signal that does vary with iron concentration is probably due to signals from several sites superimposed to form the broad signal. These appear to all have been etched away by the time 10% of the mass of pigment has been removed.

5.6 CONCLUSIONS

The samples showed good crystallinity in the X-ray and I.R. results. Etching with HF removes areas of high Al and Fe content implying that the surfaces are more heavily doped than the bulk of the crystallite. However

FIG. 5.9   VARIATION OF SIGNAL AMPLITUDE WITH ETCHING
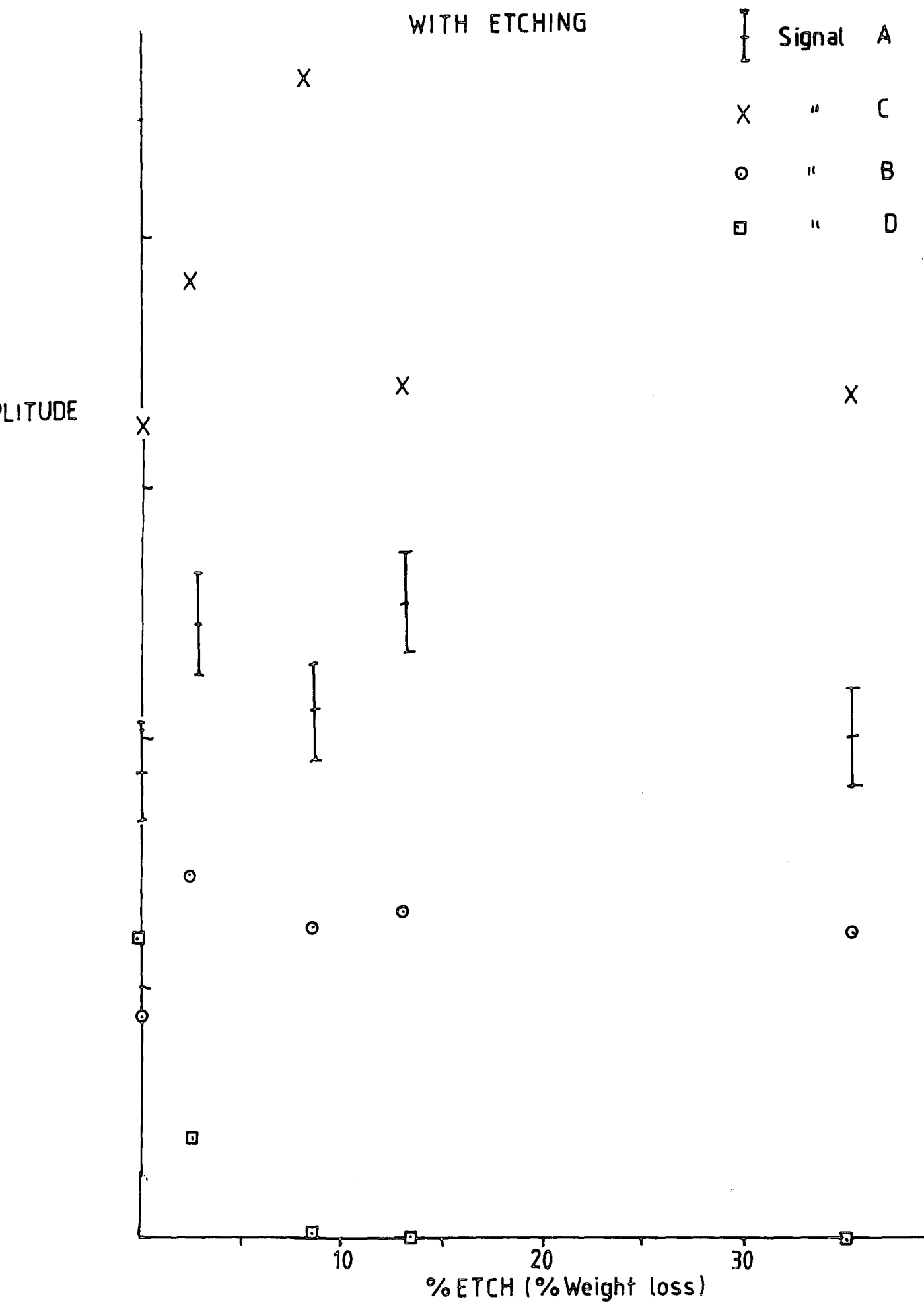
FIG.5·10 EFFECT ON IRON CONCENTRATION OF ETCHING
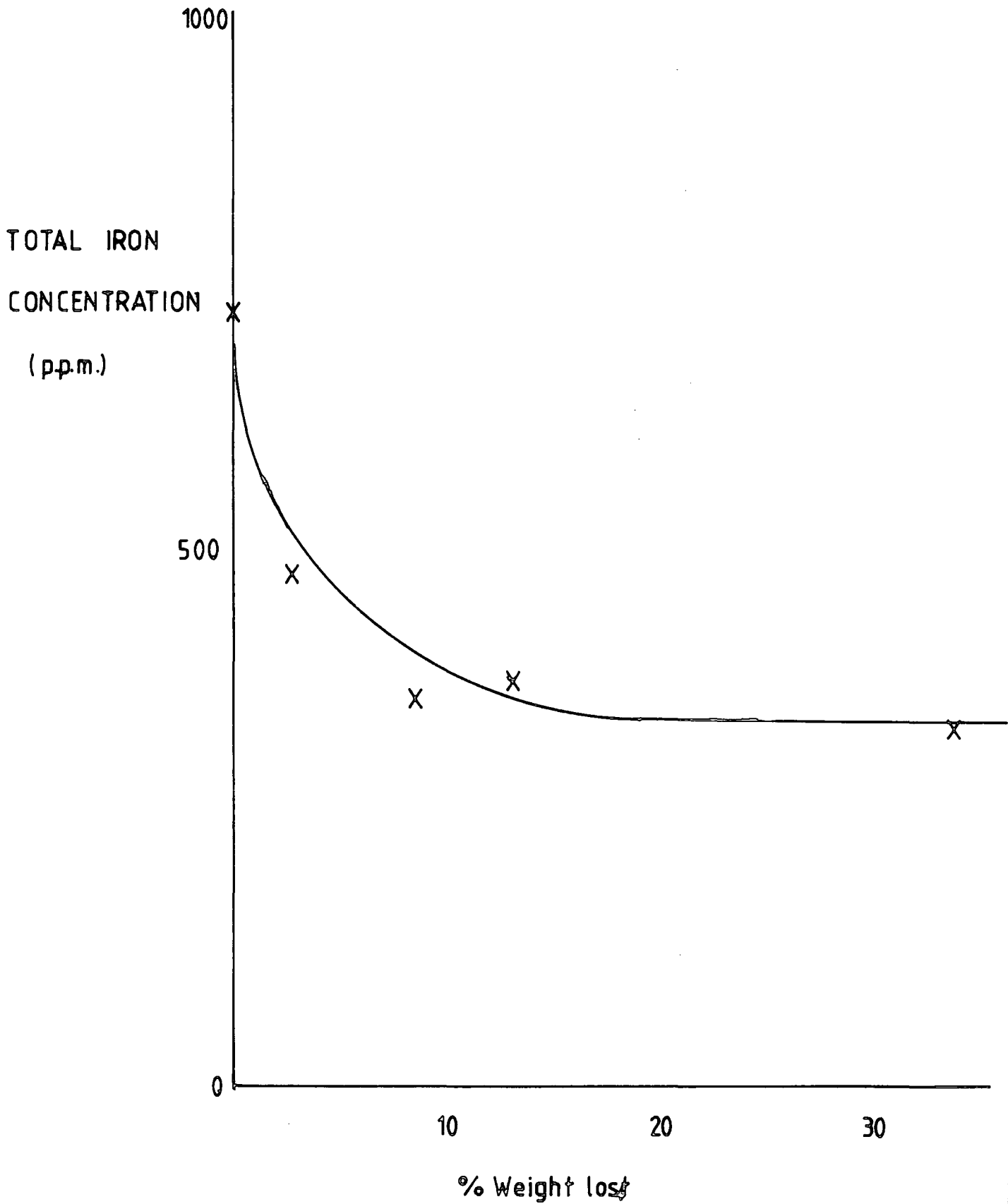
E.P.R. measurements show that neither iron in a substitutional site or in a site of rhombic symmetry decrease with etching so the iron removed must be in some other site or charge state.

The only E.P.R. spectra to be affected by the etching signal at about g = 2 is not seen in the highly etched samples and as was explained in Chapter 3, is probably due to defects, in view of this evidence probably surface defects.

Doping the pigments causes sintering which will not affect the E.P.R. spectra because the bulk of each particle is unaffected by the process.

CHAPTER 6

EFFECT OF U.V. IRRADIATION ON RUTILE PIGMENTS

6.1   EXPERIMENTAL

The samples were irradiated at a variety of temperatures using light from a 250 watt mercury lamp through some slots in the side of the cavity which allowed 50% of the incident light through. A set of band pass filters was used to find the wavelength of the light necessary to cause the various processes to occur. There were two main effects ; a new line with a g value of $\simeq 2.00$ (signal G) was seen and the amplitudes of the other spectra were also changed. After the experiment the absorbtion of the empty cavity was monitored to ensure that no centres were formed in the quartz by the irradiation.

6.2   RESULTS

Most of the spectra were affected by the irradiation but for most the effect was small. At low liquid helium temperatures the amplitude of most spectra was reduced. There were two major effects on Signal G and Fe^{3+} substitutional ions which are detailed in the following sections. Fig 6.1 shows the amplitude of signal F (the adsorbed He) during irradiation. This is the most noticeable of the results of irradiation on the remaining spectra. The effect on signal C was very small and decreased but was too small to measure accurately because of the width of the line. Signal D showed no change in irradiation.

6.2.1 Fe^{3+} Substitutional Ion

When the samples were irradiated with light below 40 K the amplitude of the line decreased (Fig 6.2). As the width of the line did not change this means that the number of Fe^{3+} ions has decreased.

FIG.6·1   EFFECT OF LIGHT ON SIGNAL F

SIGNAL
AMPLITUDE

(ARBITRARY

UNITS)

LAMP ON

NO FILTERS

LAMP OFF

LAMP ON

RED

FILTER

LAMP
OFF

LAMP ON

350 nm.

BAND-PASS

FILTER

LAMP OFF

5   10   15
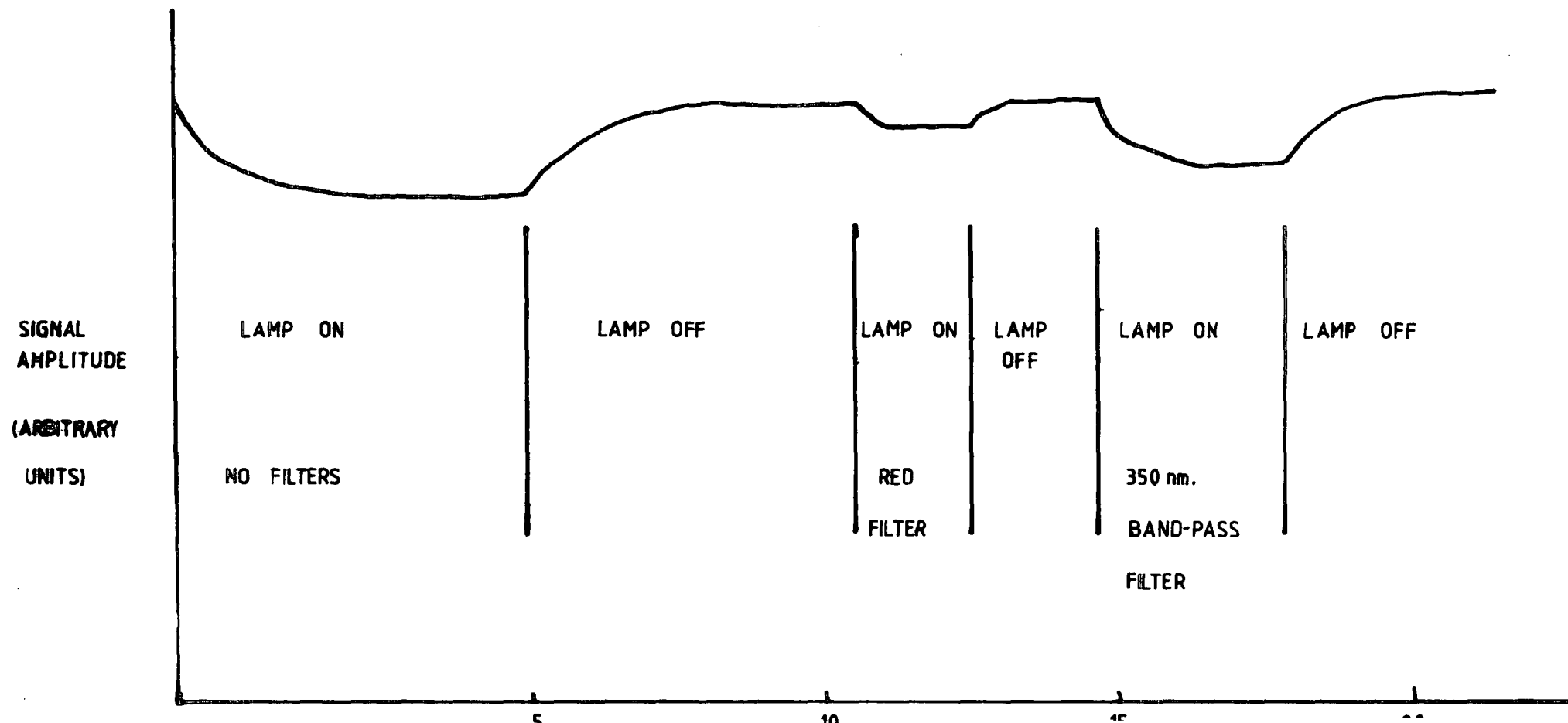
FIG. 6·2

EFFECT OF LIGHT ON THE Fe^{3+} SUBSTITUTIONAL FEATURE.

NOTE THAT THAT THE WIDTH (H_u-H_L) IS THE SAME FOR BOTH LINES AND THAT THE SHAPE IS UNCHANGED.

SAMPLE X11/1000
TEMPERATURE 5 K
H_u-H_L = 11 Gauss

LINE IN DARK

LINE AFTER ILLUMINATION

I_0

I_L

$I_0/2$

$I_L/2$

DIFFERENTIATED ABSORPTION

MAGNETIC FIELD

H_L H_0 H_u
793 Gauss
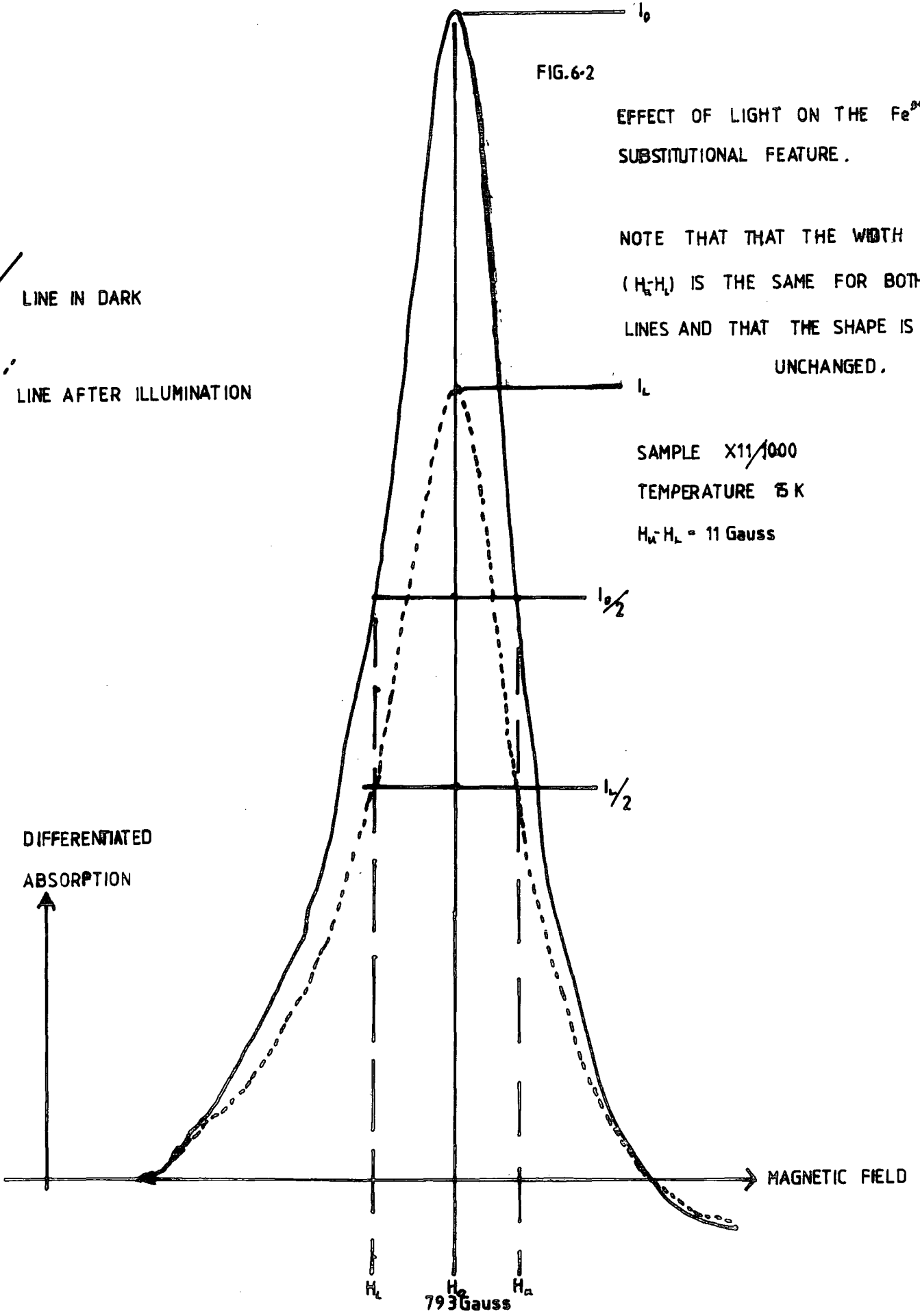
This was repeated at a variety of temperatures and the results are shown in Fig 6.3. The vertical axis shows the change in number of the Fe^{3+} ions I_L/I_D where

I_L = line intensity in light

I_D = line intensity in dark.

No change was seen above 40 K and a maxima in the effect was observed at 10 K. Where the light is removed the signal amplitude is restored to its original value.

The next experiment was to observe the effect of varying the wavelength of the illumination. Up to this state all the measurements were done with no filter between the lamp and sample. Figure 6.4 shows the effect on a few filters to illustrate the experiment. First the sample is in the dark and then a shutter opens and the signal amplitude is reduced. (This curve was drawn not by sweeping the magnetic field but just monitoring the peak of the Fe^{3+} feature and watching its height change). The introduction of either a 350 nm or 400 nm band pass filter had the same effect as closing the shutter but other filters had less effect. This shows that light of band gap energy ($\sim$ 3 eV) has no effect on the lines but light of a lower energy does effect the amplitude. The lines were most sensitive to light of wavelengths longer than about 700 nm (about 1.8 eV).

Several previous workers have looked at the effect of optical irradiation on the substitutional ion but they have all just examined the lines in single crystals. (Faughnan and Kiss (1968) ; Mizushima et al (1979), Hodgskiss (1981)). They all see changes in the iron spectra at 77 K and Hodgskiss reports changes up to 200 K. Also Mizushima et al (1979) show that their Fe^{3+} ions are most affected by light of about 3 eV, i.e. greater than the band gap and Faughnan uses light of 400 nm which changes the amplitude
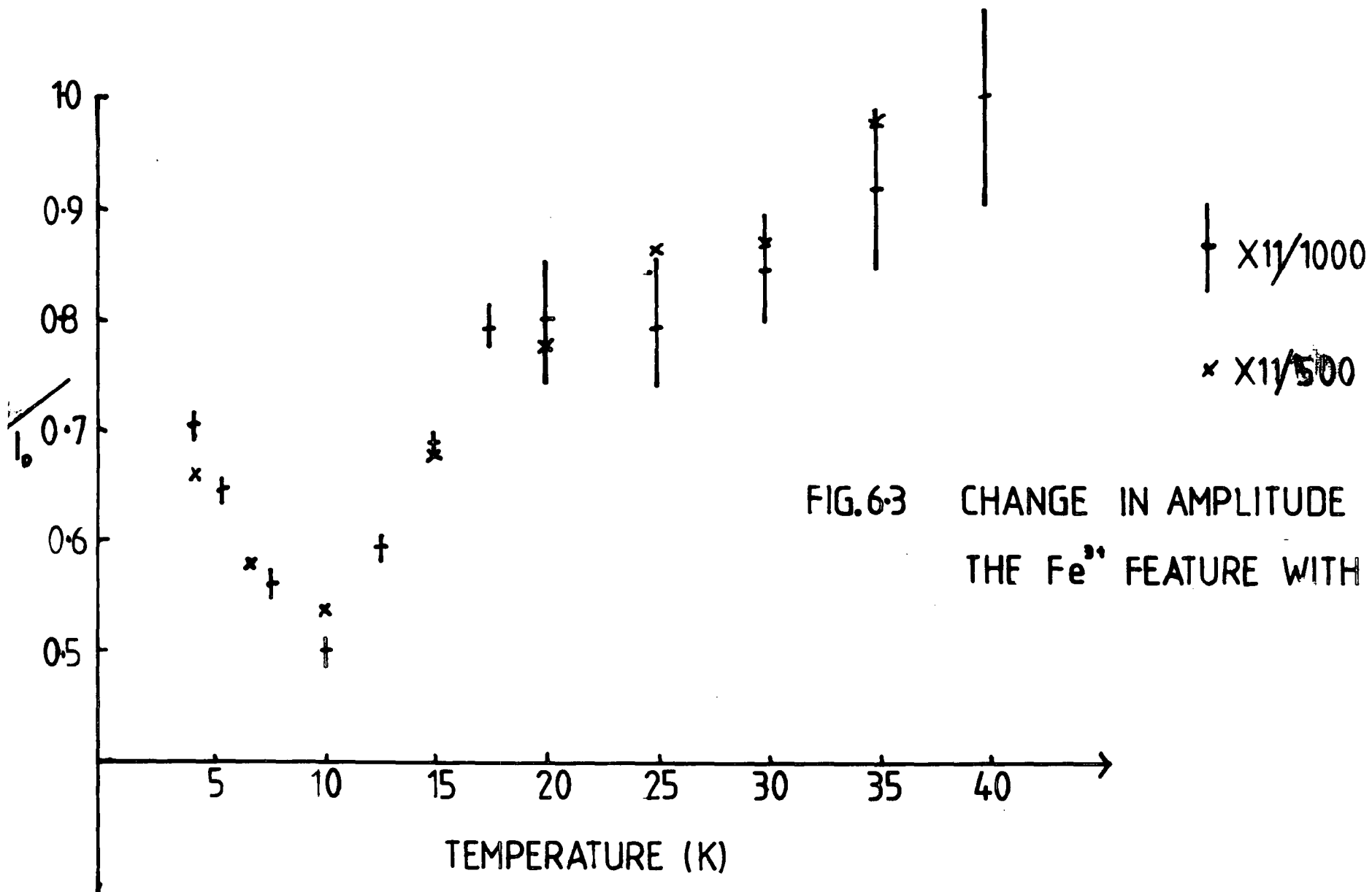
FIG.6.3   CHANGE IN AMPLITUDE OF
THE Fe'' FEATURE WITH ILLUMINATION

FIG. 6·4 EFFECT OF LIGHT ON THE $g = 8·18$ Fe^{3+} LINE.
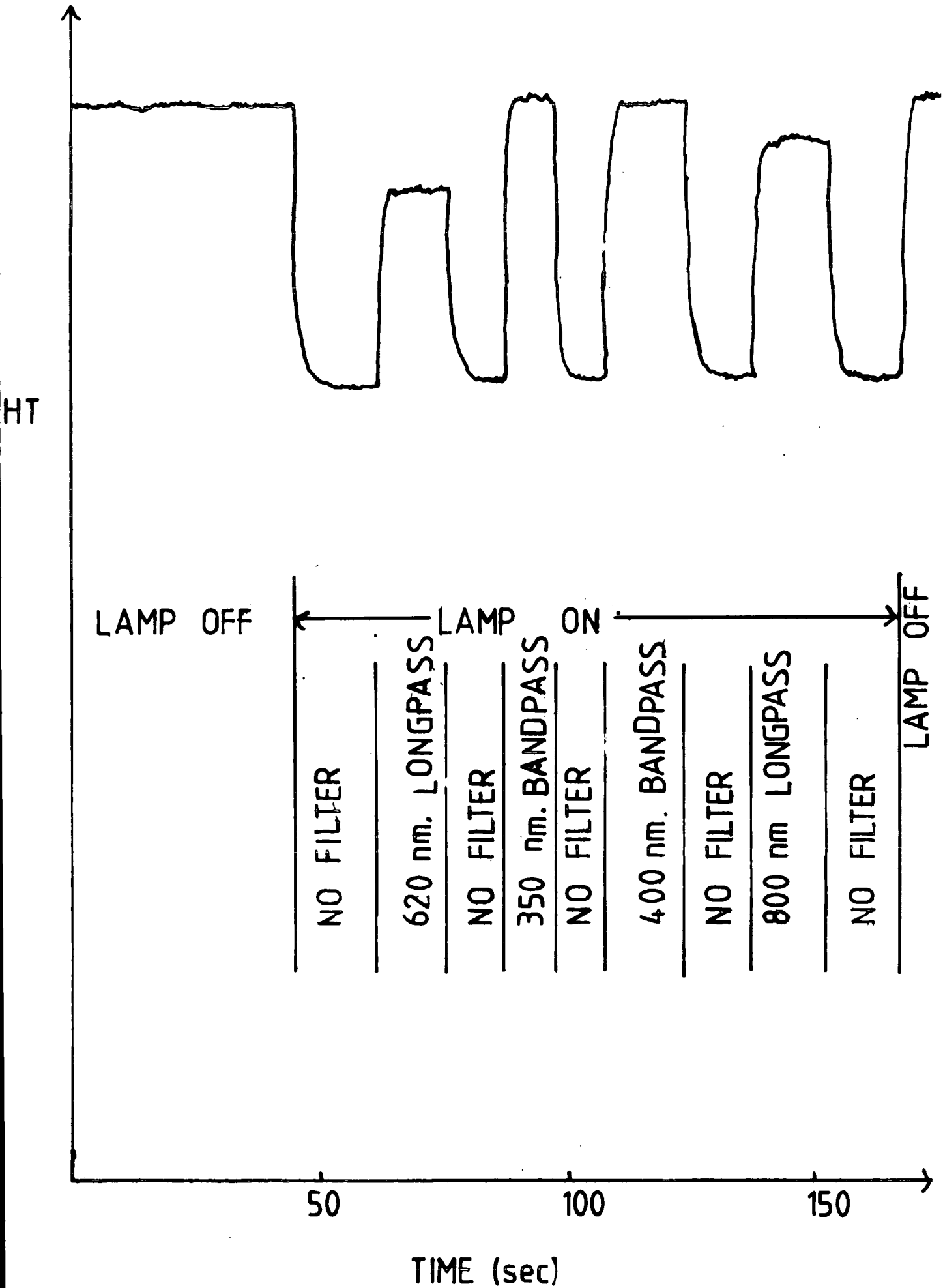
of his lines by more than 50%. It is clear that different mechanisms are important in rutile pigments.

A third set of measurements was performed on the iron lines. When the illumination ceased, the lines regained their original size. The rate at which they regained their original amplitudes was monitored (Fig 6.5). When these graph plots were redrawn on a graph of log $(I_D - I_t)$ v. time, where I_t is the intensity of the line time t seconds after stopping the illumination, Fig 6.6 gives two examples.

If we assume that the "decay" back to the original line amplitude is exponential we can characterize each decay by a relaxation time τ as follows :-

$$I_t = I_D - (I_D - I_L) \, e^{-t/\tau}$$

i.e.

$$\ln \frac{I_D - I_t}{I_D - I_L} = - t/\tau$$

so plotting $\ln(I_D - I_t)$ V. t should give a line of slope $- 1/\tau$.

τ was calculated and the result for the sample X11/1000 is given in Fig 6.7. Values of τ above 20 K could not be calculated because the change in amplitude irons becoming comparable to the signal-to-noise ratio (see Fig.6.2). The main feature is that τ increases with temperature. In Fig 6.6 it can be seen that only the initial points lie on the straight line. This implies that the behaviour is not a simple exponential as would be expected if there was only one transition involved in the restoration of the Fe^{3+} population.

6.2.2 Signal, G

This line showed a dramatic response to illumination at temperatures up to 100 K. This response was dependent on the amount of iron the sample had been doped with. Fig 6.8 shows the response of this line to illumination. These illustrate a general result that in the dark before illumination the

LAMP OFF

LAMP OFF

T=10

T= 7·5

5 sec.
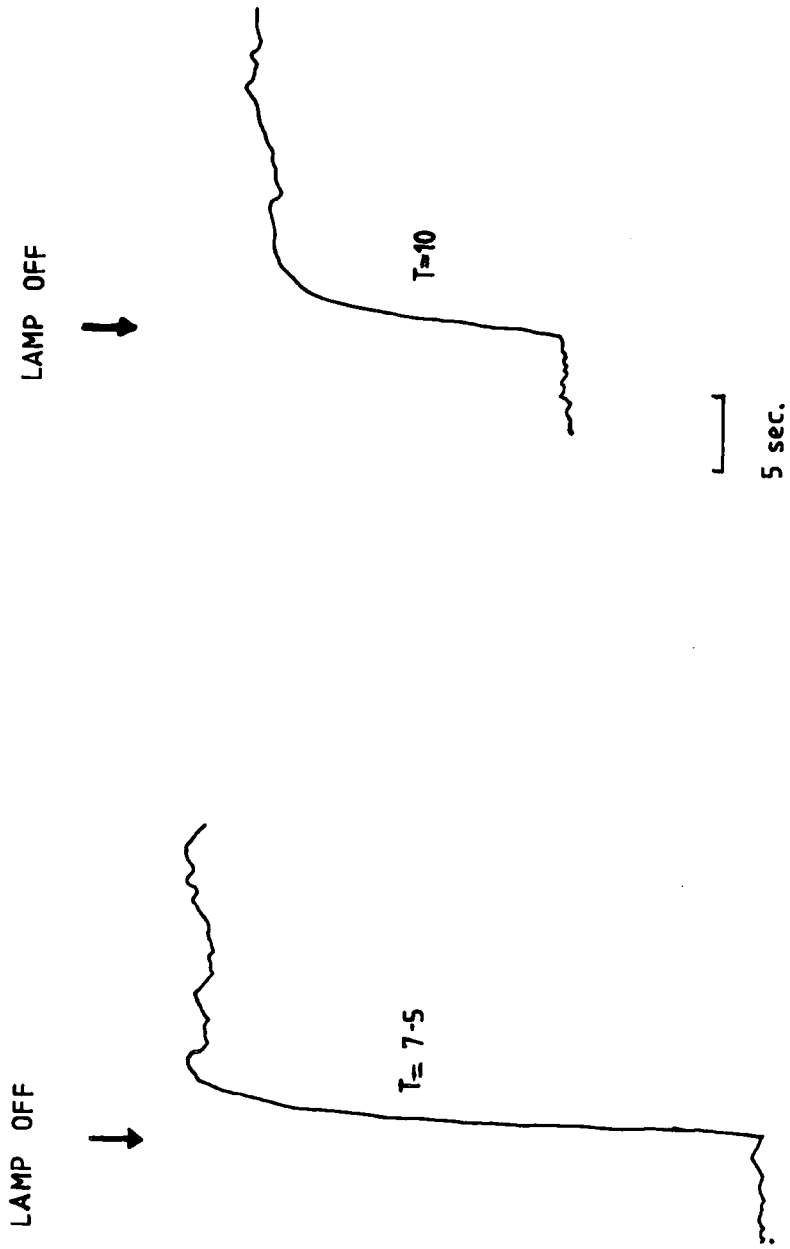
FIG. 6·5   AMPLITUDE OF SUBSTITUTIONAL Fe^{3+} AFTER IRRADIATION WITH A 250W Hg LAMP

FIG. 6·6   RECOVERY   OF
OF g=8·18 Fe^{3+} LINE AFTER
IRRADIATION WITH LIGHT.
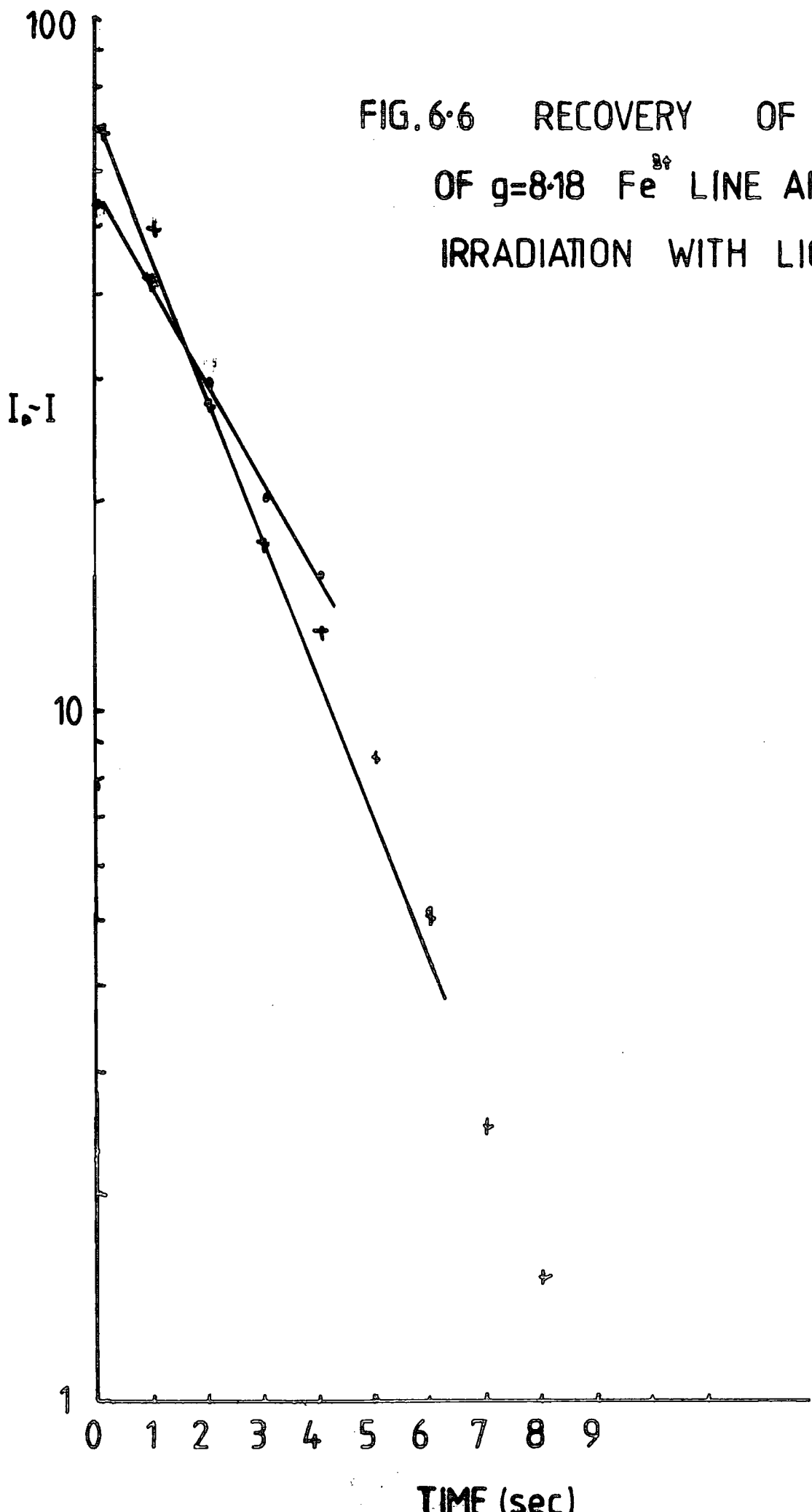
FIG.6·7   RELAXATION TIME, τ, FOR Fe$^{D\circ}$ SUBSTITUTIONAL IONS IN PIGMENT X11/1000
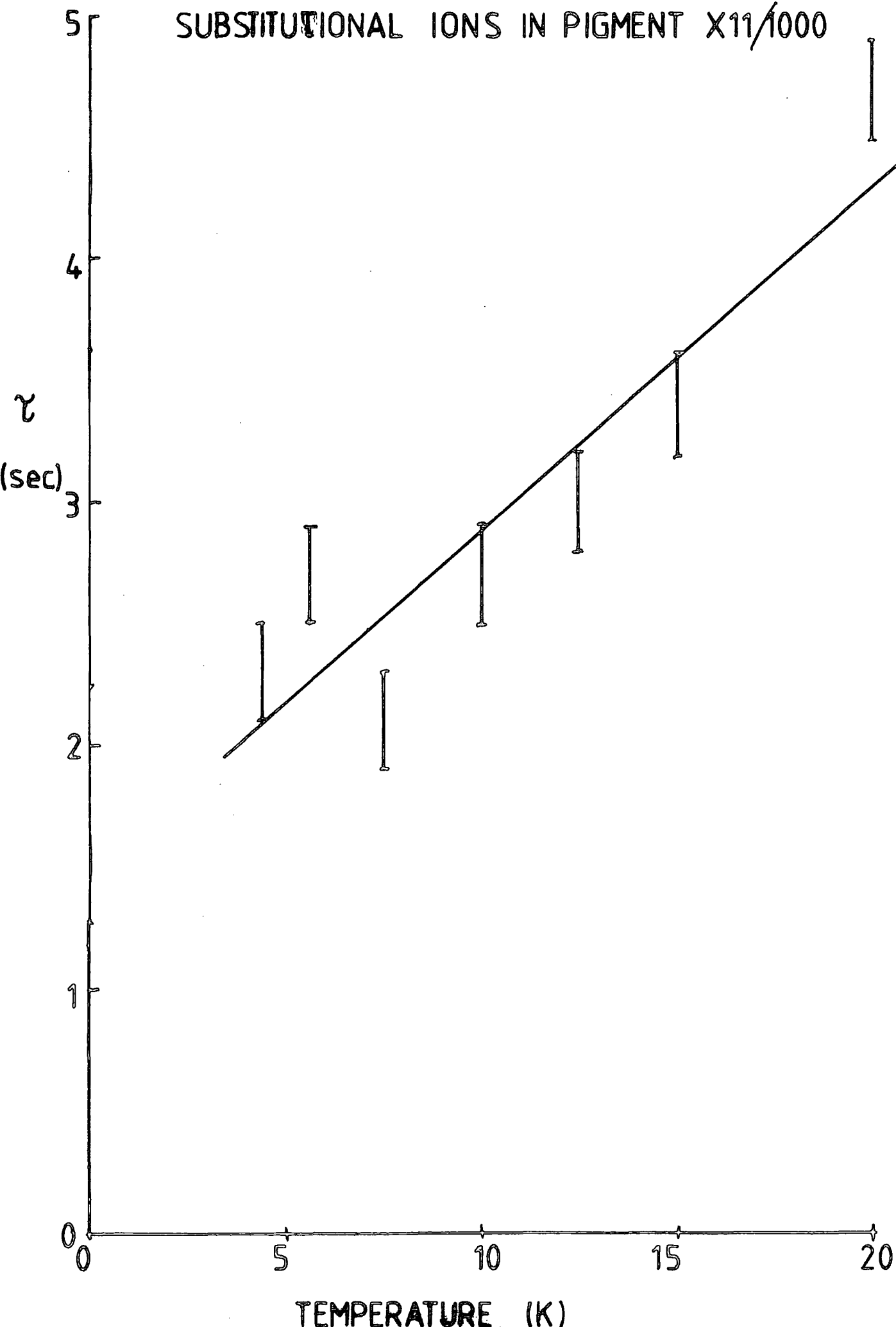
FIG.68   RESPONSE OF SIGNAL G   TO U.V. IRRADIATION
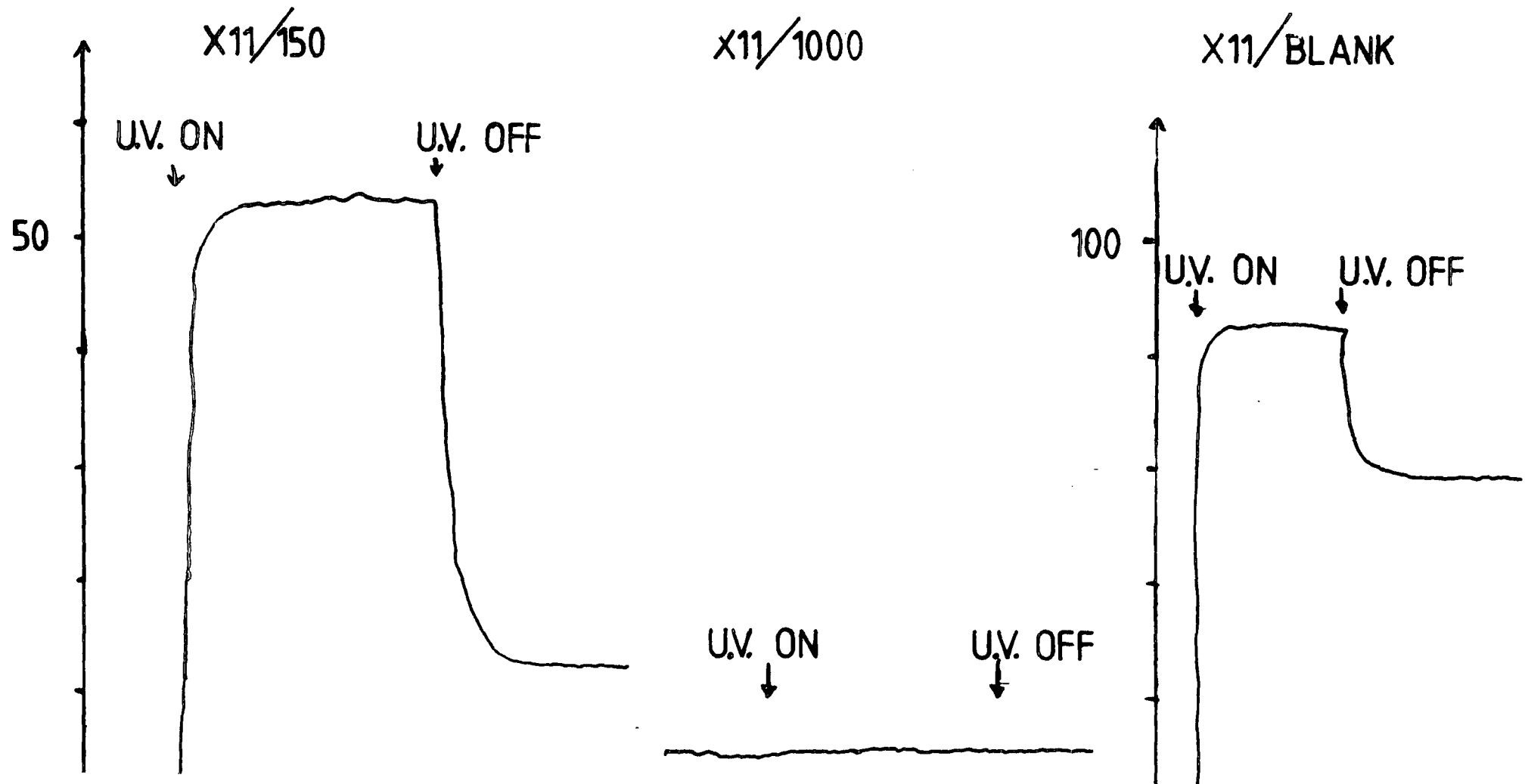
amplitude of the signal was very small and dependent on the amount of iron. On illuminating the samples the increase of the signal for the undoped sample was of the order of two orders of magnitude. The sample X11/1000 (ppm 400) showed no change and the samples with intermediate Fe concentrations showed intermediate results (Fig 6.9).

Using filters as described in the previous section, wavelengths shorter than about 700 nm were required for this effect and the largest effect was in the wavelengths 400 nm approximately, i.e. about the band gap energy of 3 eV.

6.2.3 Discussion of these results

In the previous section, it was noted that pre-ious workers who had studied the Fe^{3+} substitutional ion in single crystal samples had seen somewhat different results. Hodgskiss (1981) also looked at powders but did not examine the iron spectra. Table 6.1 details these results and contrasts them with the effects seen in this work. Mizushima et al (1979) explained their results as follows.

There exist in the band gap of rutile two sets of levels, E_1 and E_2, (Fig 6.10), which are related to surface states and to a defect in bulk of the crystal respectively. The $Fe^{3+} : d^5$ level is mostly occupied at equilibrium as it is just above the valence band but the Fe^{2+} level is close enough to E_c to be accessible and the $Fe^{4+} : d^4$ is also accessible. So a photoexcitation from one isolated Fe^{3+} ion to another would create both a Fe^{2+} and a Fe^{4+} ion.

$$2Fe^{3+} + h\nu \rightarrow Fe^{2+} + Fe^{4+}$$
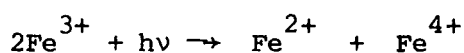
Excitations can occur from E_1 to the conduction band for $\lambda < 700$ nm but only wavelengths of $\lambda < 650$ nm affect the population of the Fe^{3+} level so that the Fe^{2+} level is just above the conduction band as shown. Light of $\lambda < 650$ nm excites electrons from E_1 to the Fe^{2+} level $e^- + h\nu + Fe^{3+} \longrightarrow Fe^{2+}$.

FIG. 6·9   RESPONSE OF SIGNAL G TO U.V. IRRADIATION AS A
FUNCTION OF IRON CONCENTRATION

+ U.V. ON

⊙ DARK (before irradiation)

× DARK (after irradiation)
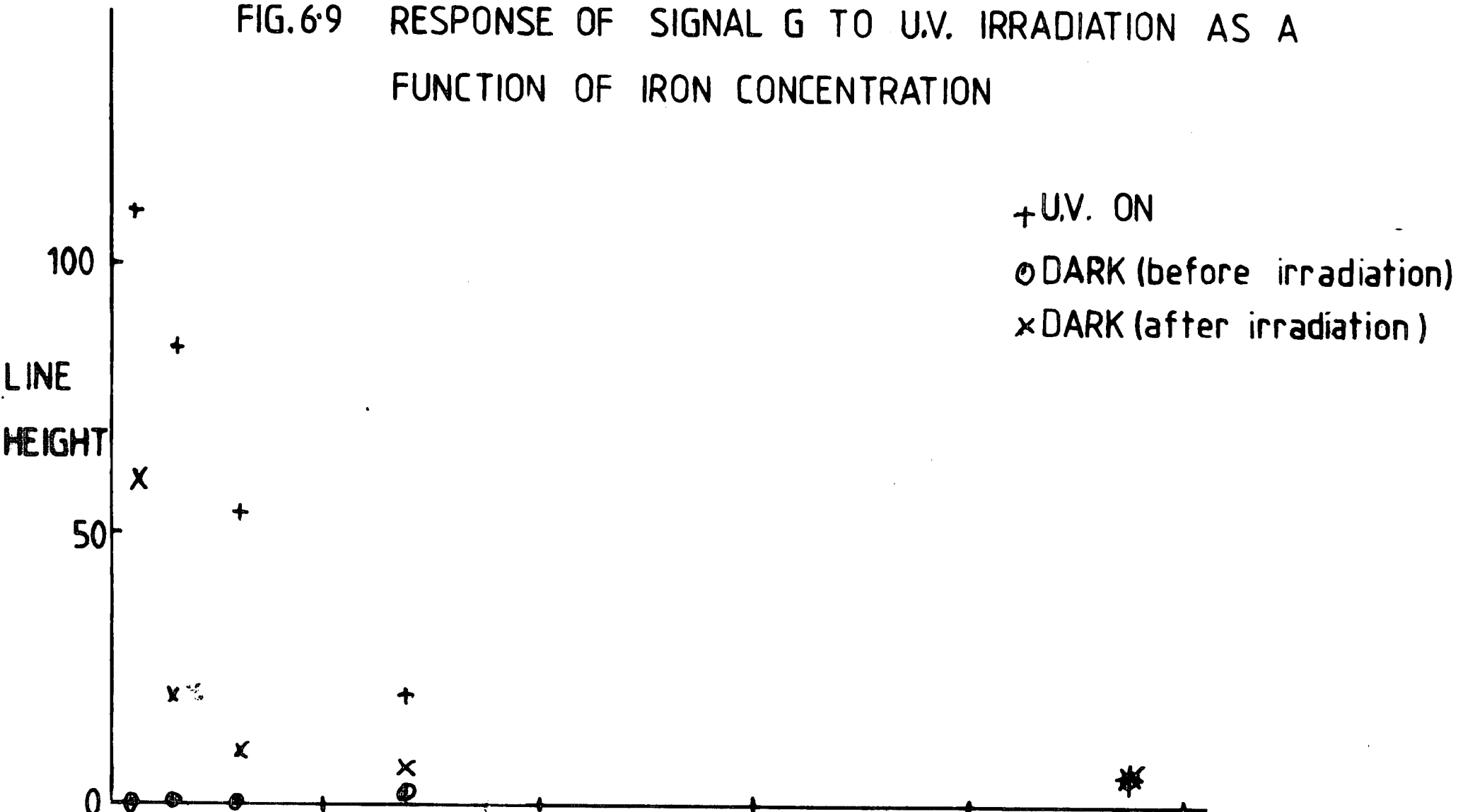
FIG. 6·10   ENERGY LEVEL DIAGRAM OF
            Fe:TiO$_2$ ACCORDING TO
            MIZUSHIMA et al (1979)

0 eV ———— Fe^{2+} //////// conduction band

-1eV

                                              E$_1$

-2eV
                                    E$_2$

        ———— Fe^{3+}
        ———— Fe^{4+} valence band
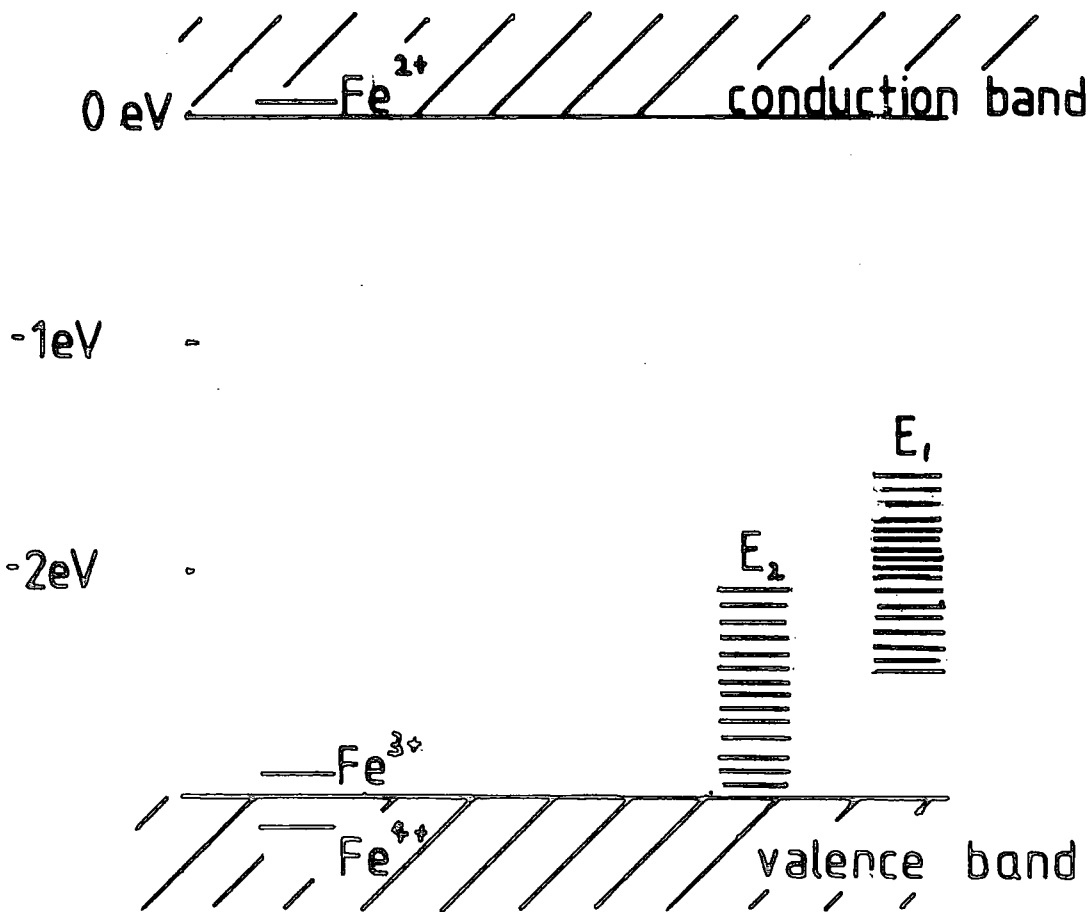
E$_1$ are surface states.

E$_2$ are bulk defects.

When $h\nu \simeq \left[(E_c - E(Fe^{3+}))\right]$ a sharp reduction in the intensity of the Fe^{3+} ion is seen because of direct excitations to the conduction band.

$$2Fe^{3+} + h\nu \longrightarrow Fe^{4+} + Fe^{2+}$$

with .

However, in the powder samples discussed here light $\lambda < 700$ nm produced no change and in fact only $\lambda > 700$ nm caused an effect. The direct opposite of the experiment described above !

One reason for the absence of any reduction in Fe^{3+} concentration during irradiation with light with $\lambda < 700$ nm could be that any electrons excited to the conduction band are trapped at sites other than the Fe^{2+} levels. If there were a large number of traps just below the conduction band these would trap electrons long before they were able to be trapped by a neighbouring Fe^{3+} ion, converting it to a Fe^{2+} ion. There is some evidence for the existence of such a level because signal G is generated by light of about 400 nm and so transitions requiring this amount of energy do occur. Also, as these samples are oxidized they will have a very low conductivity and so the probability of the excited electrons travelling far enough to be trapped Fe^{2+} states, is small.

This still requires that the reduction in Fe^{3+} concentration for wavelengths greater than 700 nm (energies less than 2 eV) be explained. It was shown in Chapter 4 that the crystallites are strained and distorted and this presumably leads to more states in the band gap. Excitations of less than band gap energy could excite electrons from a Fe^{3+} ion to a higher level and so lead to an increase in Fe^{4+} concentrations.

$$Fe^{3+} + h\nu \longrightarrow Fe^{4+} + e^{-}$$
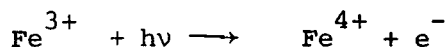
After the irradiation ceases these are retrapped at the Fe^{3+} level restoring the number of Fe^{3+} ions.

If the response time is plotted on a log τ versus reciprocal temperatures an activation energy E can be estimated. This assumes that $\tau \, \alpha \, \exp(E/kT)$

Fig 6.11 shows the result. E can be calculated from the slope and gives

an answer of E = 0.0002 eV. This suggests that most of the electrons

being retrapped at the Fe^{3+} centre are coming from levels with very nearly

the same energy. This would agree with the idea of a broad "band" of

defect states in the band gap. Electrons are excited to higher levels

(about 1 or 2 eV above Fe^{3+}) and then the Fe^{3+} state is filled with an

electron from a neighbouring defect state and the excited electron re-

combines on a defect state. It was noted that the relaxation of the Fe^{3+}

population after irradiation is not a simple exponential as transitions

from more than one state to the Fe^{3+} level are involved. This would be

expected if there are a "band" of defect states as has been assumed.

The behaviour of signal G is considerably more complicated. As

was noted in Chapter 3 it is likely to be due to a trapped hole. A

difficulty arises in understanding how the response to light can fall so

dramatically with increasing iron concentration while at the same time the

number of holes trapped in these sites in areas before irradiation increases.

A suggestion is that the number of these hole traps is reduced by

the addition of iron. It is known that in rutile much of the iron is in

states that do not give E.P.R. signals (Anderson et al, 1974) and

in these samples Fe^{3+} in rhombic symmetry has been observed. So if iron

associates with the empty hole trap forming a completely new site, the

behaviour of Fig 6.9 can be explained. Exposing the samples to radiation

of about band gap energy raises electrons to the conduction band and leaves

behind holes which can be trapped giving rise to spectrum G. As the con-

centration of iron increases so the number of these sites fall and the

fall of the population in the light is observed. However, substituting

Fe^{3+} for Ti^{4+} introduces holes and these can be trapped at the site giving,

in the dark before any irradiation, an increase in the amplitude of the

signal. So if signal G represents trapped holes the amplitude of spectrum

FIG. 6.11 PLOT OF $\log \tau$ v $\frac{1}{T}$
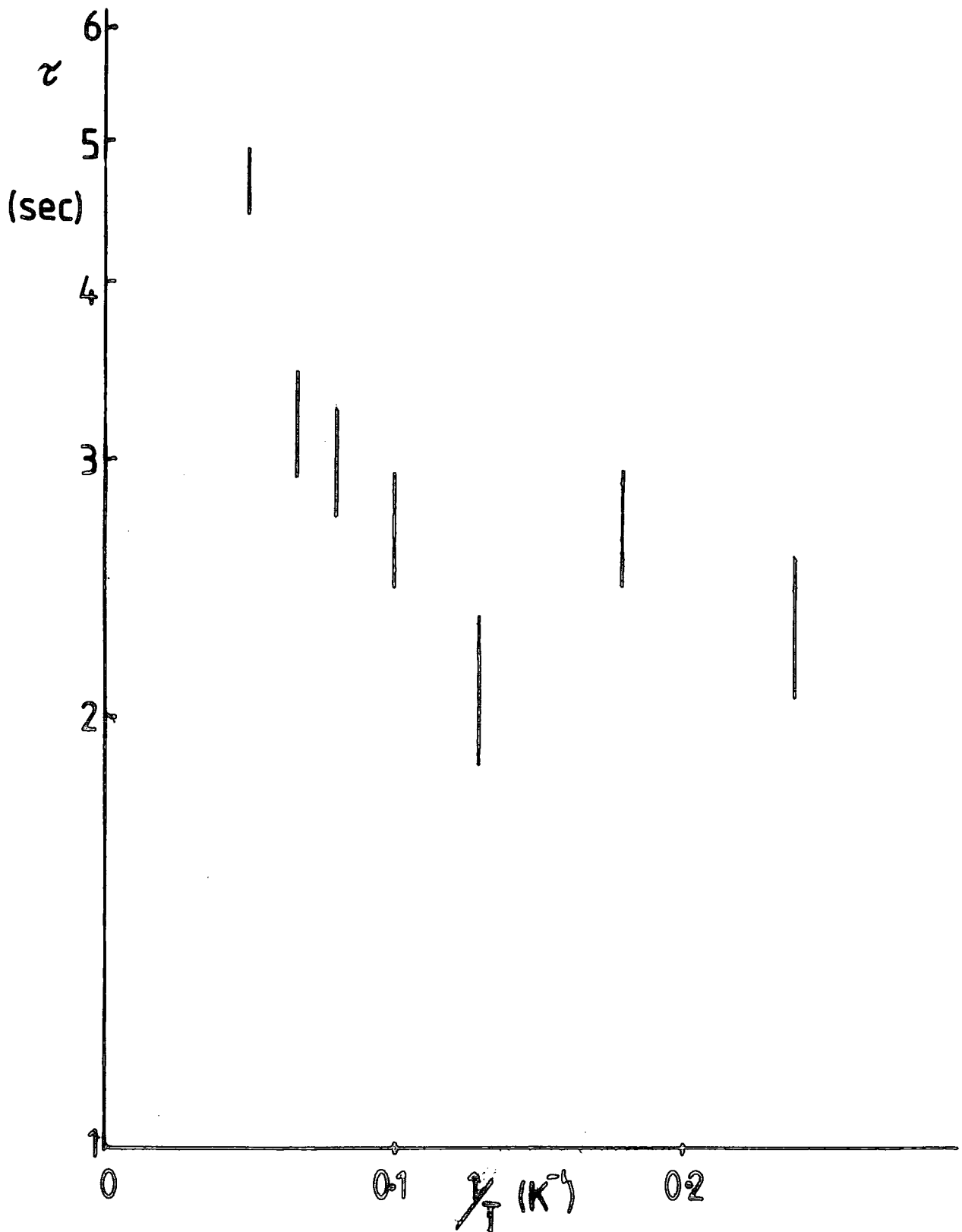
TABLE 6.1 : Comparison of results of optically irradiating Fe^{3+} : TiO_2

Ref.	Faughnan & Kiss (1968)	Mizushima et al (1979)	Hodgskiss (1981)	This Work
Sample	Single Crystals. Doped with Fe & Mo	Oxydized Single Crystal Doped with iron	Single Crystal Doped with Fe,Ni,Cr & Me	Pigments Doped with Fe
Wavelengths used to alter population	400 nm	400-850 nm max change at > 400 nm see Fig 1.9	400 nm Hg lamp with Cu_2S_4O soln and filter	λ< 700 nm NO CHANGE WITH λ = 400 or 350 nm
Temps at which effects observed	77 K not seen at room temperature No comment about lower temperatures	77 K	4.2 $\longrightarrow$ 230 Fe^{3+} concentration reduced over entire range.	4.2 $\longrightarrow$ 40 NO CHANGE ABOVE 40 K
Does effect on Fe^{3+} remain after illumination ceases? (Is a meta stable state induced ?)	?	YES	YES	NO

G is proportional to the number of trapped holes and these holes are formed either by Fe doping or by exposure to light.

6.3 CONCLUSIONS

The behaviour of rutile pigments is totally different from that reported for single crystals but this can be explained by the increased number of states in the band gap and by the distorted nature of the crystal lattice. The Fe^{3+} site is only affected by light greater than 700 nm while shorter wavelengths affect the hole trap G. The number of this hole trap that exist are reduced by the introduction of iron, so while different phenomena are observed these can be explained by a different model, based on the presence of many more states.

APPENDIX 1

SAMPLE ANALYSIS

These analyses were performed by Tioxide International Limited at their Central Laboratories using X-ray fluorescence and mass spectroscopy.

TABLE A1

CLDD 1372/1 $\longrightarrow$ /8.

Sample	ppm Fe before strip	ppm Fe after 5% strip
CLDD 1372/1	35	15
" /2	70	20
" /3	135	55
" /4	405	195
Sample	ppm Cr before strip	ppm Cr after strip
" /5	48	27
" /6	95	34
" /7	225	103
" /8	313	143

the base material contains 1.34% Al_2O_3.

TABLE A2

X5 BLANK

	Before	After 5% Strip
% Al_2O_3	0.57	0.22
% SiO_2	0.03	<0.01
% P_2O_5	0.03	0.03
% SO_3	0.03	0.03
ppm CaO	<20	20
" ZnO	<20	<20
" Fe	10	<10
" Sn	70	40
" ZrO_2	<20	<20
" Pb	<10	<10
" K_2O	20	10
" Nb_2O_5	<10	<10
" Sb_2O_3	<20	<20
" Cl	50	60

TABLE A3 X5

Intended dopant concentration	% Al_2O_3		ppm Fe		
	Before	After	Before	After	5% strip
10	0.58	0.22	20	10	
50	0.59	0.22	60	30	
100	0.60	0.20	100	50	
150	0.60	0.21	130	70	
250	0.59	0.20	190	110	
500	0.56	0.19	350	240	
1000	0.59	0.17	620	400	

TABLE A4   X11

	Before	After	5% strip
% Al_2O_3	1.80	1.07	
% SiO_2	0.03	<0.01	
% P_2O_5	0.03	0.02	
% SO_3	0.03	0.03	
ppm CaO	<20	20	
" ZnO	<20	<20	
" Fe	10	10	
" Sn	<20	<20	
" ZrO_2	<20	<20	
" Pb	<10	<10	
" K_2O	20	10	
" Nb_2O_5	<10	<10	
" Sb_2O_3	<20	<20	
" Cl	<50	110	

TABLE A5   X11

| Intended Fe | Measured 5% Strip | | | |
| | % Al$_2$O$_3$ | | ppm Fe Concentration | |
	Before	After	Before	After
10	1.81	1.03	30	10
50	1.80	1.08	60	30
100	1.80	1.02	100	50
150	1.81	0.98	110	60
250	1.77	0.96	170	100
500	1.79	1.07	290	150
1000	1.82	1.07	670	500

TABLE A6   X11 A → E

Sample	Measured Fe (ppm)	% weight of sample removed by HF etch
A	730	unstripped
B	480	2.7
C	360	8.5
D	380	13.1
E	330	33.5

The intended Fe concentration was 1000 ppm.

TABLE A7 KENT BOULE

MgO	70 ppm
Al_2O_3	0.03 %
SiO_2	0.06 %
P_2O_5	0.03 %
SO_3	0.2 %
Cl_2	90 ppm
CaO	0.02 %
Fe	1.5 %
ZnO	0.02 %
ZrO_2	0.02 %
Bi	0.05 %
SrO	80 ppm
Y_2O_3	40 ppm

(all others less than 30 ppm)

APPENDIX 2

Equation 1.7 can be solved to find the resonant field of a particular transition and its transition probability (i.e. its intensity) as shown below. This can be used to derive powder spectra but because of the complexity alternative methods were derived which are described in Chapter 3.

A2.1   SOLUTION OF THE SPIN HAMILTONIAN

The single crystal spectra may be calculated by inserting in $\mathcal{H}_{sp}$, the Spin Hamiltonian, the appropriate parameters and finding the eigenfunctions and eigenvalues by the normal quantum mechanical methods. The time dependent (transition-inducing) interaction with a monochromatic field (H_o) is included to first order, using semi-classical perturbation theory (MacKay et al, 19).

Calculation of single crystal E.S.R. spectrum is equivalent to solving, for fixed values of the static applied field, H_o and H_1, the time dependent Schrödinger equation :-

$$\mathcal{H}_{sp} \mid \psi(t)> \ = \ - \ i \ h \ \frac{\partial}{\partial t} \mid \psi(t)> \tag{A2.1}$$

If $\mathcal{H}_{sp}$ can be written as $\mathcal{H}_{sp} = \mathcal{H}_{stat} + \mathcal{H}_{rad}$, where $\mathcal{H}_{stat}$ is a large time independent term and $\mathcal{H}_{rad}$ a small time dependent term, one would first solve the static case,

$$\mathcal{H}_{stat} \mid V_k> \ = \ E_k \mid V_k> \tag{A.2.2}$$

and then include $\mathcal{H}_{rad}$; Eqn A.2.1 is solved in the approximation that $\mid \psi(t)>$ is a linear combination of the stationary eigenstates $\mid V_k>$ with time-dependent coefficients so that the population of the states are linear functions of the duration of application of $\mathcal{H}_{rad}$, (Schiff, 1955). Suppose that $\mid V_k>$ is expanded in a complete set of orthonormal states (basis vectors)

$|u_m(j)>$, which are eigenfunctions of J^2 and J_z (eigenvalues $j(j+1)$ and m respectively) with J being the angular momentum operator as usual. Then

$$|V_k> = \sum_m |u_m(j)> < u_m |V_k> \qquad (A2.3)$$

(This is equivalent to expanding an ordinary 3.D vector in a basis $\underline{e}_1, \underline{e}_2, \underline{e}_3$ as $\underline{v} = \underline{e}_1 (\underline{e}_1 \cdot \underline{v}) + \underline{e}_2 (\underline{e}_2 \cdot \underline{v}) + \underline{e}_2 (\underline{e}_3 \cdot \underline{v})$, except that the scalar products $|u_m |V_k>$ are in a complex Hilbert space). If the Hamiltonian can be written in terms of angular momentum operators :-

$$\mathcal{H} |V_k> = |V_e> \sum_{mm'} |u_{m'}(j)>< u_{m'}|\mathcal{H}|u_m> < u_m| V_k> \qquad (A2.4)$$

where $<u_{m'}|\mathcal{H}|u_m> = \mathcal{H}_{mm'} \equiv \int u_{m'}^*(j) \; u_m(j) \; d\tau \qquad (A2.5)$

is a matrix element of $\mathcal{H}$. Now $|V_e>$ is a vector in the space spanned by $|u_m>$ so :-

$$|V_e> = \sum_{m'} |u_{m'}(j)> < u_{m'}| V_e> \qquad (A2.6)$$

and using (A2.4) and (A2.6) $|V_e> = \mathcal{H} |V_k>$ can be written :-

$$<u_{m'}| V_e> = \sum_m <u_{m'}|\mathcal{H}|u_m> < u_m| V_k> \qquad (A2.7)$$

where the coefficients $<u_m | V_k>$, $(m = j, j-1, \ldots -j)$, may be thought of as a column vector ; for example the basis vectors are the set

$$\begin{bmatrix} \delta_{j,m} \\ \delta_{j-1,m} \\ \vdots \\ \delta_{-j\,m} \end{bmatrix}$$

Using this notation (A2.2) can be rewritten as

$$\sum_m \langle u_{m'} | \mathcal{H}_{stat} | u_m \rangle \quad \langle u_m | v_k \rangle = E_k \langle u_{m'} | v_k \rangle \tag{A2.8}$$

Consider the set of eigenvectors $\langle u_m | v_k \rangle$ for all eigenvalues E_k. These are orthogonal, i.e.,

$$\sum_m \langle v_e | u_m \rangle \langle u_m | v_k \rangle = \delta_{ek} \tag{A2.9}$$

hence the set $\langle u_m | v_k \rangle$ may be written as the columns of a unitary matrix, U_{mk}, and may be written

$$\sum_m \mathcal{H}_{m'm} U_{mk} = E_k U_{m'k} \tag{A2.10}$$

Using equation (1.17), A.2.9

$$\sum_{m',m} U^+_{1m} \mathcal{H}_{mm'} U_{mk} = \sum_{m'} U_{1m'} U_{m'k} E_k = \delta_{1k} E_k = D_{1k} \tag{A2.11}$$

or

$$U^+ \mathcal{H}_{stat} . U = D \tag{A2.12}$$

Thus to solve equation (A2.2) the problem reduces to finding the unitary transformation which reduces the Hermition matrix $\mathcal{H}_{stat}$ (element $\mathcal{H}_{mm'}$) to diagonal form with elements $E_k \, \delta_{1k}$.

Equation (1.9) can be written,

$$\sum_k a_k(t) \langle v_j | \mathcal{H}_{rad}(t) | v_k \rangle = -ih \sum_k \dot{a}_k(t) \langle v_j | v_k \rangle = -ih \dot{a}_j(t) \tag{A2.13}$$

We want a solution of (A2.13) with $\mathcal{H}_{rad}(t) = \mathcal{H}_{rad}(o)\,e^{i\omega t}$ and $a_j(t=o) = 1$, $a_k(o) = o$, $k \neq j$. The corresponding form of (A2.13) is :-

$$\dot{a}_j(t) = -(i\,h)^{-1} \sum_k a_k(t)\,e^{i\omega t}\ \langle v_j|\ \mathcal{H}_{rad}(o)\ |\ v_k\rangle \qquad (A2.14)$$

which may be solved by standard methods (Schiff, 1955) to give :-

$$I_{jk}\ \alpha\ |\ \langle v_j\ |\ \mathcal{H}_{rad}(o)\ |\ v_k\rangle\ |^2 \qquad (A2.15)$$

where I_{jk} is the intensity of the transition from state k to state j or the power absorbed in the resonance line $k \rightarrow j$. To reduce (A2.15) to matrix notation we use (A2.3) to give

$$\langle v_j|\ \mathcal{H}_{rad}\ |v_k\rangle = \sum_{mm'} \langle v_j|\ u_{m'}\rangle\ \langle u_{m'}|\ \mathcal{H'}_{rad}(o)|\ u_m\rangle\langle\ u_m|\ v_k\rangle$$

$$= \sum_{m'm} U^+_{jm'}\ \mathcal{H}_{rad}(o)_{m'm}\ U_{mk}$$

$$= (U^+\ \mathcal{H}_{rad}(o)\ U)_{jk}$$

so

$$I_{jk}\ \alpha\ |(U^+\mathcal{H}_{rad}(o)\ U)_{jk}|^2 \qquad (A2.16)$$

In a typical E.S.R. experiment, the oscillating field, $H_1 e^{i\omega t}$ is perpendicular to the static field H. With $\mathcal{H}_{rad} = \mathcal{H}_1 e^{i\omega t}$ the transition probability connecting the states k and j has been taken on (Aasa and Vanngard, 1975).

$$I_{jk}^2 = |\langle v_j|\mathcal{H}_1\ |\ v_k\rangle|^2 \Big/ (\beta H_1)^2 \qquad (A2.17)$$

To simulate E.S.R. spectra I_{jk} has to be multiplied by a shape function $S(H)$ normalized such that :-

$$\int S(H) \, dH = 1 \qquad (A2.18)$$

However, from time dependent perturbation theory the transition probability is a frequency dependent quantity (Abragam and Bleaney, 1970), given by $I_{jk}^2 f(\nu)$, with $f(\nu) \, d\nu = 1$). Since the E.S.R. spectrometer works at a constant frequency, the intensity integrated over the magnetic field becomes :-

$$\int I_{jk}^2 S(H) \, dH = \int I_{jk}^2 f(\nu) \frac{dB}{d\nu} \, d\nu \qquad (A2.19)$$

For narrow lines $I_{jk}^2 \frac{dB}{d\nu}$ can be taken as a constant over the line width and the integrated intensity becomes $I_{jk}^2 \frac{dB}{d\nu}$, which is the factor that should multiply a normalized shape function $S(B)$ in simulations of E.S.R. spectra.

In cases where $S > \frac{1}{2}$ the situation is complicated because $\frac{dB}{d\nu}$ depends on the field. To derive powder spectra we will use an effective spin of $S^* = \frac{1}{2}$ and a resonance condition $h\nu = g \, \beta H$, which implies that $\frac{dB}{d\nu}$ is proportional to $\frac{1}{g}$. We can now define an intensity factor, W,

$$W = \frac{I_{jk}}{g} \qquad (A2.20)$$

This factor was pointed out by Aasa and Vanngard, (1975) and has been used by some authors to improve their simulated spectra (Conesa and Sarice 1979 and Pilbrow 1978). Even if I_{jk} is assumed to be a constant, the variation in W due to the $1/g$ dependence should be included in any calculations.

Thus from Equations (1.20) and (1.25) the energy levels, and the magnitude of the transition between them may be computed. Dowsing and Gibson (1969), Aasa (1970) and Barry (1967) have used a Spin Hamiltonian of the form

$$\mathcal{H} = \underline{H}.g.\underline{s} + D\left[S_z^2 - \frac{1}{3}S(S+1)\right] + E\left[S_x^2 - S_g^2\right] \qquad (A2.21)$$

to describe a d^5 ion without any hyperfine interaction (i.e. Fe^{3+}). They use computational procedures to solve this equation and have derived powder spectra from it. Fe^{3+} in a substitutional site in rutile needs two further terms to adequately describe its behaviour and these terms combined with the facts that g is isotropic and s = 5/2 (Section 1.3.2) give :-

$$\mathcal{H} = g\,\underline{H}.\underline{S} + D\left[S_z^2 - \frac{32}{12}\right] + E\left[S_x^2 - S_y^2\right] + \frac{a}{6}\left[S_x^4 + S_y^4 - \frac{707}{10}\right]$$

$$+ F\left[S_z^4 - \frac{95}{14}S_z^2 + \frac{81}{16}\right] \qquad (A2.22)$$

To rewrite this in an Energy Matrix form we must replace the operators by their matrix representations discussions of matrix representations of spin and angular momentum operators given in most text books (e.g. Dicke & Wittke (1961). They give the following relations :-

$$\left[\frac{S_-}{}\right]_{m_s m_s'} = \sqrt{(s-m_s')(s-m_s'+1)}\;\delta_{m_s, m_s'-1} \qquad (A2.23)$$

$$\left[\frac{S_+}{}\right]_{m_s', m_s} = \left[\frac{S_-}{}\right]_{m_s, m_s'} \qquad (A2.24)$$

$$\left[\frac{S_z}{}\right]_{m_s, m_s'} = m_s'\;\delta_{m_s, m_s'} \qquad (A2.25)$$

where S_+ and S_- have the usual definitions of "step-up" and "step-down" operators.

$$S_x = \frac{1}{2}(S_+ + S_-) \tag{A2.26}$$

$$S_y = \frac{-i}{2}(S_+ - S_-) \tag{A2.27}$$

Substituting for S = 5/2 we find :-

$$S_x = \begin{pmatrix} 0 & \sqrt{5}/2 & 0 & 0 & 0 & 0 \\ \sqrt{5}/2 & 0 & \sqrt{2} & 0 & 0 & 0 \\ 0 & \sqrt{2} & 0 & 3/2 & 0 & 0 \\ 0 & 0 & 3/2 & 0 & \sqrt{2} & 0 \\ 0 & 0 & 0 & \sqrt{2} & 0 & \sqrt{5}/2 \\ 0 & 0 & 0 & 0 & \sqrt{5}/2 & 0 \end{pmatrix} ; S_y = i\begin{pmatrix} 0 & -\sqrt{5}/2 & 0 & 0 & 0 & 0 \\ \sqrt{5}/2 & 0 & -\sqrt{2} & 0 & 0 & 0 \\ 0 & \sqrt{2} & 0 & -3/2 & 0 & 0 \\ 0 & 0 & 3/2 & 0 & -\sqrt{2} & 0 \\ 0 & 0 & 0 & \sqrt{2} & 0 & -\sqrt{5}/2 \\ 0 & 0 & 0 & 0 & \sqrt{5}/2 & 0 \end{pmatrix}$$

$$S_z = \begin{pmatrix} 5/2 & 0 & 0 & 0 & 0 & 0 \\ 0 & 3/2 & 0 & 0 & 0 & 0 \\ 0 & 0 & 1/2 & 0 & 0 & 0 \\ 0 & 0 & 0 & -1/2 & 0 & 0 \\ 0 & 0 & 0 & 0 & -3/2 & 0 \\ 0 & 0 & 0 & 0 & 0 & -5/2 \end{pmatrix} \tag{A2.28}$$

These are substituted into equation (A2.22) and the resulting matrix is shown in Table A2.1. To find the energy levels for an arbitrary applied magnetic field the field has to be reduced into its components along the x,y and z axes and then substituted into the matrix of Table A2.1. This matrix was diagonalized on a computer with the aid of the NAG subroutine library of the Numerical Algorithms group. An example program is listed on the next page. This program calculates the principle values for Fe^{3+} ions given the Spin

Hamiltonian parameters D, E, F and a for the three cases with the magnetic field along the three directions x, y and z defined in Chapter One. The results are given in Table 3. 3. This program first acts up a matrix which has all the terms of the Spin Hamiltonian matrix which are not field dependent. Next the field is chosen and described in terms of the field along the three axis, i.e. $\underline{H}$ = (H_x, H_y, H_z) ; and then a subroutine called SOLVE is used. SOLVE calculates all the field dependent terms and then uses the appropriate subroutines to diagonalize the matrix. The array DARR contains the six eigenvalues which are the energies of the energy levels for that particular field $\underline{H}$.

Similar programs using SOLVE were used to determine the energy levels of Fe^{3+} ions and the graphs of Figs 3. (, however it required too much time to evaluate a powder spectra because the number of field values needed would be very large and the time needed to evaluate SOLVE many times would be prohibitive.

This is because the spectra must be evaluated at discrete points, H_i, and the spacing between these points must be considerably smaller than the linewidth of the line broadening function chosen. This means that the width of each field interval in the simulation should be of the order of one Gauss. Now to evaluate a powder spectra the values of resonant field H_R must be found for a large number of orientations of the crystal lattice with respect to the magnetic field. (Each orientation can be described by $\underline{\Omega}$ = (Θ_x, Θ_y, Θ_z) where the Θ_i are the direction cosines of the magnetic field with the z crystallographic axis). H_R is found for many different $\underline{\Omega}$ and each time a $\underline{\Omega}$ gives a H_R has a value in the range $H_i - \frac{\Delta}{2}$ to $H_i + \frac{\Delta}{2}$ (where $\Delta = H_{i+1} - H_i$) an array $D(H_i)$ is incremented by one. The "noise" of the simulation, the random variation of the value of $D(H_i)$, is given simply as $\dfrac{\sqrt{D(H_i)}}{D(H_i)}$. Now for a 10% noise $D(H_i) = 100$.

TABLE A2.1 Energy Matrix for Fe^{3+}

Note that $G_i = g\beta H_i$.

If the Energy Matrix is $\underline{E}$, Eigenvalues λ are given by $|\underline{E} - \lambda\,\underline{I}| = 0$

where $\underline{I}$ is identity, and Eigenvectors $\underline{x}$ satisfy the relation $\underline{E}\,\underline{x} = \lambda\,\underline{x}$

	5/2	3/2	1/2	-1/2	-3/2	-5/2
5/2	$\frac{5}{2}G_z + \frac{10}{3}D + \frac{a}{2} + \frac{F}{3}$	$\frac{\sqrt{5}}{2}(G_x - iG_y)$	$\sqrt{10}\;E$	0	$\frac{\sqrt{5}}{2}a$	0
3/2	$\frac{\sqrt{5}}{2}(G_x + iG_y)$	$\frac{3}{2}G_z - \frac{2}{3}D - \frac{3}{2}a - F$	$\sqrt{2}(G_x - iG_y)$	$3\sqrt{2}\;E$	0	$\frac{\sqrt{5}}{2}a$
1/2	$\sqrt{10}\;E$	$\sqrt{2}(G_x + iG_y)$	$\frac{1}{2}G_z - \frac{8}{3}D + a + \frac{2}{3}F$	$\frac{3}{2}(G_x - iG_y)$	$3\sqrt{2}\;E$	0
-1/2	0	$3\sqrt{2}\;E$	$\frac{3}{2}(G_x + iG_y)$	$-\frac{1}{2}G - \frac{8}{3}D + a + \frac{2}{3}F$	$\sqrt{2}(G_x - iG_y)$	$\sqrt{10}\;E$
-3/2	$\frac{\sqrt{5}}{2}a$	0	$3\sqrt{2}\;E$	$\sqrt{2}(G_x + iG_y)$	$-\frac{3}{2}G - \frac{2}{3}D - \frac{3}{2}a - F$	$\frac{\sqrt{5}}{2}(G_x - iG_y)$
-5/2	0	$\frac{\sqrt{5}}{2}a$	0	$\sqrt{10}\;E$	$\frac{\sqrt{5}}{2}(G_x + iG_y)$	$-\frac{5}{2}G_z + \frac{10}{3}D + \frac{1}{2}a + \frac{F}{3}$

In practice by choosing a regular array of directions $\underline{\Omega}$ the required number of $D(H_i)$ can be reduced. (Instead of selecting $\underline{\Omega}$ at random which would describe a random selection of crystallites, the $\underline{\Omega}$ are chosen so that the angles between them subtend equal units of solid angle. This is valid for a large number of particles where the total number of crystallites is so large that each orientation is equally present).

Now as $\Delta = 1$ G and the powder spectra of iron is over 1 Tesla wide, i.e. 10,000 G, we would need 10,000 intervals H_i and for each to give a $D(H_i) \simeq 100$ this would mean 1,000,000 different values of $\underline{\Omega}$ being chosen. As explained in Chapter 3 a simpler method was used which is identical to that used in the next section.

A2.2   SIMULATION OF A POWDER SPECTRA

A typical program is shown in Fig A2.2.

The subroutines are :-

H   -   This determines the resonant field given values of g_x, g_y, g_z and Θ and ϕ the orientation of the crystallite with respect to the magnetic field.

G   -   Gaussian lineshape function.

F   -   Lorentzian lineshape function.

An array corresponding to the $D(H_i)$ of the previous section is set up as well as two more which just store the values of Θ and ϕ used. Then H_R is found for every Θ and ϕ (Ω) used and $D(H_i)$ incremented. $D(H_i)$ is called IN(K) in the example shown. Then the line is broadened and differentiated for comparison with experiment.

Program SIM.

```
>     1              DIMENSION HH(201),A(101),AA(201),BR(200),DIFF(200),IN(200),
>     2            @AM(6),G1(5)
>     3             DATA HH/201*0.0/
>     4             DATA A/101*0.0/
>     5             DATA AA/201*0.0/
>     6             DATA BR,DIFF/400*0.0/
>     7             DATA IN/200*0/
>     9             DATA G1/2.0030,2.0471,2.0335,2.0202,2.00070/
>    10             DATA G2,G3/2.0110,2.0110/
>    11             DATA PL,UU,BETA,WA1,WA2,WA3/0.66261E-26,0.910E10,0.92729E-20,
>    12            @9.0,8.9,8.8,
>    13             DATA SIGMAG/3.0/
>    14     C
>    15     C   SET UP FIELD ARRAY
>    16     C
>    17             HH(1)=3150.0
>    18             DO 1 I=2,201
>    19           1 HH(I)=HH(I-1)+1.0
>    20     C
>    21     C   SET UP ARRAY CORRESPONDING TO THETA
>    22     C
>    23             DO 2 I=1,101
>    24           2 A(I)=ARCOS(FLOAT(I-1)/100.0)
>    25     C
>    26     C   SET UP ARRAY CORRESPONDING TO PHI
>    27     C
>    28             PAI=4.0*ATAN(1.0)
>    29             AA(1)=0.0
>    30             DO 3 I=2,201
>    31           3 AA(I)=AA(I-1)+PAI/200.0
>    32     C
>    33     C   FIND VALUE OF RESONANT FIELD AND INCREMENT CORRESPONDING ELEMENT OF IN
>    34     C
>    35             DO 20 I=1,101G=???
>    36             DO 20 J=1,201)x??a
>    37             IF (J.EQ.101) GO TO 7
>    39      ..     X=H(G1(1),G2,G3,A(I),AA(J),UU,BETA,PL,WA1,WA2,WA3)
>    40             K=INT(X-3150.0)
>    41           7 IN(K)=IN(K)+1
>    42          20 CONTINUE
>    43     C
>    44     C   CONVOLUTE WITH LINE BROADENING FUNCTION AND PUT RESULT IN BR
>    45     C
>    45.5           DO 8 ISIG=1,60,5
>    45.7           SIGMAG=FLOAT(ISIG)
>    46             DO 10 I=1,200
>    47             YY=FLOAT(IN(I))
>    48             S=HH(I)+0.5
>    49             DO 10 J=1,200
>    50             SS=HH(J)+0.5
>    51             XX=F(S,SS,PAI,SIGMAG)
>    52             YG=XX*YY
>    53             BR(J)=BR(J)+YG
>    54          10 CONTINUE
```

Program SIM (con.)

```
>   55      C
>   56      C   DIFERENTIATE LINESHAPE AND PUT RESULT IN DIFF
>   57      C
>   58          DO 13 I=1,199
>   59       13 DIFF(I)=BR(I+1)-BR(I)
>   61          DO 8 KK=1,200
>   61.2     8 WRITE(7,300) HH(KK),DIFF(KK)
>   65      200 FORMAT(4X,I4,14X,E12.5,11X,I6,10X,E12.5,8X,E12.5)
>   65.5    300 FORMAT(1X,E12.5,1X,E12.5,1X)
>   66          STOP
>   67          END
```

Subroutines for SIM

```
>   68      C
>   69      C   LORENTZIAN LINE BROADENING
>   70      C
>   71          FUNCTION F(H,HI,PAI,SIGMA)
>   72          F=(2.0*SIGMA)/(PAI*(4.0*(H-HI))**2+SIGMA**2)
>   73          RETURN
>   74          END
>   75      C
>   76      C   GAUISSIAN LINE BROADENING
>   77      C
>   78          FUNCTION G(H,HI,PAI,SIGMA)
>   79          G=1.0/((SQRT(2.0*PAI))*SIGMA)*EXP(-((H-HI)**2)/
>   80         @(2.0*SIGMA**2))
>   81          RETURN
>   82          END
>   83      C
>   84      C FIND RESONANT FIELD
>   85      C
>   86          FUNCTION H(G1,G2,G3,THETA,FAY,UU,BETA,PL,WA1,WA2,WA3)
>   87          G=SQRT((G1*SIN(THETA)*SIN(FAY))**2+(G2*SIN(THETA)*COS(FAY))**2+
>   88         @(G3*COS(THETA))**2)
>   91          H=(PL*UU)/(G*BETA)
>   92          RETURN
>   93          END
```

END OF FILE

Program P.VALUES

```
>    1          COMPLEX*16 EE(6,6),AA,BB,A1,B,C,DD
>    2          REAL*8 AR(6,6),AI(6,6),R(6),WK1(6),WK2(6),WK3(6)
>    3          REAL*8 A,CO1,CO2,CO3,C11,C22,C33,D,E,F,GX,GX1,GY,GY1
>    4          REAL*8 GZ,GZ1,HX,HY,HZ,DARR(6),EARR(6),TOL,EPS,X,Y,Z,FREQ
>    5          COMMON HX,HY,HZ,GX1,GY1,GZ1,DARR,EE,C11,C22,C33????~
>    6          WRITE(6,99)
>    7          IFAIL=0
>    8          FREQ=9.2
>    9          READ(5,1)NUM
>   10          DO 15 III=1,NUM
>   11          READ(5,2)GX1,GY1,GZ1
>   12          READ(5,4)D,E,F,A
>   13          WRITE(6,5)GX1,GY1,GZ1,D,E,F,A????a
>   14          AA=(0.0D0,0.0D0)
>   15          EE(5,2)=AA
>   16          EE(1,4)=AA
>   17          EE(2,5)=AA
>   18          EE(1,6)=AA
>   19          EE(3,6)=AA
>   20          EE(4,1)=AA
>   21          EE(3,2)=AA
>   22          EE(6,1)=AA
>   23          EE(6,3)=AA
>   24          BB=DCMPLX(3.162278*E,0.0D0)
>   25          EE(1,3)=BB
>   26          EE(3,1)=BB
>   27          EE(4,6)=BB
>   28          EE(6,4)=BB
>   29          BB=DCMPLX(DSQRT(2.0D0)*3.0D0*E,0.0D0)
>   30          EE(2,4)=BB
>   31          EE(4,2)=BB
>   32          EE(3,5)=BB
>   33          EE(5,3)=BB
>   34          BB=DCMPLX(DSQRT(5.0D0)/2.0D0*A,0.0D0)
>   35          EE(1,5)=BB
>   36          EE(5,1)=BB
>   37          EE(2,6)=BB
>   38          EE(6,2)=BB
>   39          C11=10.0D0/3.0*D+A/2.0+F/3.0
>   40          C22=(-2)*D/3.0-3.0/2.0*A-F
>   41          C33=A+2.0/3.0*F-8.0/3.0*D
>   42          Z=0.25D0
>   43          HZ=0.0D0
>   44          HY=0.0D0
>   45          HX=0.0
>   46          CALL SOLVE
>   47          WRITE(6,11)DARR(1),DARR(2),DARR(3),DARR(4),DARR(5),DARR(6)
>   48          SP1=DARR(3)-DARR(1)
>   49          SP2=DARR(5)-DARR(3)
>   50          WRITE(6,19)SP1,SP2
>   51          WRITE(6,9)
>   52          HX=Z
>   53          Y=Z
>   54       22 CALL SOLVE
>   55          X=DABS(DARR(2)-DARR(1))
```

```
>    56          Y=Y/2D0
>    57          IF(Y-0.00002)12,13,13
>    58      13  IF(FREQ-X)21,12,23
>    59      21  HX=HX-Y
>    60          GOTO 22
>    61      23  HX=HX+Y
>    62          GOTO 22
>    63      12  WRITE(6,39)HX
>    64          HX=Z
>    65          Y=Z
>    66      36  CALL SOLVE
>    67          X=DABS(DARR(4)-DARR(3))
>    68          Y=Y/2D0
>    69          IF(Y-0.00002)32,33,33
>    70      33  IF(FREQ-X)34,32,35
>    71      34  HX=HX-Y
>    72          GOTO36
>    73      35  HX=HX+Y
>    74          GOTO36
>    75      32  WRITE(6,39)HX
>    76          HX=Z
>    77          Y=Z
>    78      46  CALL SOLVE
>    79          X=DABS(DARR(6)-DARR(5))
>    80          Y=Y/2D0
>    81          IF(Y-0.00002)42,43,43
>    82      43  IF(FREQ-X)44,42,45
>    83      44  HX=HX-Y
>    84          GOTO 46
>    85      45  HX=HX+Y
>    86          GOTO 46
>    87      42  WRITE(6,39)HX
>    88          WRITE(6,8)
>    89          Z=0.25D0
>    90          HZ=0.0D0
>    91          HX=0.0D0
>    92          HY=Z
>    93          Y=Z
>    94     722  CALL SOLVE
>    95          X=DABS(DARR(2)-DARR(1))
>    96          Y=Y/2D0
>    97          IF(Y-0.00002)712,713,713
>    98     713  IF(FREQ-X)721,712,723
>    99     721  HY=HY-Y
>   100          GOTO 722
>   101     723  HY=HY+Y
>   102          GOTO 722
>   103     712  WRITE(6,39)HY
>   104          HY=Z
>   105          Y=Z
>   106     736  CALL SOLVE
>   107          X=DABS(DARR(4)-DARR(3))????/
>   108          Y=Y/2D0
>   109          IF(Y-0.00002)732,733,733
>   110     733  IF(FREQ-X)734,732,735
```

```
>   111      734 HY=HY-Y
>   112          GOTO 736
>   113      735 HY=HY+Y
>   114          GOTO 736
>   115      732 WRITE(6,39)HY
>   116          HY=Z
>   117          Y=Z
>   118      746 CALL SOLVE
>   119          X=DABS(DARR(6)-DARR(5))
>   120          Y=Y/2D0
>   121          IF(Y-0.00002)742,743,743
>   122      743 IF(FREQ-X)744,742,745
>   123      744 HY=HY-Y
>   124          GOTO 746
>   125      745 HY=HY+Y
>   126          GOTO 746
>   127      742 WRITE(6,39)HY
>   128          WRITE(6,7)
>   129          Z=0.25D0
>   130          HX=0.0D0
>   131          HY=0.0D0
>   132          HZ=Z
>   133          Y=Z?????
>   134      622 CALL SOLVE
>   135          X=DABS(DARR(2)-DARR(1))
>   136          Y=Y/2D0
>   137          IF(Y-0.00002)612,613,613
>   138      613 IF(FREQ-X)621,612,623
>   139      621 HZ=HZ-Y
>   140          GOTO 622
>   141      623 HZ=HZ+Y
>   142          GOTO 622
>   143      612 WRITE(6,39)HZ
>   144          HZ=Z
>   145          Y=Z
>   146      636 CALL SOLVE
>   147          X=DABS(DARR(4)-DARR(3))
>   148          Y=Y/2D0
>   149          IF(Y-0.00002)632,633,633
>   150      633 IF(FREQ-X)634,632,635
>   151      634 HZ=HZ-Y
>   152          GOTO 636
>   153      635 HZ=HZ+Y
>   154          GOTO 636
>   155      632 WRITE(6,39)HZ
>   156          HZ=Z
```

```
>  157          Y=Z
>  158      646 CALL SOLVE
>  159          X=DABS(DARR(6)-DARR(5))
>  160          Y=Y/2D0
>  161          IF(Y-0.00002)642,643,643
>  162      643 IF(FREQ-X)644,642,645
>  163      644 HZ=HZ-Y
>  164          GOTO 646
>  165      645 HZ=HZ+Y
>  166          GOTO 646
>  167      642 WRITE(6,39)HZ
>  168       15 WRITE(6,99)
>  169        1 FORMAT(I2)
>  170       99 FORMAT('1')
>  171       39 FORMAT(3X,2(D12.6,3X))?????
>  172        5 FORMAT(3X,'GX=',F6.4,3X,'GY=',F6.4,3X,'GZ=',F6.4,7X,
>  173          @'D=',F6.2,2X,'E=',F6.2,2X,'F=',F6.2,2X,'A=',F6.2)
>  174        2 FORMAT(3(F6.4,1X))
>  175        4 FORMAT(4(F6.2,1X))
>  176        9 FORMAT(////,' X',/)?*??/
>  177       19 FORMAT(' THE SPLITTINGS BETWEEN THE DOUBLETS ARE ',F12.6,' AND ',F
>  178          @12.6,' GHZ')
>  179        8 FORMAT(//,' Y',/)
>  180        7 FORMAT(//,' Z',/)
>  181        6 FORMAT(3(F5.2,1X))
>  182       11 FORMAT(//,'  THE ZERO FIELD ENERGY LEVELS ARE :- ',/,6(10X,F12.6,'
>  183          @ GHZ',/),////)
>  184          STOP
>  185          END
```

Subroutine   SOLVE

```
>   186          SUBROUTINE SOLVE
>   187          COMPLEX*16 EE(6,6),AA,BB,A1,B,C,DD
>   188          REAL*8 GZ,GZ1,HX HY,HZ,DARR(6),EARR(6),TOL,EPS,X,Y,Z
>   189          REAL*8 AR(6,6),AI(6,6),R(6),WK1(6),WK2(6),WK3(6)
>   190          REAL*8 A,CO1,CO2,CO3,C11,C22,C33,D,E,F,GX,GX1,GY,GY1,FREQ
>   191          COMMON HX,HY,HZ,GX1,GY1,GZ1,DARR,EE,C11,C22,C33
>   192          IAR=6
>   193          IAI=6
>   194          GX=GX1*HX*13.996
>   195          GY=GY1*HY*13.996
>   196          GZ=GZ1*HZ*13.996
>   197          CO1=DSQRT(5.0D0)/2.0D0
>   198          CO2=DSQRT(2.0D0)
>   199          CO3=1.5
>   200          EE(1,1)=DCMPLX(GZ*5.0D0/2.0D0+C11,0.0D0)
>   201          EE(2,2)=DCMPLX(GZ*3.0D0/2.0D0+C22,0.0D0)
>   202          EE(3,3)=DCMPLX(GZ/2.0D0+C33,0.0D0)
>   203          EE(4,4)=DCMPLX(C33-GZ/2.0D0,0.0D0)
>   204          EE(5,5)=DCMPLX(C22-GZ*3.0D0/2.0D0,0.0D0)
>   205          EE(6,6)=DCMPLX(C11-GZ*5.0D0/2.0D0,0.0D0)
>   206          A1=DCMPLX(CO1*GX,CO1*GY*(-1))
>   207          EE(1,2)=A1
>   208          EE(5,6)=A1
>   209          B=DCMPLX(CO1*GX,CO1*GY)
>   210          EE(2,1)=B
>   211          EE(6,5)=B
>   212          C=DCMPLX(CO2*GX,(-1)*CO2*GY)
>   213          EE(2,3)=C
>   214          EE(4,5)=C
>   215          DD=DCMPLX(CO2*GX,CO2*GY)
>   216          EE(3,2)=DD
>   217          EE(5,4)=DD
>   218          EE(3,4)=DCMPLX(CO3*GX,CO3*(-1)*GY)
>   219          EE(4,3)=DCMPLX(CO3*GX,CO3*GY)
>   220          DO 20 I=1,6
>   221          DO 20 J=1,6
>   222          AR(I,J)=DREAL(EE(I,J))
>   223          AI(I,J)=DIMAG(EE(I,J))
>   224       20 CONTINUE
>   225          CALL X02AAF(EPS)
>   226          CALL X02ADF(TOL)
>   227          CALL F01BCF(6,TOL,AR,IAR,AI,IAI,DARR,EARR,WK1,WK2)
>   228          CALL F02AVF(6,EPS,DARR,EARR,IFAIL)
>   229          RETURN
>   230          END
```

REFERENCES

Aasa R., (1970), J.Chem.Phys 52, 3919.

Aasa R., Vanngard T., (1975), J. Magn. Reson. 19, 308.

Abragam A., Bleaney B., (1970), "E.P.R. of Transition Metal Ions",

Clarendon Press.

Allen J.W., (1964), Proc. 7th Inter.Conf. on Semiconductors, Paris, p 781.

Al'tshuler S.A., Kozyrev B.M., (1974), "E.P.R. in Compounds of Transition

Elements", John Wiley & Sons.

Anderson P.O., Kollberg E., (1973), Phys. Rev. B8, 4956.

Anderson P.O., Kollberg E., Jelinsky A., (1974), J.Phys. C.Solid State

Phys. 7, 1868.

Assenheim H.M., (1966), "Introduction to E.S.R.", Adam-Hilger.

Barry T.I., (1967), N.P.L. report l.M.U. Ex 6.

Blandin M.G., Fairsant P., Picard C., Ezzo M., Fontain G., (1980)

Phys.Stat.Sol. A60, 357.

Blandin M.G., Bursill C.A., Hutchinson J.L., Gai P.L., (1981),

J. Physique (France) C3 42, 95.

Bleaney B., Stevens K.W., (1953) Rept. Prog.Phys. 16, 108.

Bleaney B., Trenham R.S., (1951), Proc.Roy.Soc (London) A 205, 175.

Blumberg W.E., (1967) in "Magnetic Resonance in Biological Systems",

eds. Erhenberg A., Malustrŏm B.E., Vǎngard T., Pergamon Press, p119.

Bogomolov V.N., Sockava L.S., (1968), Sov.Phys.Sol.Stat. 9, 2677.

Carter D., Okaya A, (1960), Phys.Rev.118, 1485.

Castner T., Newell G.S., Holton W.C., Slichiter C.P., (1960),

J.Chem.Phys. 32, 668.

Chandrashekhev G.V., Titte R.S., (1976), J. Electrochem. Soc. 123, 392.

Chester P.F., (1961), J. Appl.Phys. 32, 866.

Chester P. F., (1964), C.E.R.L. Report RD/C/R 1267.

Clark W., Broadhead P., (1970), J.Phys. C3, 1047.

Conesa J.C., Sarice J., J. Magn. Reson. 33, 298.

Cronemayer O.C., Phys. Rev. 87, 876.

De Vore J.R., (1951), J. Opt.Soc.Am. 41, 416.

Dicke R.H., Wittke J.P., (1961), "Introduction to Quantum Mechanics",
     Addison Wesley Pub.Co.

Dowsing R.D., Gibson J.F., J. Chem.Phys. 30, 294.

Dyrek C., Schindler R.N., (1977), Z. Naturforsch 32a, 501..

Eggleston H.S., (1980), "E.S.R. Studies of Doped Rutile",
     M.Sc. Thesis, Durham University.

Eggleston H.S., Thorp J.S., (1981), J.Mat.Sci, 16, 537.

Faughnan B.W., Kiss Z.J., (1968), Phys.Rev.Lett. 21, 1331.

Frederikse H.P.R., (1961), J.App.Phys. 32, 2211.

Goni M.S., McPherson R., (1980), J.Mat.Sci. 15, 1915.

Gerritsen H.J., Sabiskey E.S., (1962), Phys.Rev. 125, 1853.

Gerritsen H.J., Harrison S.E., (1959), Phys. Rev.Lett 2, 153.

Gerritsen H.J., Harrison S.E., (1950), J.Appl.Phys. 31, 1566.

Gerritsen H.J., Sabiskey E.S., (1963), Phys.Rev. 132, 4507.

Gibb R.M., Anderson J.S., (1972), J.Sol.Stat.Chem.5, 212.

Grant F.A., (1959), Res.Mod Phys. 31, 646.

Griffith J.S., (1961), "The Theory of Transition Metal IOns",
     Cambridge.

Hodgskiss S.W., (1981) " Electron Spin Resonance Studies of Impurity Ions
     in Rutile",
     Ph.D.Thesis, Durham University.

Huntington M., Sullivan G., (1965), Phys.Rev.Lett. 14, 177.

Ikebe M., Miyako Y., Date M., (1969), J.Phys.Soc. Japan 26, 43.

Kersen J., Volger J., (1973) Physica 69, 535.

Kittel C., Abrahams E., (1953), Phys.Rev. 90, 238.

Lichenberger G.J., Addison J.R., (1964), Phys.Rev. 184, 381.

Low L., Offenbacker E.L., Sol.Stat.Phys. 17, 135.

McDevitt N.J., Baun W.L., (1964), Spectrochim.Acta. 20, 799.

Mackay J.H., Kopp M., Tyman E.L., Tek Fu Yen, in "E.S.R. of Metal
    Complexes", ed. Teh Fu Yen, Adam Hilger Ltd, London.

Madan M.P., (1964), Can J.Phys. 42, 583.

Manenkov A.A., Milgaeo V.A., Prokhovov A.M., (1962), Sov.Phys.Sol.Stat 4
    280.

Matossi F., (1951), J.Chem.Phys. 19, 1543.

Mizushima K., Tanaka M., Asai I., Iida S, (1973), Am.Inst.Phys.Conf.
    Proc 18, 1044.

Mizushima K., Tanaka M., Asai I., Iida S., Goodenough J.B., (1979),
    J.Phys. Chem.Sol 40, 1129.

Mizushima K., Tanaka M., Iida S., (1972), J.Phys.Soc. Japan 32, 1519.

Naccache C., Meriaudeau P., Che M., (1971), Trans For Soc 67, 506.

NaragansonP.S., (1950), Proc.Ind. Acad.Sci A32, 279.

NaragansonP.S., (1953), Proc.Ind.Acad.Sci A37, 411.

Orbach R., Stapleton H.J., (19   ),in "Electron Paramagnetic Resonance",
    ed. Geschwind S, Ch.2, Plenum.

Pilbrow J.R., (1978), J.Magn.Reson. 31, 479.

Poole C.P., Farach H.A. (1971), "Relaxation in Magnetic Resonance",
    Academic Press.

Poole C.P., Farach H.A., (1972) "The Theory of Magnetic Resonance"
    Wiley - Interscience.

Purcell T., Weeks R.A., (1971), J.Chem.Phys. 54, 2800.

Schiff C.I., (1955), "Quantum Mechanics", McGraw-Hill, Chapters VI and VIII.

Schollmeier G., (1966), Proc. IEEE 54, 690.

Shannon R.D., Prewitt C.T., (1969), Acta Cryst B25, 925.

Shen L.N., Johnson O.W., Oklesen W.D., De Ford J.W.,(1974),
    Phys. Rev. B10, 1823.

Sierro I., Müller K.A.,Lacroix R., (1960), Arch Sci (Geneva) 12, 122.

Silobee R.H. (1972) in "Electron Paramagnetic Resonance" ed. Ceschwind S,
p 504, Plenum.

Sochava L.S., Reshina I.I., Mirkin D.N., (1970), Sov.Phys.Sol Stat. 12, 942.

Sochava L.S., Tolparas Yu. N., (1972), Sov.Phys.Sol Stat 13, 1802.

Spitzer W.G., Miller R.C., Kleinman D.A., Howarth L.E., (1951),
     J.Chem.Phys. 19, 1543.

Shevets V.A., Kazanskii V.B., (1971), Kinet Catal. USSR 12, 332.

Standley K.J., Vaughan R.A., (1969), "Electron Spin Relaxation
     Phenomena in Solids", Adam Hilger.

Stoneham A.M., (1966), Proc.Phys. Soc, 89, 909.

Stoneham A.M. (1967), Colloque Ampère XIV, Session 19 No.6, p 852.

Stoneham A.M., (1968), Proc. Phys.Soc. (Ser 2) 1, 565.

Tanaka S., Mizushima K., Iida S., (1980), J.Phys.Soc.Japan 44, 1291.

Taylor P.L., Bougher J.F., Kritz H.M., (1974), Chem Res 75, 203.

Turner G.P.A. (1967), "Introduction to Paint Chemistry", Science
     Paperbacks, Chapman & Hall.;

Tioxide International Ltd., "Tioxide Pigments : a guide to selection"
     BTP 182.

Van Hooff J.H.C., (1968), J.Catal. 277.

Van Vleck J.H. (1948), Phys.Rev. 74, 1168.

Van Vleen G., (1978), J. Magn. Reson, 30, 91.

Von Hippel A. , Kalnajs J. Westphal W.B., (1962), ᠁Phys.Chem.Solids
     23, 779.

Weeks A.A., (1961), Bull.Am.Phys.Soc. 6, 178.

Young C.G., (1961), Ball.Am.Phys.Soc 6, 248.

Zerfoss S., Stokes R.G., Moore C.H., (1948), J.Chem.Phys. 16, 1166.

Zvingel D., (1976), Sol Stat.Comm. 20, 397.